INVESTIGATION OF FLOW AND SCOUR AROUND HEAD OF A VERTICAL WALL BREAKWATER

A THESIS SUBMITTED TO
THE GRADUATE SCHOOL OF NATURAL AND APPLIED SCIENCES
OF
MIDDLE EAST TECHNICAL UNIVERSITY

BY

KADİR KARAKAŞ

IN PARTIAL FULFILLMENT OF THE REQUIREMENTS
FOR
THE DEGREE OF MASTER OF SCIENCE
IN
CIVIL ENGINEERING

AUGUST 2019

Approval of the thesis:

INVESTIGATION OF FLOW AND SCOUR AROUND HEAD OF A VERTICAL WALL BREAKWATER

submitted by **KADİR KARAKAŞ** in partial fulfillment of the requirements for the degree of **Master of Science in Civil Engineering Department, Middle East Technical University** by,

Prof. Dr. Halil Kalıpçılar
Dean, Graduate School of **Natural and Applied Sciences** _____

Prof. Dr. Ahmet Türer
Head of Department, **Civil Engineering** _____

Assist. Prof. Dr. Cüneyt Baykal
Supervisor, **Civil Engineering, METU** _____

Examining Committee Members:

Prof. Dr. Ali Melih Yanmaz
Civil Engineering, METU _____

Assist. Prof. Dr. Cüneyt Baykal
Civil Engineering, METU _____

Prof. Dr. Ahmet Cevdet Yalçıner
Civil Engineering, METU _____

Assoc. Prof. Dr. Kubilay Cihan
Civil Engineering, Kırıkkale University _____

Assist. Prof. Dr. Gülizar Özyurt Tarakcıoğlu
Civil Engineering, METU _____

Date: 27.08.2019

I hereby declare that all information in this document has been obtained and presented in accordance with academic rules and ethical conduct. I also declare that, as required by these rules and conduct, I have fully cited and referenced all material and results that are not original to this work.

Name, Surname: Kadir Karakaş

Signature:

ABSTRACT

INVESTIGATION OF FLOW AND SCOUR AROUND HEAD OF A VERTICAL WALL BREAKWATER

Karakaş, Kadir
Master of Science, Civil Engineering
Supervisor: Assist. Prof. Dr. Cüneyt Baykal

August 2019, 104 pages

In this study, wave induced hydrodynamic and morphodynamic processes around the head of a vertical wall breakwater are investigated by numerical and physical modeling. An open source computational fluid dynamics code was used to investigate the flow around the head of structure. The code solves incompressible Reynolds-Averaged Navier-Stokes equations with a k-omega turbulence closure. For investigating flow and scour around the structure, small-scale physical model tests were carried out in the random wave flume of Middle East Technical University, Department of Civil Engineering, Coastal and Ocean Engineering Laboratory. The experiments are composed of two stages where in the first stage the flow around the structure on a fixed bed is investigated by means of flow visualization techniques, and Acoustic Doppler Velocimeter measurements and in the second stage the scour around the structure mounted on a movable sandy bed under the same wave conditions is observed. The experiments are carried out for various Keulegan-Carpenter numbers and wave steepnesses. The wave induced scour depths are observed via underwater camcorders, and bed evolution is analyzed via semi-automatic laser scanner. When the results of scour experiments performed under regular and random waves are examined; in the dimensionless time scale, regular waves reached 25 times faster to the equilibrium state than random waves. When the KC number is around 5.5, the

scour depths formed under random waves are 7 times the scour depths formed under regular waves. In the experiments, waves with different steepnesses but similar KC numbers are examined, and no significant difference was observed in the scour depths of these waves. When the shape effect of the breakwater head under random waves is examined, it is concluded that the scour depths in the tests with sharp-edged head structure are higher than the models with round head shape by 20% to 25%. Numerical model results and physical model results are found to be in agreement for the lee-wake vortex dimensions and velocity distribution measurements. In both numerical and physical model results, when the velocity distribution measurements are examined, it is observed that the velocities converge to the undisturbed velocities beyond 10B distance from the tip of the breakwater head and there is no blockage effect after this distance. It is observed that, contrary to regular and random waves, the equilibrium scour depths of solitary waves occur at the leeward of the structure, not in front of the breakwater head. Furthermore, while solitary waves have the same wave height but occur at different depths are examined, scour depth increases with increasing water depth.

Keywords: Vertical Wall Breakwater, Scour, Flow Visualization, OpenFOAM®

ÖZ

DÜŞEY YÜZLÜ DALGAKIRAN MÜZVARI ÇEVRESİNDEKİ AKIM VE OYULMANIN ARAŞTIRILMASI

Karakaş, Kadir
Yüksek Lisans, İnşaat Mühendisliği
Tez Danışmanı: Dr. Öğr. Üyesi Cüneyt Baykal

Ağustos 2019, 104 sayfa

Bu çalışmada, düşey yüzlü dalgakıranının müzvar kısmındaki dalga kaynaklı hidrodinamik ve morfodinamik süreçler sayısal ve fiziksel modelleme ile incelenmiştir. Yapı etrafındaki akışı araştırmak için açık kaynak hesaplamalı akışkanlar dinamiği kodu kullanılmıştır. Kod, k-omega türbülans kapatmasıyla sıkıştırılamaz Reynolds Ortalamalı Navier Stokes denklemlerini çözmektedir. Yapı etrafındaki akım ve oyulmayı araştırmak için, Orta Doğu Teknik Üniversitesi, İnşaat Mühendisliği Bölümü, Kıyı ve Deniz Mühendisliği Laboratuvarı'nın düzensiz dalga kanalında küçük ölçekli fiziksel model deneyleri yapılmıştır. Deneyler, birinci aşamada sabit bir taban üzerinde yapının etrafındaki akımın, akım görüntüleme teknikleri ve akustik Doppler hız ölçümleri ile araştırıldığı ve ikinci aşamada, aynı hareket altındaki hareketli bir kumlu yatak üzerine monte edilen yapının etrafındaki oyulmanın araştırıldığı iki aşamadan oluşmaktadır. Deneyler çeşitli Keulegan-Carpenter (KC) sayıları ve dalga diklikleri için gerçekleştirilmiştir. Dalgaların sebep olduğu oyulma derinlikleri su altı kameralarla gözlenmiş ve yarı otomatik lazer tarayıcıyla taban değişimi kaydedilmiştir. Düzenli ve düzensiz dalgalar altında gerçekleştirilen oyulma deneylerinin sonuçları incelendiğinde; boyutsuz zaman ölçeğinde, düzenli dalgaların düzensiz dalgalara göre 25 kat daha hızlı denge durumuna ulaştığı gözlemlenmiştir. KC sayısı 5 mertebelerinde iken düzensiz dalgalar

altında oluşan oyulma derinlikleri düzenli dalgalar altında oluşan oyulma derinliklerinin 7 katı kadar gerçekleşmiştir. Deneyler kapsamında farklı diklikteki ancak benzer KC sayısına sahip dalgalar incelenmiş ve bu dalgaların oyulma derinliklerinde belirgin bir farklılık gözlemlenmemiştir. Düzensiz dalgalar altında dalgakıranın kafa şeklinin etkisi incelendiğinde, keskin kenarlı kafa yapısına sahip modellerde oyulma derinliklerinin 20%'den 25%'e kadar yuvarlatılmış kafa şekline sahip modellere göre daha fazla olduğu sonucuna ulaşılmıştır. Öte yandan, sayısal model sonuçları ile fiziksel model sonuçlarının ard-alan girdap boyutları ve akıma dik yöndeki hız dağılımı ölçümleri açısından benzer olduğu gözlemlenmiştir. Hem sayısal hem de fiziksel model sonuçlarında, hız dağılımı ölçüm sonuçları incelendiğinde yapı önünden 10B mesafede hızların bozulmamış hızlara yakınsadığı gözlemlenmiş ve bu mesafeden sonra tıkanma etkisinin ortadan kalktığı anlaşılmıştır. Soliter dalgalar altında denge oyulma derinliklerinin düzenli ve düzensiz dalgaların aksine yapı önünde değil, yapının ardında oluştuğu gözlemlenmiştir. Ayrıca aynı dalga yüksekliğine sahip ancak farklı derinliklerde oluşan soliter dalgalar incelendiğinde su derinliğinin artmasıyla oyulma derinliği artmaktadır.

Anahtar Kelimeler: Düşey Yüzlü Dalgakıran, Oyulma, Akım Görüntüleme, OpenFOAM®

dedicated to virtuous ones…

ACKNOWLEDGEMENTS

First of all, I would like to thank my supervisor Dr. Cüneyt Baykal who always make me search for perfection, his work discipline is beyond measure. The precision of this research is not only because of me but also his exertion. I am heartily grateful to have such an excellent professor.

Secondly, I would like to thank Prof. Dr. Ayşen Ergin for her Coastal Engineering lecture book which gives me the opportunity to meet with coastal engineering. Without her and her book, this thesis would not be existed. Her extraordinary energy and caressing attitude to the students are irreplaceable.

My honorable professors; Prof. Dr. Ahmet Cevdet Yalçıner, Dr. Işıkhan Güler and Dr. Gülizar Özyurt Tarakcıoğlu, I would like to thank you for your inexhaustible effort to teach and lead.

For his guidance and comments, I would sincerely thank to PhD candidate Hasan Gökhan Güler.

I also would thank to my dear colleagues Can Özsoy, Cem Bingöl, Ghazal Khodkar, Koray Deniz Göral and Mehmet Sedat Gözlet and many others for their moral support and warm friendship. Last two years became outstanding with their companionship.

Last but not the least, I would like to thank my father Arslan Karakaş and my mother Kadire Karakaş, for their immeasurable supports. I would also thank to my brother Deniz Can Karakaş, and my sister Madame Judge Aslı Hilal Karakaş Kuzucu for their endless encouragements. Finally, I am deeply grateful to my sister and one of my best friends Asmin Güneş Karakaş, for giving meaning to my life in every sense and pushing me to applicate METU.

This study is supported by the “Numerical and Physical Modeling of Scour Around Head of a Vertical Wall Breakwater” (Grant no:YÖP-303-2018-2674) project of METU Scientific Research Projects.

TABLE OF CONTENTS

LIST OF TABLES

TABLES

LIST OF FIGURES

FIGURES

LIST OF ABBREVIATIONS

ABBREVIATIONS

2D	2 Dimensional
3D	3 Dimensional
ADV	Acoustic Doppler Velocimeter
CFD	Computational Fluid Dynamics
DHI	Danish Hydraulic Institute
RANS	Reynolds-averaged Navier-Stokes

LIST OF SYMBOLS

SYMBOLS

B	Width of breakwater
d_{50}	Median diameter of the sediment
g	Gravitational acceleration
h	Water depth
H	Wave height
H_m	Mean wave height
H_s	Significant wave height
H/L	Wave steepness
$H\{\cdot\}$	Heaviside step function
k	Turbulence kinetic energy
KC	Keulegan-Carpenter number
KC_r	Keulegan-Carpenter number for random waves
K_r	Reflection coefficient
L	Wave length
L_s	Wave length corresponding to significant wave height
L_X	Vortex dimension on X axis
L_Y	Vortex dimension on Y axis
m_{0U}	Zeroth spectral moment of flow velocity
p	Pressure

s	Relative density of the sediment
S	Scour depth
S_g	Gradation coefficient of the sediment
S_{ij}	Average expansion rate tensor
t	Time
t^*	Dimensionless time scale
T	Wave period
T_{mU}	Mean period of oscillating flow for random waves
T_U	Period of oscillating flow for regular waves
T_p	Peak wave period
T_s	Wave period corresponding to significant wave height
T_Z	Mean value of zero-up crossing period of wave series
T^*	Time scale of scour process
u_i	Velocities
U_m	Maximum horizontal velocity of water particles
$U_{m,r}$	Maximum horizontal velocity of water for random waves
U_{m0}	Undisturbed maximum horizontal velocity of water particles
U_{rms}	Root mean square of the flow velocity
x_i	Cartesian coordinates
ρ	Density of water
σ_U	Root mean square of the flow velocity

τ_{ij}	Reynolds stress tensor
v	Kinematic viscosity
v_T	Turbulent viscosity
ω	Specific rate of dissipation of the turbulence kinetic energy
ωt	Phase angle of a wave

CHAPTER 1

INTRODUCTION

Breakwaters are the main engineering structures constructed to create calm sea areas safe for marine activities and sea vehicles such as yachts and ships. These structures can be classified in four major categories: i) sloped rubble-mound, ii) vertical wall, iii) floating and iv) composite breakwaters where the sloped and vertical types are used in combination. These breakwater types are selected based on site conditions, project specifications, requirements and constraints. More information about breakwaters, types and design of these structures could be found in engineering manuals and guidelines.

In the design procedure of breakwaters, understanding the wave-seabed-structure interactions, resulting flow features and morphological changes in the close vicinity of the structure is a major step. As the name implies, the breakwaters are constructed against the wave forces. However, the direct impact of the waves is not the only mechanism that endangers the stability of these structures. The physical processes generated as a result of wave-seabed-structure interactions such as scour and liquefaction could also result in failure of these structures even in milder wave conditions than the design conditions. Therefore, these processes should also be considered in the design stage, and the necessary precautions need to be taken.

In this study, the hydro- and morpho-dynamic processes around the head of a vertical wall type breakwater with no foundation and scour protection are investigated by physical model experiments and numerical modeling. In the study, two different shapes of the breakwater head are considered: a) rounded in the form of a semi-circle with a diameter equal to the width of the breakwater and b) sharp-edged where the head is like a rectangle with sharp corners.

The physical model tests are carried out in mainly three stages: i) wave calibration, ii) flow and iii) scour stages. In the first stage, the time series of the wave conditions to be considered in the tests are determined. The tests are carried out for three different wave types: regular, random and solitary waves. In the second stage, flow around the structure is investigated observing the flow features around the structure and visualizing these features by injecting dissolvable dye into the water. In this stage, the possible blockage effect by the structure in the wave flume is also investigated through transverse velocity measurements from the tip of the structure to ensure the scour processes are not agitated due to the converging flow in the flume. In the third stage, the morphological changes around the head of a vertical wall breakwater placed on a non-cohesive sand bed are investigated measuring the scour depths before and after the wave series. For the numerical modeling part, the flow around the head is also investigated by means of a computational fluid dynamics (CFD) code which has been extensively validated and verified for the flow and scours around the vertical cylinders and pipelines under various flow conditions (e.g., Baykal et al. 2015, 2017; Fuhrman et al. 2014; Larsen et al. 2017).

The flow and scour around the head of a vertical wall breakwater has already been studied by Sumer and Fredsøe (1997) for regular waves by physical model experiments. They report the vortex regimes around the tip of the breakwater under various wave conditions, blockage effect, scour depths around the structure under regular waves. This study extends their discussion to the random and solitary waves and searches for answers to the following major questions:

i. How is the flow (vortex) regime, observed for regular waves around the head of a vertical wall breakwater, affected by the irregularity of the wave train for similar wave conditions (in wave height and period)?
ii. If any changes in the flow regime occur for random waves, then how the equilibrium scour depths around the structure are affected?
iii. Similarly, how are the flow and scour changes for solitary waves, which are commonly used in tsunami research?

iv. How does the shape of the head of the breakwater affect the flow and scour depths?

v. Could the flow features and sizes of these features with respect to various regular wave conditions around the head of a vertical wall breakwater given by Sumer and Fredsøe (1997) be simulated in a numerical model? Additionally, what should be the dimensions and resolution of the computational domain?

In Chapter 2, previously done studies about scouring around vertical walls, abutments, and piles are presented. Those studies consist both numerical and physical model tests. Flow characteristics of reviewed studies are steady/unsteady flows, waves, and combined currents and waves.

Numerical studies are presented with hydrodynamic and turbulence equations, flow conditions, model properties in Chapter 3. 2D and 3D simulations are performed in the scope of this study and presented comparatively with regard to numerical model properties.

In Chapter 4, experimental studies presented. Experimental studies consist of hydrodynamic tests, flow visualization tests, and scour tests. Results of experimental studies under various types of waves are compared with each other. Numerical simulation results obtained in Chapter 3 are also compared with physical model results in this chapter.

Finally, conclusions and future recommendations about the present study are listed in Chapter 5.

CHAPTER 2

LITERATURE REVIEW

Vertical wall breakwaters are preferred to create protected coastal areas against wind waves where the water depth increases rapidly and generally depth at the toe of the structure is larger than 15 m in coastal engineering. In the literature, scour induced damage under wave action is considered among failure types for this type of structures. (e.g., Franco 1994; Oumeraci 1994; Takahashi 1996) are examples of these studies. Franco (1994) remarks breakwater damages in his study that he discusses the design and construction of vertical wall breakwater. One of Franco's breakwater examples that he studied in his work is the breakwater in Gela, Sicily. This breakwater was damaged in 1991 after a storm with a significant wave height of 6 meters. The depth of scour at the tip of the structure was reached 1.5 meters. Based on the examples he examined, Franco also cited scour in front of the structure besides wave overtopping and ground liquefaction for the tilting failures of caisson type breakwaters. Oumeraci (1994) examined the damage varieties for the vertical wall breakwaters and introduced the developed design strategies. In his study, Oumeraci mentioned the Mustapha Breakwater in Algeria as an example of scour induced damage. The Mustapha Breakwater was damaged by tilting on its side due to scours. Takahashi (1996) in his work on the design of vertical wall breakwaters, examined the damage situation of the built breakwaters by observing on-site. Among the main causes of damage is the scour around the breakwater. One of the examples is the Mutsu-Ogawahara Port’s composite breakwater which has rubble base and caisson blocks. A severe storm hit northern Japan on 16 February 1992 with a recorded significant wave height of 9.94 m which is greater than the design wave. Due to the storm, one of the listed damage that observed is 1 m to 2 m scouring in front of the structure at the sandy sea bottom. Settlement and deformation at the rubble foundation

are caused by the scours although no damage at the caisson blocks. Another example is Sendai Port's 700 m offshore vertical wall breakwater in Japan. In 1991 as a result of typhoon's devastating effect, several caisson blocks are moved from their original place, Figure 2.1. Caisson blocks that have 11.8 m widths were placed at 21 m water depth and on 6 m high rubble base. The significant wave height and wave period of this storm were given as 6.8 m and 12 s, respectively. The KC number of this wave is calculated as 1.9 with the linear wave theory. The occurred damage at the head of breakwater can be seen in Figure 2.2. This tilting and sliding caused not by the wave forces but scouring at the sea bed.

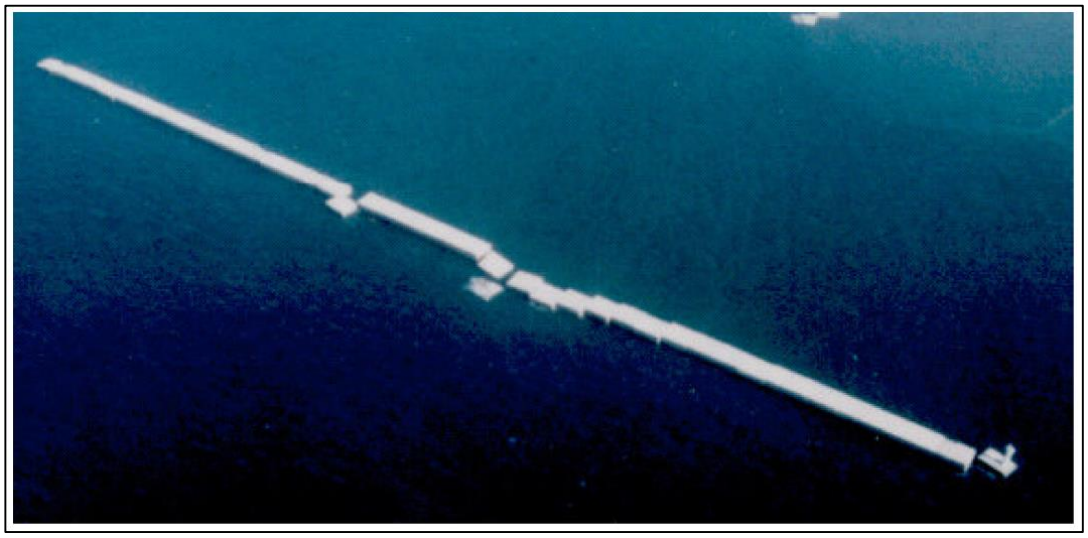

Figure 2.1. Sendai Port's damaged offshore breakwater under Typhoon 9119 (19th typhoon in 1991) (Kim 2009)

Figure 2.2. Damaged breakwater head of Sendai Port under Typhoon 9119 (19th typhoon in 1991) (Kim 2009)

Design wave height of the vertical wall breakwaters is generally chosen from 50 or 100 years return wave heights. In order to compute KC numbers for vertical wall breakwaters under waves have 10-12 s wave periods at a 15-20 m water depth, maximum horizontal velocities of water particles can be calculated as approximately U_m=2-5 m/s with the linear wave theory. Width of the breakwater varies between 10-20 m with regard to wave height and period and KC numbers are in the order of O(1) under design waves. When the wave characteristics are relatively moderate, the KC number will decrease as well.

There are many experimental studies about structure-flow interaction induced scour around coastal and offshore structures, bridge piers, and other hydraulic structures. (e.g., Melville and Raudkivi 1977, 1996; Raudkivi and Ettema 1977, 1983; Raudkivi 1986, 1998; Melville and Sutherland 1988; Ettema et al. 1998) can be given as examples of experimental studies on scouring around bridge piers under unidirectional flow. (e.g., Lim 1997; Yanmaz and Altınbilek 1991; Eroğlu et al. 2001; Güney et al. 2011; Zhao et al. 2012) can be given as examples for the scouring around square cross-

section structures under unidirectional flow conditions. Lim (1997) studied the maximum scour depth in front of bridge abutments under fixed-bed (no sediment movement at far-field) conditions. Abutments used in these experiments are extended from shore and perpendicular to the current. From this point of view, it is similar to the cross-section of the vertical wall breakwater head exposed to the unidirectional current (tidal, etc.) perpendicular to the breakwater direction. In the study of Yanmaz and Altınbilek (1991), they studied piles that have square and cylindrical cross-section under fixed-bed condition and offered dimensionless scour depth curves. Zhao et al. (2012) studied scour around single submerged caisson blocks experimentally which have square and rectangular cross-sections with different angular placement (0°,45°, and 90° orientations). Eroğlu et al. (2001) studied scour around spur-dikes under live-bed (sediment movement at far-field) condition. Güney et al. (2011) studied local scour around square pile under unsteady flow.

(e.g., Sumer et al. 1992a, 1992b, 1993; Dey et al. 2006) studies can be examples about scouring around pile-based structures under regular waves induced oscillatory bi-directional flow. Carreiras et al. (2000) studied scour around single pile and multiple piles due to wave action and investigated the effect of breaking zone to scouring processes. Sumer and Fredsøe (2001), investigated scouring processes under unidirectional flow, combined flow and wave, and random wave conditions for cylindrical structures. Nielsen et al. (2010) studied flow conditions and scouring process around cylindrical single-piles with scour protection under steady current condition via physical model experiments with both live-bed and fixed-bottom conditions. Sumer et al. (1993) experimentally studied scour around square piles with 45° and 90° orientations under wave action and proposed the formulas that calculate scour depths depending on Keulegan-Carpenter (KC) Number.

$$KC = \frac{U_m T}{B} \tag{2.1}$$

Where the U_m is the maximum horizontal velocity of water particles at the near-bed, T is the wave period, and B is the width of structure. The most comprehensive

previously done study about present study's topic is Sumer and Fredsøe (1997). They studied the scour around head of vertical wall under both waves only and combined current and wave conditions and observed flow conditions. However, they used regular waves in their experiments. In their study; flow around structure (Figure 2.3), dimensions of the vortex forms, scour depths and the dimensions of scour holes, and additionally suggested dimensions of rubble scour protection base are given for the depending KC number.

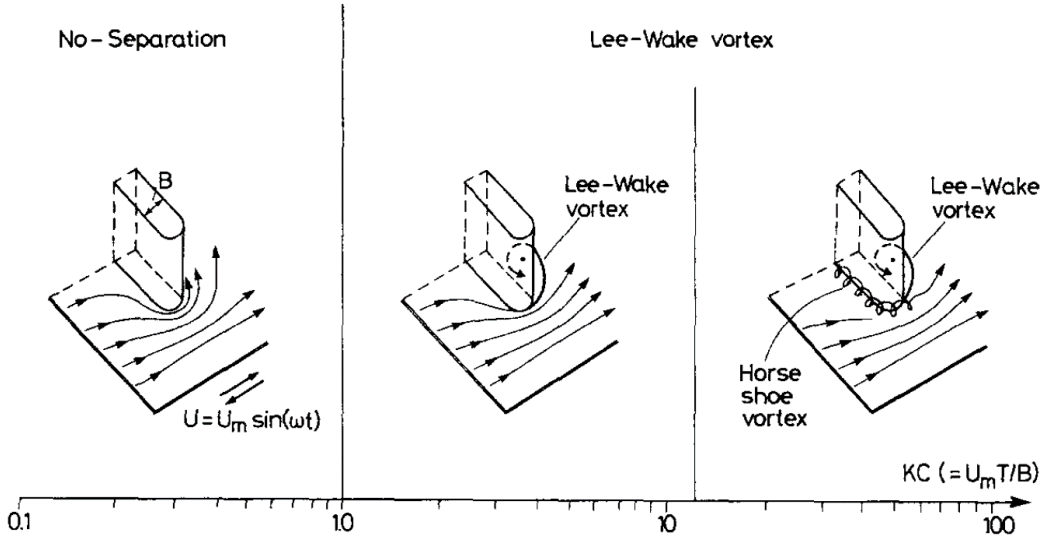

Figure 2.3. Flow around head of the vertical wall breakwater at near-bed (Sumer and Fredsøe 1997)

Sumer and Fredsøe (1997) classified flow regimes around the breakwater into 3 different categories according to KC number. The first one of them is the no-separation region without any vortex formation when the KC is smaller than 1. Secondly, there is a region that only lee-wake vortex occurs while KC number is in-between 1 and 12. Lastly, when KC number is larger than 12, both lee-wake vortex and horseshoe vortex forms simultaneously in the third region.

Flow and scouring processes around cylindrical structures are also studied with 3D numerical models, (e.g., Olsen and Melaaen 1993; Olsen and Kjellesvig 1998; Roulund et al. 2005; Göthel and Zielke 2007; Liu and Garcia 2008; Zhao and Cheng

2008; Zhao et al. 2010; Escauriaza and Sotiropoulos 2011a, 2011b; Baranya et al. 2012; Stahlmann and Schlurmann 2012; Stahlmann 2014; Jacobsen et al. 2014; Fuhrman et al. 2014; Baykal et al. 2015, 2017) studies can be given as examples for those. In the study of Roulund et al. (2005), they studied the flow conditions around a cylindrical structure that exposed to steady current for the equilibrium state. However, they couldn't take into account the lee-wake vortices because of the computational loads, and sediment transport is taken as bed load only. Stahlmann (2014) is the first study in which irregular flow regimes and suspended sediment transport is taken into account together with the free water surface under live bed conditions, and Stahlmann (2014) also developed the results that found in Roulund et al. (2005). Stahlmann (2014) studied not only scour around cylindrical piles numerically but also the numerical model is applied to the scouring problem around the foundation of the tripod type offshore turbine. The results of numerical models are presented in a comparative manner with laboratory and field measurements.

CHAPTER 3

NUMERICAL MODELING

Numerical simulations become inevitable with the development of computer technology. Due to the fact that physical model experiments are demanding and time consuming, researchers are eager to work with numerical models. However, numerical models also have some insufficiencies. For instance, numerical models need to be calibrated by experimental or site data. Another deficiency for numerical models is determining the adequate cell size in the computational domain. Since a model with coarse resolution may give inaccurate results or unnecessarily fine resolution may extend computational time. Therefore, creating a numerical model can be challenging too.

Nowadays, various types of open source or commercial software are available for Computational Fluid Dynamics (CFD) modeling. In this part of study, 2D and 3D hydrodynamic simulations carried out by using open source CFD software, OpenFOAM® (version 1.6-ext, 2010) are presented. Reynolds-averaged Navier-Stokes (RANS) equations are solved with finite volume methods in the model. In the OpenFOAM® software, there are already available solvers with various turbulence closure models for the solution of Navier-Stokes equations in different flow conditions such as steady/unsteady, laminar/turbulent.

3.1. Structure of the Numerical Model

3.1.1. Hydrodynamic and Turbulence Equations

The numerical model used in this study is a 3D computational fluid dynamics model coupled with a sediment transport, and morphology model. The RANS equations were solved in 3D with the k-omega turbulence model. Those equations are listed below.

$$\frac{\partial u_i}{\partial t} + u_j \frac{\partial u_i}{\partial x_j} = -\frac{1}{\rho}\frac{\partial p}{\partial x_i} + \frac{\partial}{\partial x_j}\left[2\nu S_{ij} + \frac{\tau_{ij}}{\rho}\right] \tag{3.1}$$

$$\frac{\partial u_i}{\partial x_i} = 0 \tag{3.2}$$

$$\frac{\partial k}{\partial t} + u_j \frac{\partial k}{\partial x_j} = \frac{\tau_{ij}}{\rho}\frac{\partial u_i}{\partial x_j} - \beta^* k\omega + \frac{\partial}{\partial x_j}\left[\left(\nu + \sigma^* \frac{k}{\omega}\right)\frac{\partial k}{\partial x_j}\right] \tag{3.3}$$

$$\frac{\partial \omega}{\partial t} + u_j \frac{\partial \omega}{\partial x_j} = \alpha \frac{\omega}{k}\frac{\tau_{ij}}{\rho}\frac{\partial u_i}{\partial x_j} - \beta\omega^2 + \frac{\sigma_d}{\omega}\frac{\partial k}{\partial x_j}\frac{\partial \omega}{\partial x_j} + \frac{\partial}{\partial x_j}\left[\left(\nu + \sigma \frac{k}{\omega}\right)\frac{\partial \omega}{\partial x_j}\right] \tag{3.4}$$

$$\sigma_d = \mathcal{H}\left\{\frac{\partial k}{\partial x_j}\frac{\partial \omega}{\partial x_j}\right\}\sigma_{d0} \tag{3.5}$$

$$f_\beta = \frac{1 + 85x_\omega}{1 + 100x_\omega} \tag{3.6}$$

$$x_\omega \equiv \left|\frac{\Omega_{ij}\Omega_{jk}S_{ki}}{(\beta^*\omega)^3}\right| \tag{3.7}$$

$$\Omega_{ij} = \frac{1}{2}\left(\frac{\partial u_i}{\partial x_j} - \frac{\partial u_j}{\partial x_i}\right) \tag{3.8}$$

$$S_{ij} = \frac{1}{2}\left(\frac{\partial u_i}{\partial x_j} + \frac{\partial u_j}{\partial x_i}\right) \tag{3.9}$$

$$\frac{\tau_{ij}}{\rho} = -\overline{u_i' u_j'} = 2\nu_T S_{ij} - \frac{2}{3}k\delta_{ij} \tag{3.10}$$

$$k = \frac{1}{2}\overline{u_i' u_i'} \tag{3.11}$$

$$\nu_T = \frac{k}{\tilde{\omega}} \tag{3.12}$$

$$\tilde{\omega} = max\left\{\omega, C_{lim}\sqrt{\frac{2S_{ij}S_{ij}}{\beta^*}}\right\} \tag{3.13}$$

In the above mentioned equations; u_i velocities, x_i Cartesian coordinates, t time, p pressure, ν kinematic viscosity, ν_T turbulent viscosity, ρ density of water, τ_{ij} Reynolds stress tensor, S_{ij} average expansion rate tensor, k density of turbulent kinetic energy, ω specific loss rate of turbulence kinetic energy, $H\{\cdot\}$ Heaviside step function, $\sigma_{d0}=1/8$, $\sigma=1/2$, $\sigma^*=3/5$, $\alpha=13/25$, $\beta^*=9/100$, $\beta=\beta_0 \cdot f_\beta$, $\beta_0=0.0708$, $C_{lim}=7/8$ as given in (Baykal et al. 2017).

3.1.2. Boundary Conditions

In order to reflect physical model realistically to the numerical model, boundary conditions of the model are assigned with considering Neumann conditions at symmetry faces, top, bottom, and outlet. At the bottom for 3D simulations as well as the structure for 2D simulations, a generalized wall function approach developed by Fuhrman et al. (2014) is used. However, velocities that are perpendicular to the symmetry faces were assumed to be zero. In order to drive the desired flow conditions, at the inlet boundary, below given boundary conditions taken from Fuhrman et al. (2014) are imposed:

$$u = U_m sin\left(\frac{2\pi}{T_w}t\right), \quad \nu = 0 \tag{3.14}$$

$$k = k_m \left[sin\left(\frac{2\pi}{T_w}t\right)\right]^2, \quad k_m = 0.0005{U_m}^2 \tag{3.15}$$

$$\omega = \omega_m \left|sin\left(\frac{2\pi}{T_w}t\right)\right|, \quad \omega_m = \frac{k_m}{100\nu} \tag{3.16}$$

in which U_m is the maximum horizontal velocity, T_w is the wave period, k_m is the maximum value of turbulence kinetic energy density, and finally, ω_w is the maximum value of the specific loss rate of turbulence kinetic energy.

In Figure 3.1, the unscaled schematic view of boundary conditions for numerical model can be seen.

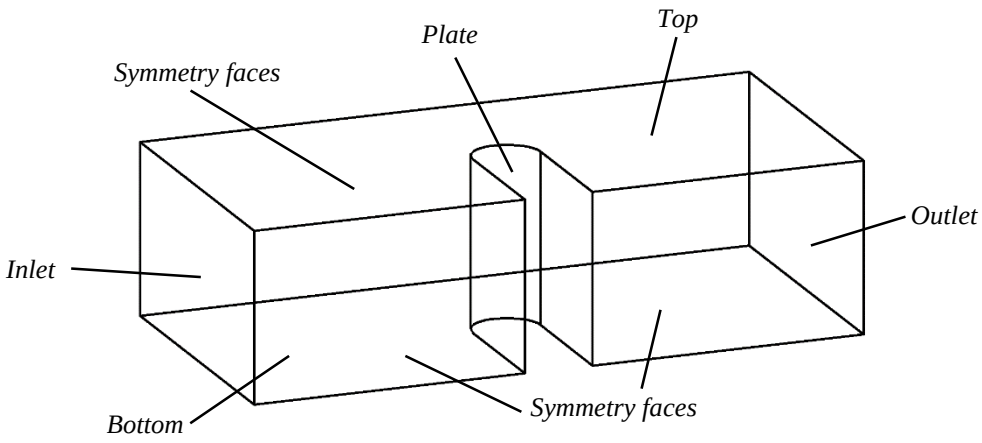

Figure 3.1. Boundary conditions of the computational domain

3.2. 2D Model Simulations

Numerical models divide into two categories in the scope of this study. First one is the 2D model to investigate hydrodynamic processes and secondly 3D model for observing vortex formation and measuring their dimensions. 2D models can be defined as spatial forms between two parallel planes with a relatively short distance from each other which is formed from one computational cell. Due to the very small distance between these two planes and the boundary conditions defined on the open surfaces of the numerical domain, a 2D model is obtained.

3.2.1. Computational Domains

The computational domain must be created first in order to give to OpenFOAM® software as an input. This computational domain is composed of blocks formed by line or arc fragments formed by spatial points. Each block consists 8 corner points and

is connected to other blocks with these vertices. As the blocks are brought together, the surface of each block is overlapped with the surface of another block. Boundary conditions should be assigned for determining how the flow will occur on open surfaces. Eventually, the numerical model is formed by putting together these blocks and defining certain boundary conditions.

While creating a numerical model with the above mentioned block structures, the shapes of these blocks are important such that the computational cells in these blocks need to be as rectangular as possible for structured computational domains. The block arrangement of the computational domain is given below with whole view and close detail in Figure 3.2 and Figure 3.3, respectively.

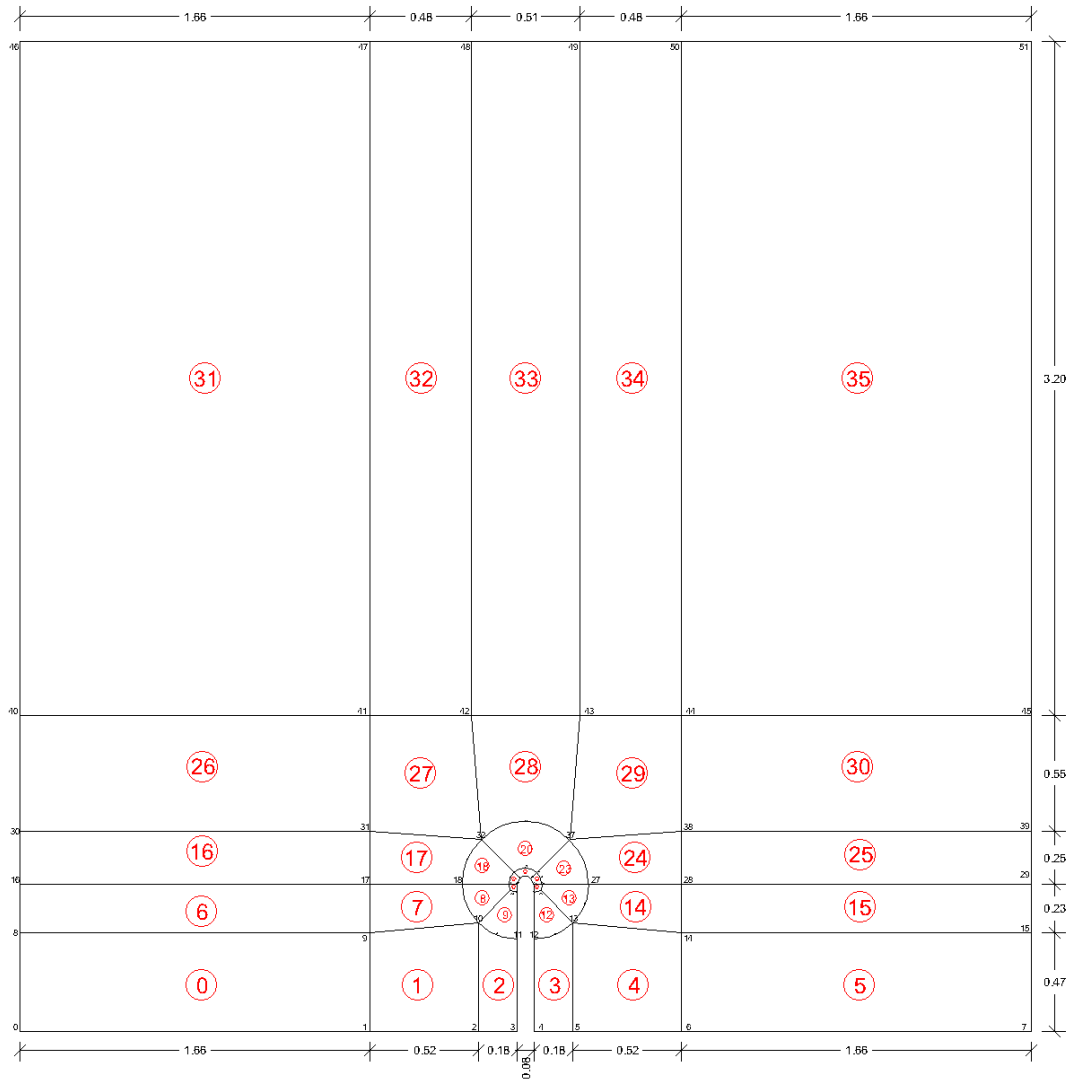

Figure 3.2. Whole view of the computational domain

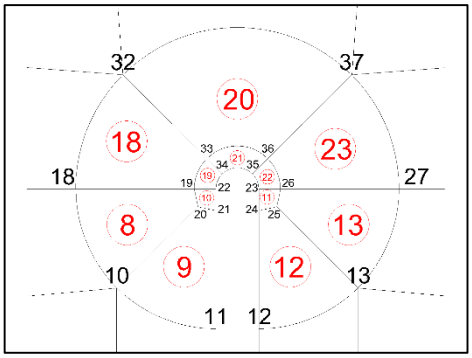

Figure 3.3. Close look around the head of the breakwater model in the computational domain

In Figure 3.2 and Figure 3.3, numbers that have black color indicate the vertices points and red colored numbers with circles mark the blocks.

In the scope of this numerical model works, 4 different cell sizes adjacent to the breakwater head chosen and computational domains created accordingly. Those are coarse mesh, medium mesh, fine mesh, and extra fine mesh. Those computational domains are prepared for the 60Bx60B dimensions. Cell sizes around the head of vertical wall are listed in dimensionless form in order to simplify the dimensions in Table 3.1.

Table 3.1. *Cell thickness of the computational domains adjacent to breakwater head*

	Cell thickness	
Mesh	Dimensionless	mm
Coarse	0.1B	8
Medium	0.05B	4
Fine	0.025B	2
Extra Fine	0.01B	0.8

The cell dimensions around the breakwater head have been kept smaller than the far-field cell dimensions in order to obtain more precise solution around the breakwater. The fact that the cell sizes that located far-field are larger than the ones around the breakwater head reduces the time required for the simulations to be completed.

Computational domains which have coarse and fine mesh are visualized by ParaView and are presented in Figure 3.4 and Figure 3.5, respectively.

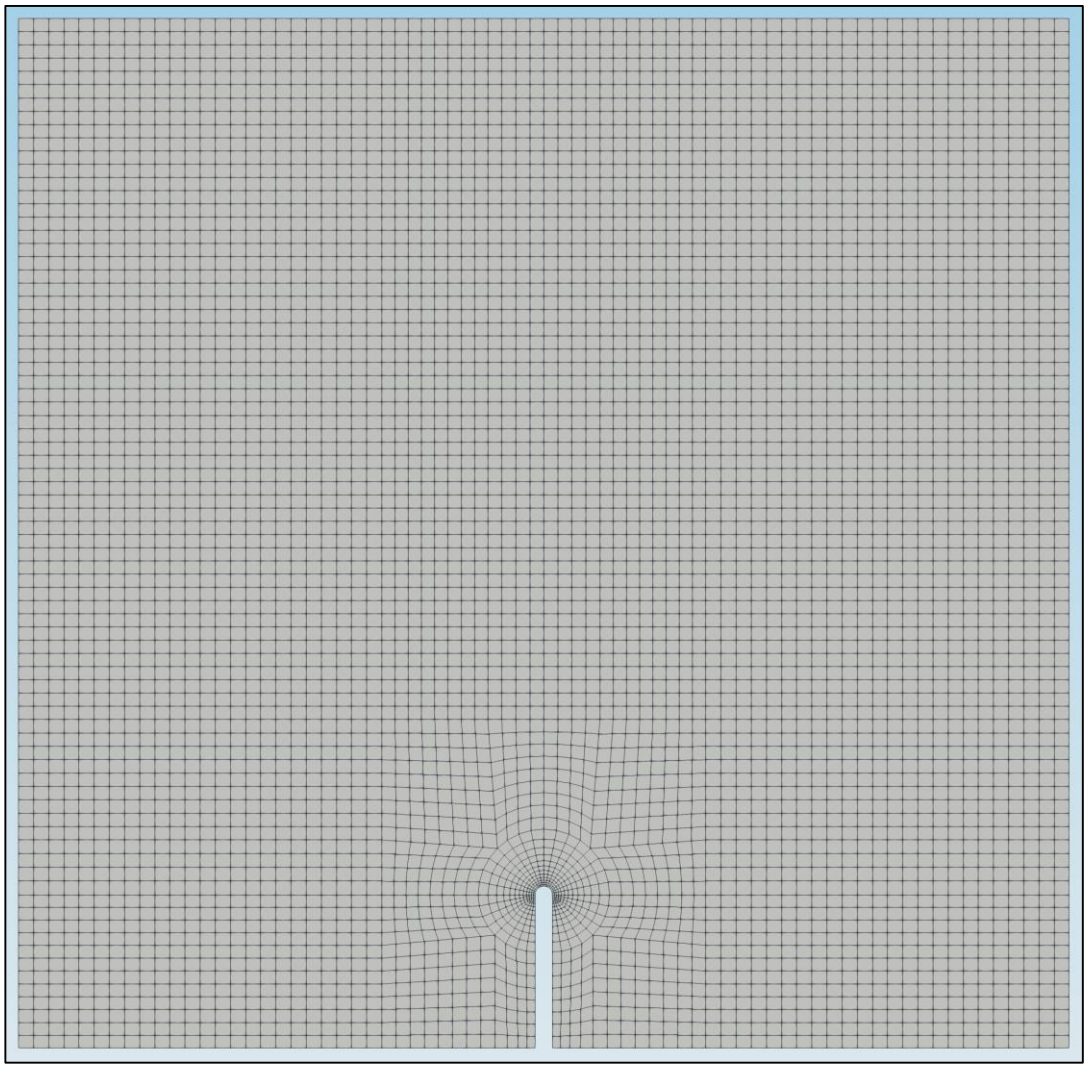

Figure 3.4. 60Bx60B model with coarse mesh

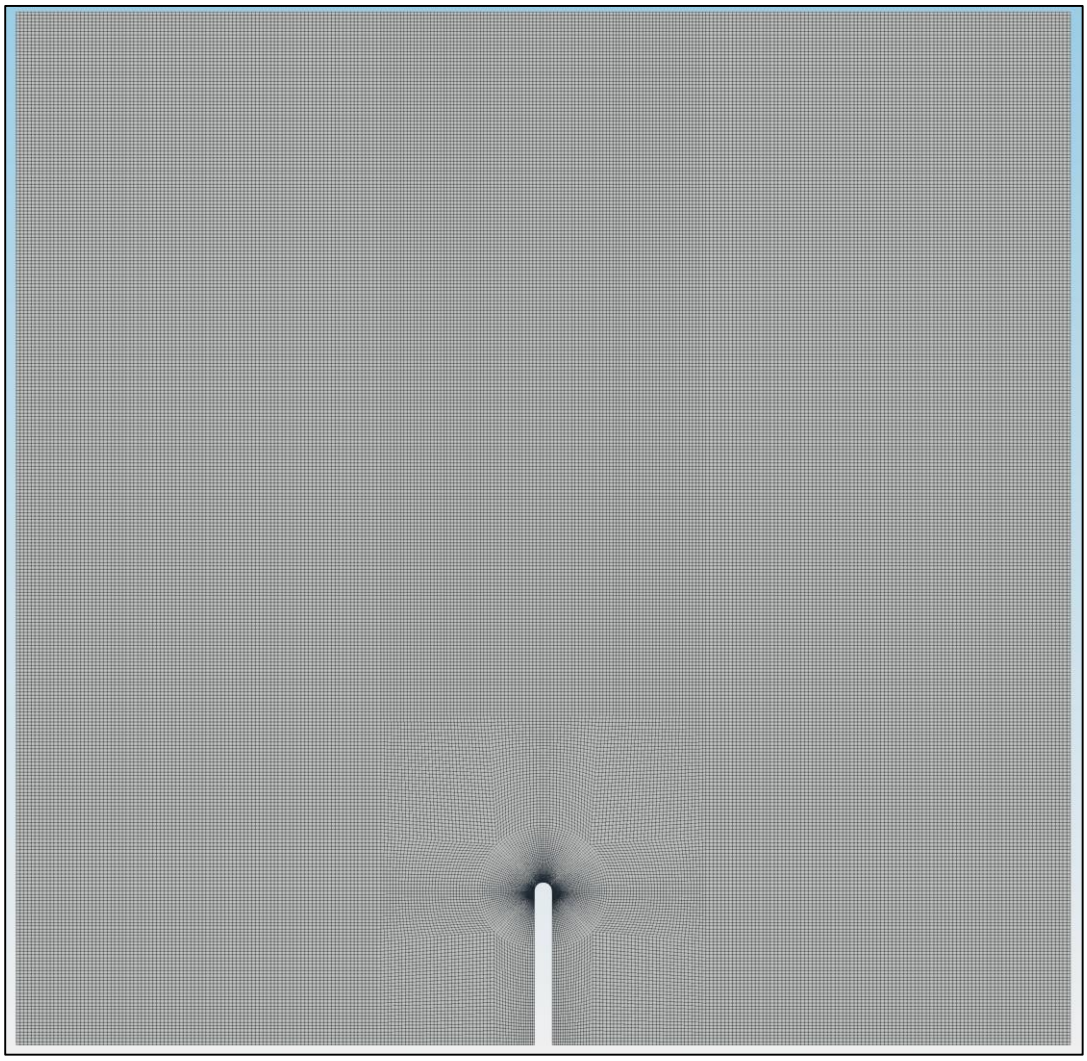

Figure 3.5. 60Bx60B model with fine mesh

In ParaView plug-in that comes with OpenFOAM® open-source software package, created numerical models can be visualized and it also provides convenience to end user with numerous tools (visualizing speed and pressure, measuring distances, creating animation, etc.).

When creating a numerical model, it is necessary to determine the dimensions of the computational domain first then boundary conditions must be defined. The center point (0.00, 0.00, 0.00) of the computational domain is accepted as the center of the semicircular arc that creates the head of the breakwater. The distance between inlet and outlet surfaces were kept constant as 60B for all models, and the breakwater model placed middle of this length. However, distance from symmetry faces needs to be determined carefully to reflect physical model to the numerical model properly. For this reason, 20B, 40B and 60B distances are chosen. 10B of those lengths is the length of the breakwater which means the clearance from tip of the structure head to the symmetry face is 10B, 30B and 50B, respectively. Finally, the thickness of all domains is selected as 1mm to ensure models act 2D. Below given Table 3.2 summarizes the selected dimensions of computational domains.

Table 3.2. *Dimensions of 2D models*

	Dimensions of Computational Domains		
	Length (B)	*Width (B)*	*Thickness (mm)*
60Bx20B	60	20	1
60Bx40B	60	40	1
60Bx60B	60	60	1

3.2.2. Flow Conditions

In this part of the study, 2 flow conditions with different KC numbers are considered. First one of these is the flow condition that is given in Sumer and Fredsøe (1997), KC=3.14. And the second one is the case that KC=1, which means stroke to diameter ratio is equal to 1. When KC=1, lee-wake vortices are not formed. In Table 3.3, flow conditions are listed according to mesh size for the 60Bx60B model.

Table 3.3. *Flow conditions for different meshes*

Breakwater Model			*Hydrodynamic Conditions*		
Computational Domain	*B (m)*	*Mesh*	U_m *(m/s)*	*T (s)*	*KC*
60Bx60B	0.08	Coarse	0.1257	2.0	3.14
60Bx60B	0.08	Medium	0.1257	2.0	3.14
60Bx60B	0.08	Fine	0.1257	2.0	3.14
60Bx60B	0.08	Extra Fine	0.1257	2.0	3.14
60Bx60B	0.08	Coarse	0.08	1.0	1.00
60Bx60B	0.08	Medium	0.08	1.0	1.00
60Bx60B	0.08	Fine	0.08	1.0	1.00

On the other hand, for the same mesh, which is medium mesh, different model dimensions, and corresponding flow conditions are given in Table 3.4.

Table 3.4. *Flow conditions for different computational domains*

Breakwater Model			*Hydrodynamic Conditions*		
Mesh	*B (m)*	*Computational Domain*	U_m *(m/s)*	*T (s)*	*KC*
Medium	0.08	60Bx20B	0.1257	2.0	3.14
Medium	0.08	60Bx40B	0.1257	2.0	3.14
Medium	0.08	60Bx60B	0.1257	2.0	3.14
Medium	0.08	60Bx20B	0.08	1.0	1.00
Medium	0.08	60Bx40B	0.08	1.0	1.00
Medium	0.08	60Bx60B	0.08	1.0	1.00

3.2.3. Results

Numerical simulations were carried out by the open-source CFD software OpenFOAM®, for the dimensions of the computational domain, mesh sizes, and KC numbers in Table 3.3 and Table 3.4. At the end of the simulations, velocities at the near field, far field, and dimensions of lee-wake vortices are compared. While reading those velocity values, ensemble average of the maximum values ($\omega t=\pi/2$) in a 20 period of time is used.

3.2.3.1. The Effect of Dimensions of Computational Domain

While determining the optimum dimensions of the computational domain, velocity distribution values are checked in 3 different domains which have same cell size adjacent to the vertical wall head. The ratio between velocity values in front of the structure to the far-field velocities are compared, and results are presented in Figure 3.6.

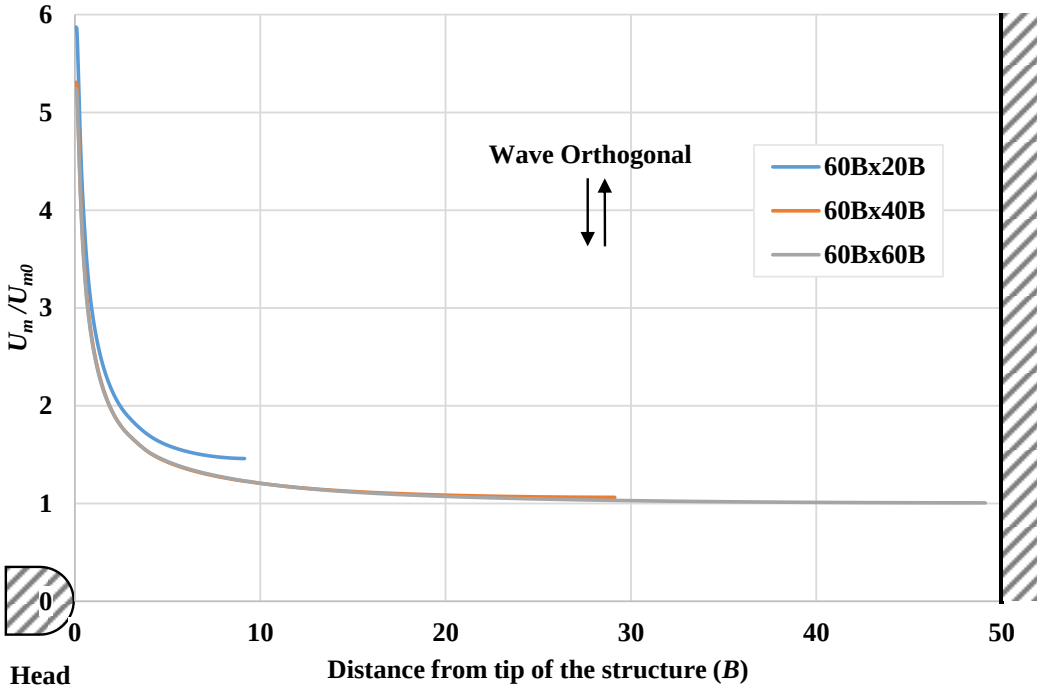

Figure 3.6. Velocity distributions for KC=3.14 with Medium Mesh

When the velocities of the water particles are examined for the 60Bx20B, 60Bx40B, 60Bx60B models, it is clear that 60Bx20B model is not sufficient for this study. When velocities in a line that perpendicular from the tip of the structure to the far-field are investigated, blockage effect disappear after 30B distance and velocities converge to the inlet velocities in that line.

In this case, 10B and 30B distance from tip of the structure to the wall is insufficient. Therefore, 60Bx60B domain which has 50B clearance becomes optimum domain size.

3.2.3.2. The Effect of Cell Thickness Adjacent to Breakwater Head

Determination of adequate cell size for a numerical model is important. Cell size affects the number of cells in a numerical model. However, when those meshes are compared in terms of computation time, the results will be exactly the opposite. Therefore, optimum cell size adjacent to the breakwater head must be determined in order to obtain precise results with a shorter time. Figure 3.7 presents the results of velocity distributions of different meshes that have same the dimensions which are 60Bx60B but different KC numbers.

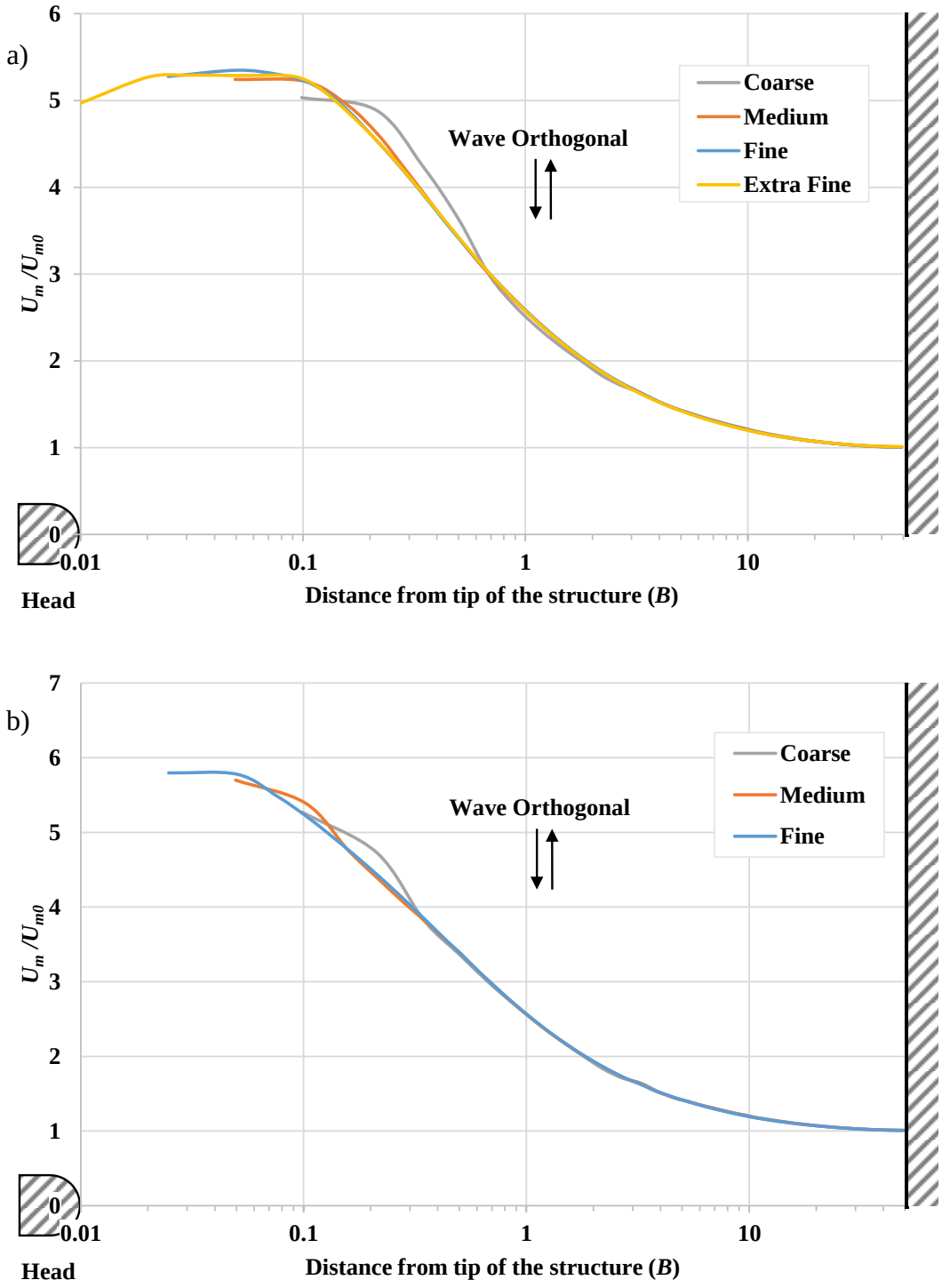

Figure 3.7. Velocity distributions for 60Bx60B computational domains a) KC=3.14, b) KC=1.0

For KC=3.14 case, it is obvious that coarse mesh and medium mesh are not sufficient. Hence, to ensure to keep computational time shorter, fine mesh is chosen for the further 3D simulations rather than extra fine mesh. On the other hand, when KC=1.0, three different models that have the same model dimensions give different results. But, as it's seen from Figure 3.7.b, only fine mesh works adequately for KC=1.0.

When the results of all coarse, medium, fine, extra fine models are compared, it's seen that coarse mesh and medium mesh are not adequate for proper simulations. However, there is no significant difference between the results of fine mesh and extra fine mesh. Thus, it can be said that the fine mesh is the optimum mesh for this study.

3.2.3.3. The Effect of Computational Domain on Vortex Formation

Lee-wake vortex dimensions are measured for both $\omega t=\pi/2$ and $\omega t=3\pi/4$. Schematic view of vortex formation is given below in Figure 3.8 and vortex that occurs in KC=3.14 case can be seen in Figure 3.9 for the 60Bx60B Extra Fine Mesh model.

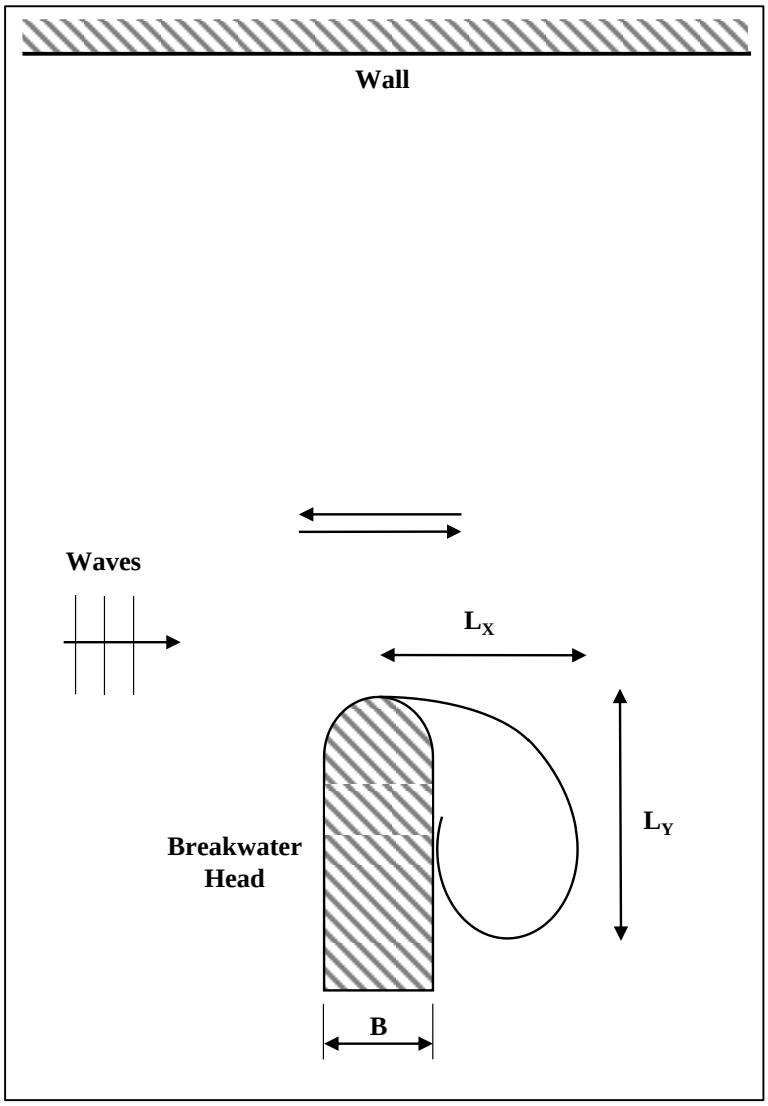

Figure 3.8. Schematic view of vortex dimensions

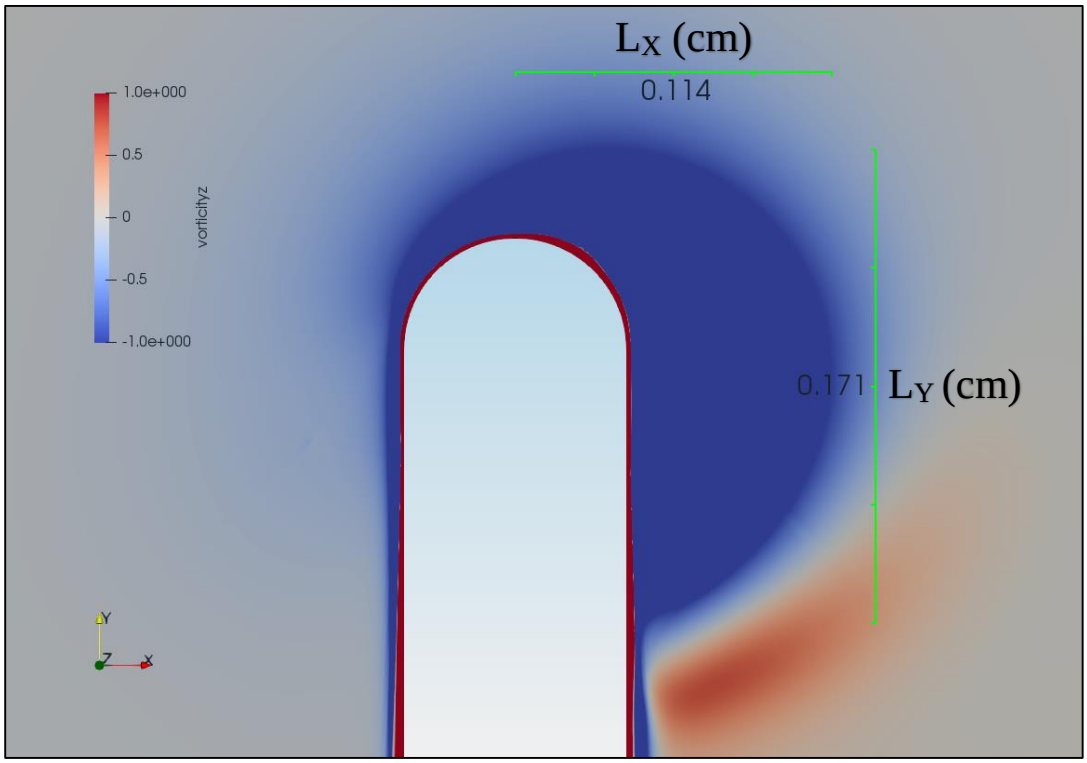

Figure 3.9. Vortex dimensions for KC=3.14 (60Bx60B – Extra Fine Mesh)

The vortex dimensions obtained from numerical studies for KC=3.14 case are listed below in Table 3.5.

Table 3.5. *Dimensions of the Lee-Wake Vortices*

Mesh	*B (m)*	*Model*	*Number of Cells*	L_X/B *(m)*	L_Y/B *(m)*
Medium	0.08	60Bx20B	8352	1.488	2.425
Medium	0.08	60Bx40B	16128	1.388	2.200
Coarse	0.08	60Bx60B	5904	1.625	2.538
Medium	0.08	60Bx60B	23616	1.388	2.250
Fine	0.08	60Bx60B	94464	1.375	2.038
Extra Fine	0.08	60Bx60B	590400	1.425	2.138

When the results of the numerical model simulations were examined and compared in between, it is seen that the ratio of vortex dimensions to the structure width, B, is similar for the all type of models for the same KC number except coarse mesh model. From this point of view, it is seen that the mesh type affects the results of numerical models. However, for the adequate meshes results are directly related to the KC number. Sumer and Fredsøe (1997) also correlated the dimensions of the lee-wake vortices with KC number in their study. It is realized that lee-wake vortices do not occur when the KC number is equal to 1, and this is consistent with Sumer and Fredsøe (1997) study.

3.3. 3D Simulations

In the scope of this study, to compare with 2D model simulations and physical model tests, 3D model simulations are performed as well. The width of the breakwater was kept constant at 8 cm to be the same as 2D simulations. There are two approaches to create 3D models. First one is increasing the thickness of the 2D model to a certain height and divide into desired cell size. So a simple 3D model is generated. Secondly, there is a truncated model that has three blocks in a row in vertical axis. These blocks have different thicknesses from each other. The bottom layer has a thickness of 3.5 times of median diameter of sediment. The middle layer has an exact thickness of sediment diameter. Finally, top layer has a thickness that complies the height of the 3D model to 2B distance. In this case, where d_{50}=0.21mm, the bottom, middle, top layers have thicknesses of 0.735 mm, 0.21 mm and 159.055 mm, respectively. The truncated mesh has exactly the same dimensions as the simple 3D mesh. It is designed for morphological simulations where the suspended sediment transport computations are carried out above 3.5 times the median grain diameter (d_{50}) away from the bottom of the domain to the top boundary. Below $3.5xd_{50}$, sediment transport is considered as bed load and therefore not modeled (e.g., Jacobsen et al. 2014; Baykal et al. 2017). Truncated 3D mesh view can be seen in Figure 3.10 below.

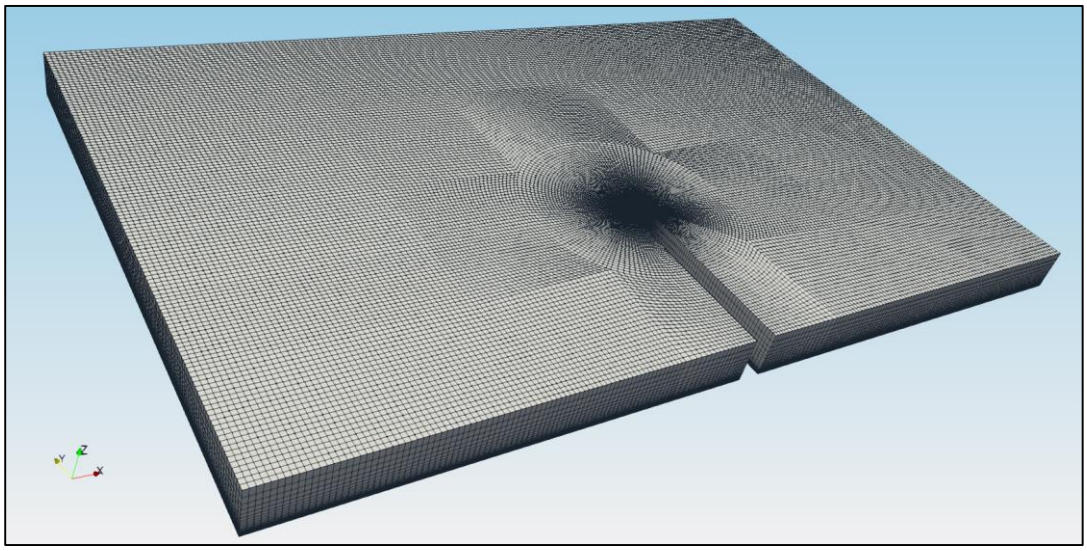

Figure 3.10. Truncated 3D mesh

Created two different 3D models run by OpenFOAM® and visualized via ParaView software. In Figure 3.11 and Figure 3.12 truncated and simple 3D models, vortex formations, and dimensions are given. Vortices visualized in $\omega t=\pi/2$ phase and visualized vortex dimensions measured at a distance of 5 cm from bottom of the models for each simulation. 5 cm distance is chosen to make convenient comparison with physical model experiments. The difference between simple and truncated model simulations appears when the vortices visualized with vorticity in (vorticity z) vertical axis.

a)

b)

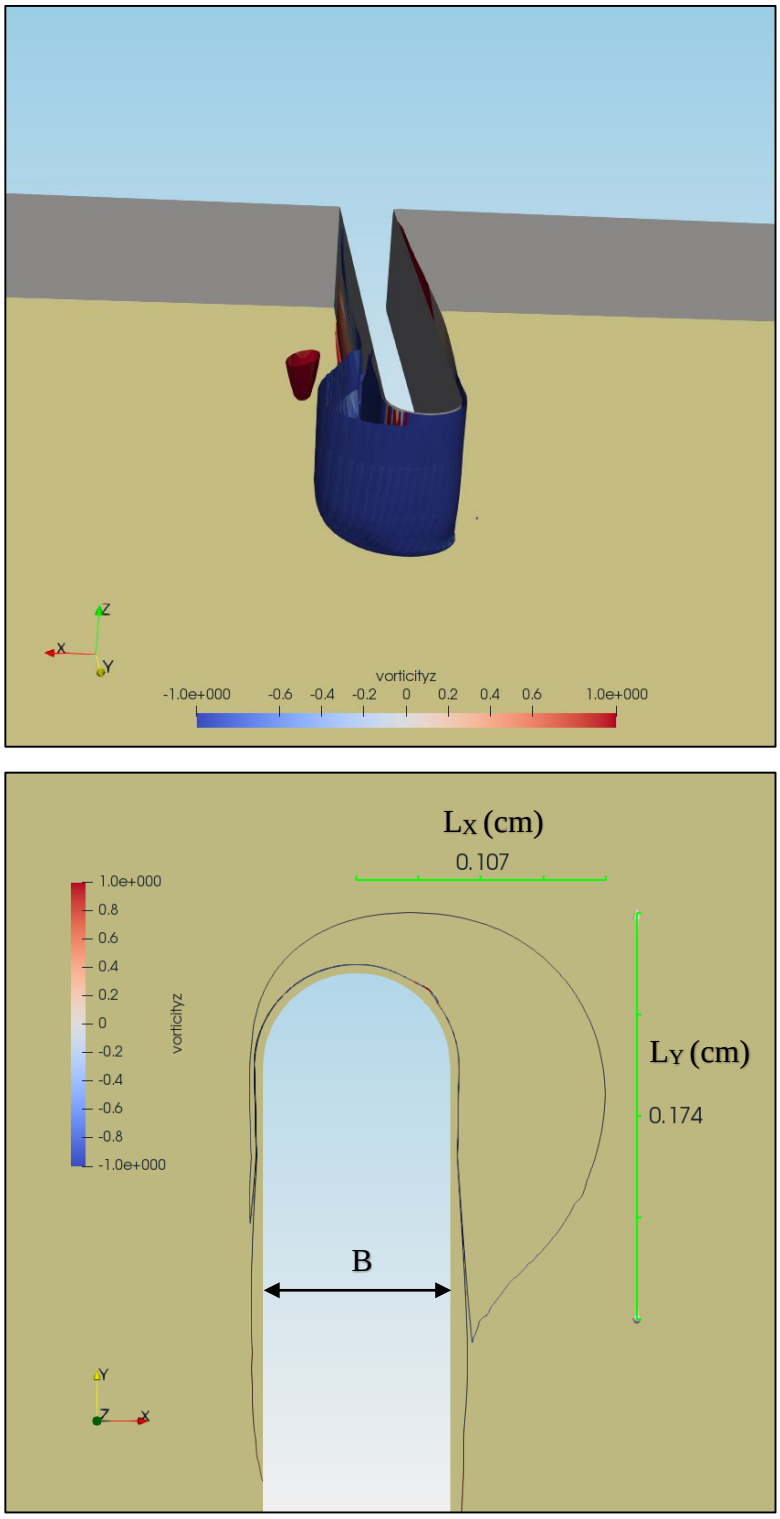

Figure 3.11. a) Vortex formation on truncated 3D model, b) vortex dimensions of truncated 3D model

a)

b)

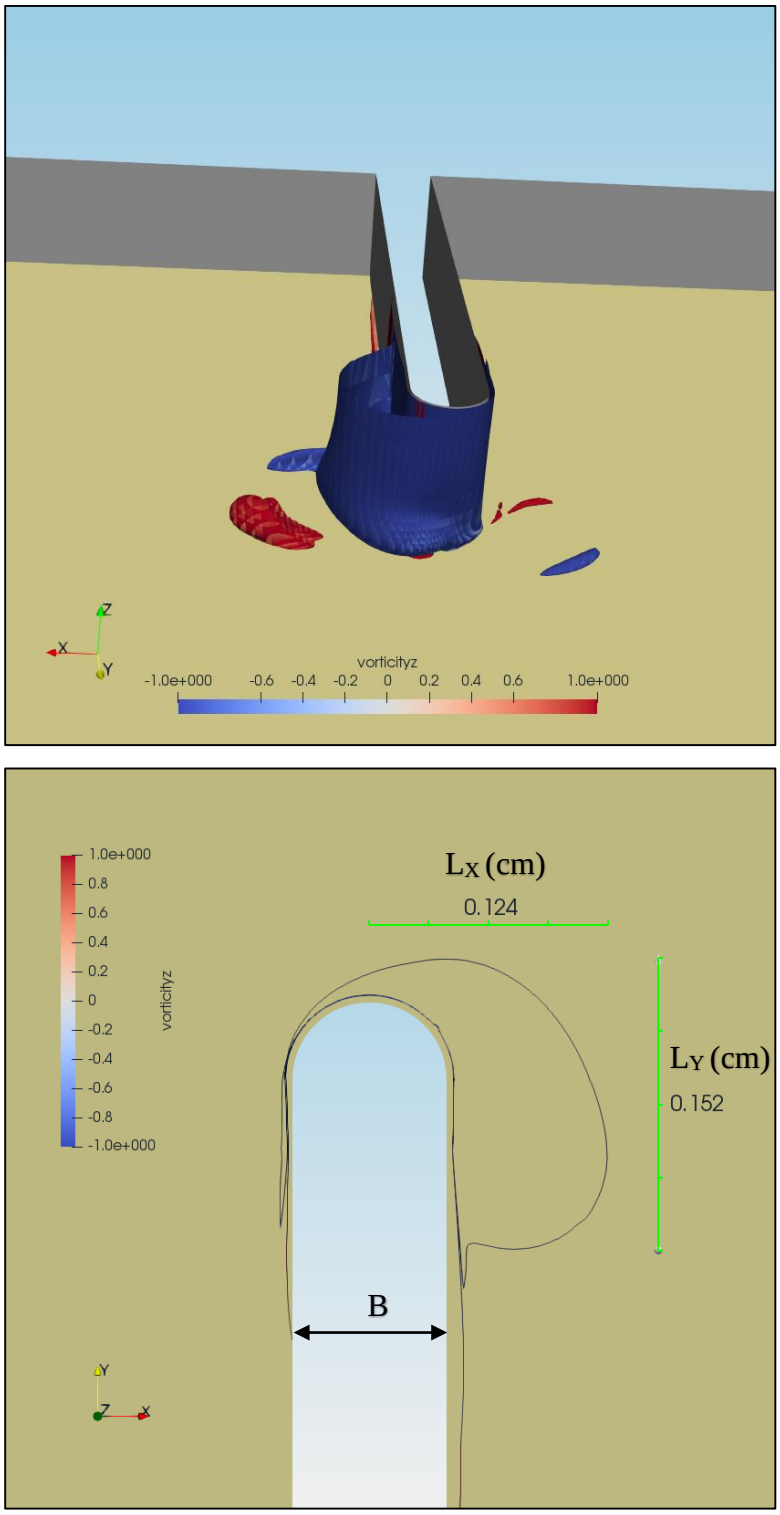

Figure 3.12. a) Vortex formation on simple 3D model, b) vortex dimensions of simple 3D model

Vortex dimensions obtained from 3D model runs with phase angle $\omega t=\pi/2$ are listed below in Table 3.6.

Table 3.6. *Lee-Wake Vortex dimensions of 3D models*

Mesh	*Model*	*Number of Cells*	L_X/B *(m)*	L_Y/B *(m)*
Fine	60Bx60B Truncated 3D	1700352	1.338	2.175
Fine	60Bx60B Simple 3D	2267136	1.550	1.900

Beside 2D Fine Mesh vortex dimensions, above given vortex dimensions obtained from 3D simulations are also presented in Flow Visualization topic in Chapter 4 with the results of Sumer and Fredsøe (1997) study. Thus, numerical and physical model results will be compared.

CHAPTER 4

PHYSICAL MODELING

In coastal engineering, hydraulic models play serious roles while designing and developing a coastal structure. Hughes (1993) defines the physical model as a small scaled reproduced system; hence, main forces affecting the system are stimulated in the model in the correct ratio to the real physical system.

Physical models have their advantages and disadvantages related to the modeling conditions and laboratory circumstances. Dalrymple (1989) indicates that data collection from a small size model reduces the cost while collecting data from prototype is more expensive and demanding. The equations of the governing processes without the assumptions in numerical models are derived from physical model experiments (Dalrymple 1989). Kamphuis (1991), states that observation of a physical model while performing it supports the understanding of the physical phenomenon. Physical model experiments are cost-effective when the size of coastal projects are considered, and physical model tests increase reliability in the design process (Le Mehaute 1990). With the developing technology, physical relations will be understood better; and by the physical models, engineers develop genuine solutions to problems (Le Mehaute 1990). Le Mehaute (1990) also indicates the controlled environment provides to check and measure parameters. However, physical models are expensive than numerical simulations (Hughes 1993). It may be impossible to reflect all forces, like wind force, to the model in the physical models (Hughes 1993). On the other hand, it is not possible to simulate actual processes in the laboratory, and physical models might be affected by laboratory effects (Hughes 1993). Le Mehaute (1990) states that scale effect may occur due to incorrect relations of the relevant parameters.

4.1. Experimental Setup

Physical model experiments are performed in a wave flume of Coastal and Harbor Laboratory of Civil Engineering Department, Middle East Technical University. It has 26 m length, 6.2 m width and 1 m depth. It is also equipped with piston-type random wave generator (Figure 4.1) and a passive wave absorption system.

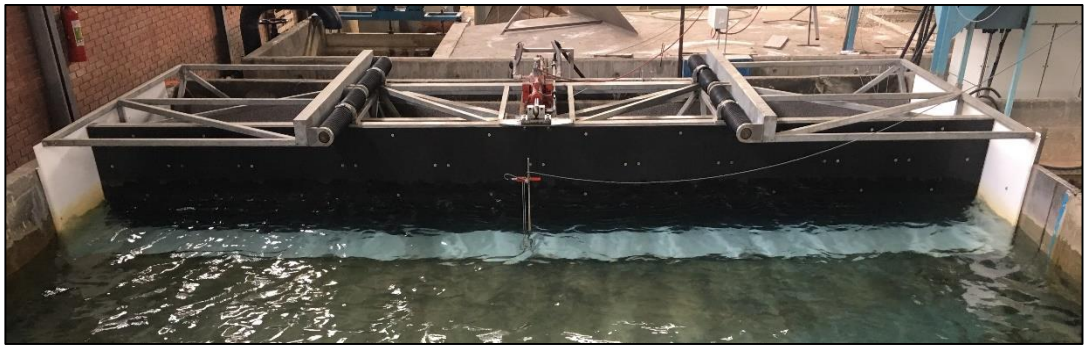

Figure 4.1. Piston-type wave generator

Although it is 6.2 m wide, experiments are performed in a 1.5 m wide inner flume which divided with glass walls. As mentioned before, this wave flume has piston-type wave generator on one end, and there are wave absorbers at the other end. In Figure 4.2, passive wave absorbers and inner flume that are made by glass panels are given.

Figure 4.2. General view of wave flume

In Figure 4.3, the unscaled drawing of experimental setup is presented.

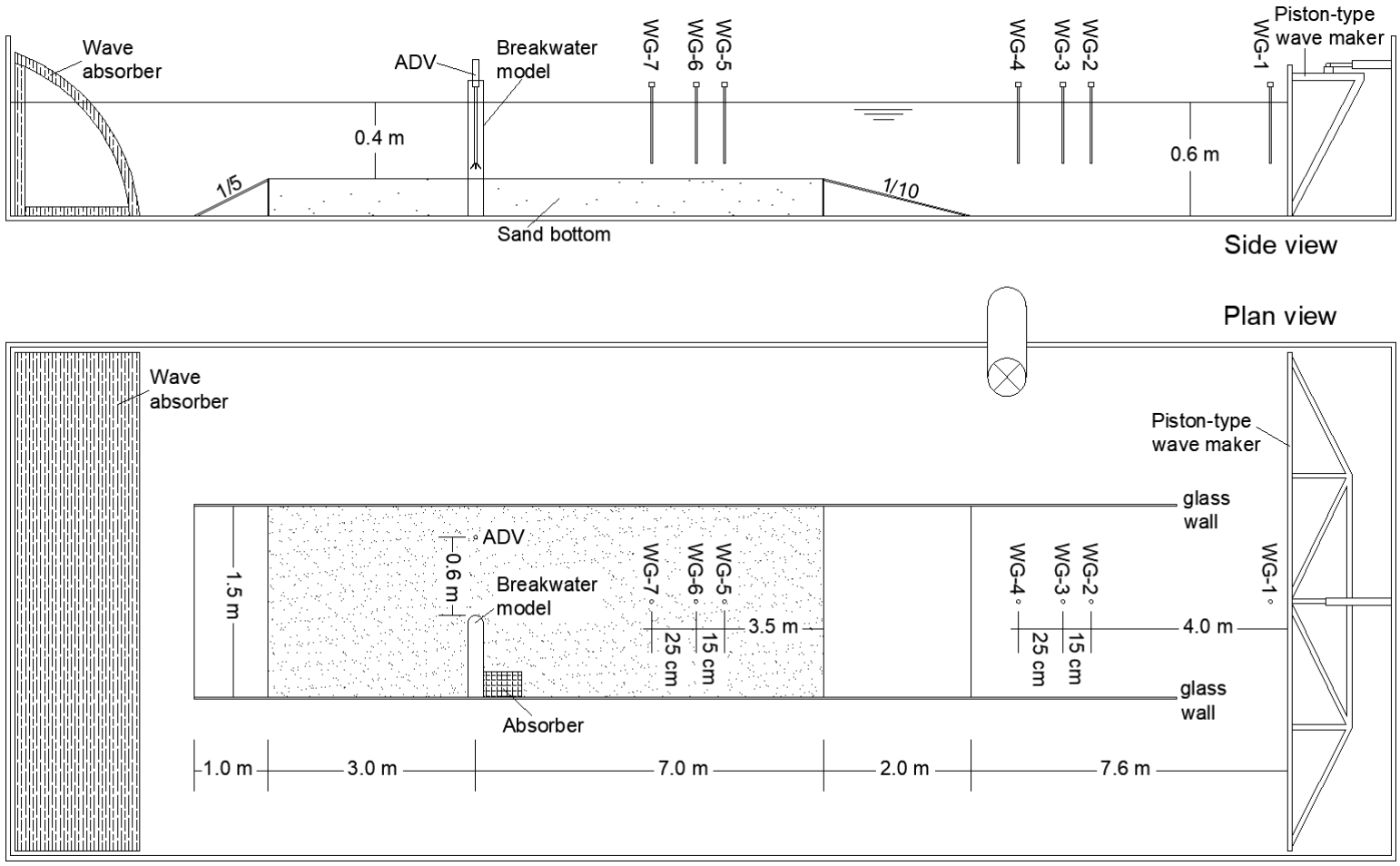

Figure 4.3. Unscaled drawing of the experimental setup

As seen from Figure 4.3, 1/10 inlet slope and 1/5 outlet slope are constructed at the two ends of 10 m long sediment pit. Before scour experiments, the plain fixed bottom is constructed in between those slopes for wave calibration and hydrodynamic experiments and flow visualization experiments. Breakwater models are made from transparent acrylic material, and they are 6 cm wide and 9B long which is 54 cm. Additionally, breakwater models emerge in all experiments. The clearance between breakwater model and glass wall is 96 cm which is 16B.

In scour experiments, to prevent scouring at the seaward face of the breakwater due to focusing waves at the corner, a wave absorber is placed. This porous wave absorber is 17 cm wide, 40 cm long and has 80 cm height. The main reason to build this absorber is to prevent scouring where breakwater model and glass wall meets. The mentioned absorber is given in Figure 4.4.

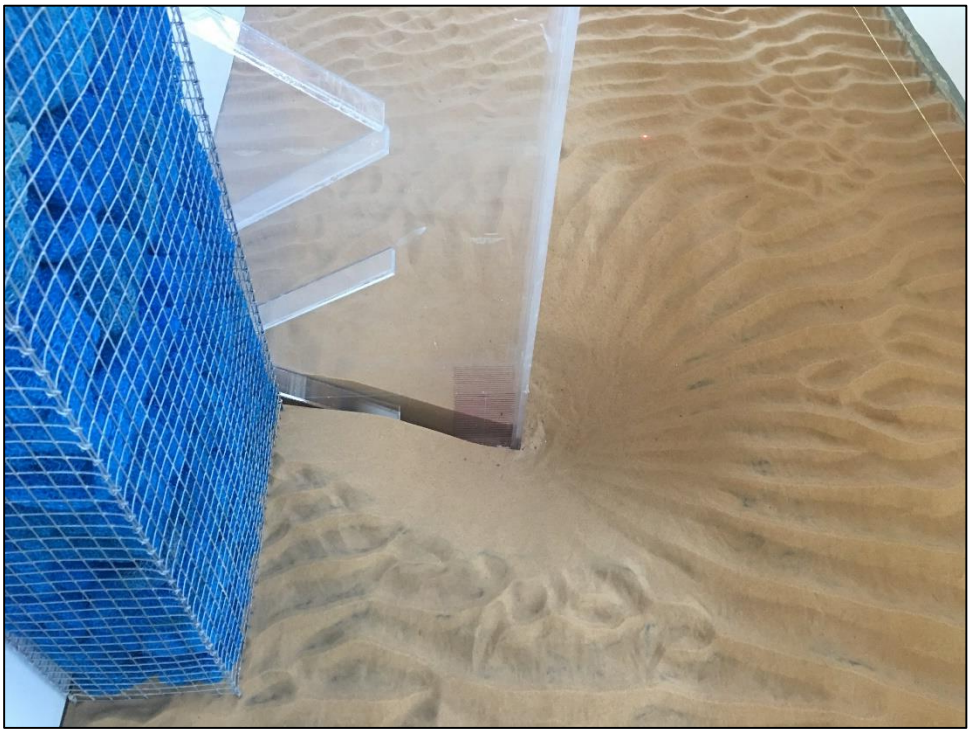

Figure 4.4. Porous wave absorber and sharp-edged breakwater model

In physical model experiments, to record the wave heights and periods, DHI 202-60 wave gauges are used. The sampling frequency of wave gauges is kept constant as 20 Hz for random and regular waves. But, it is increased to 40 Hz for the solitary waves. Nortek Group Vectrino Acoustic Doppler Velocimeter (ADV) is used to record velocity of water particles to calculate KC number of oscillating flow. ADV measurements are recorded with 200 Hz sampling frequency, and it is mounted 5 cm from the bottom of the bed for both movable bed and fixed bottom. While performing wave calibration tests, ADV measurements are performed where the breakwater model will be placed. Since there are fluctuations in the ADV measurements, filter applied to the horizontal velocity measurements.

A semi-automatic laser bed scanner is used to obtain bottom evolution. The laser scanner is a laser distance meter mounted to an aluminum frame structure and is capable of scanning 1.5 m x 3.0 m area in desired resolution in both axes and equipped with Banner® LTF24IC2LDQ Laser Diffuse Time-of-Flight Sensor. Vertical measurement accuracy of the laser bed scanner is 0.3 mm, and horizontal positioning accuracy is below 1.0 mm. Difference between scanned initial and final states gives the relative bottom change. For the most experiments areal bottom changes were scanned. However, few cases scanned at X and Y axis which are flow direction and transverse direction, respectively. Three profile measurements are performed for both axes, and those profiles have 0.5B=3 cm distance in between. For instance, profiles that are obtained in X axis measured right in front of the breakwater model. Secondly, Y axis measurements are performed leeward and seaward sides with the middle of the breakwater head. In Figure 4.5, semi-automatic laser bed scanner and experimental setup for round head structure are shown with ADV mounted at 10B distance in front of structure head.

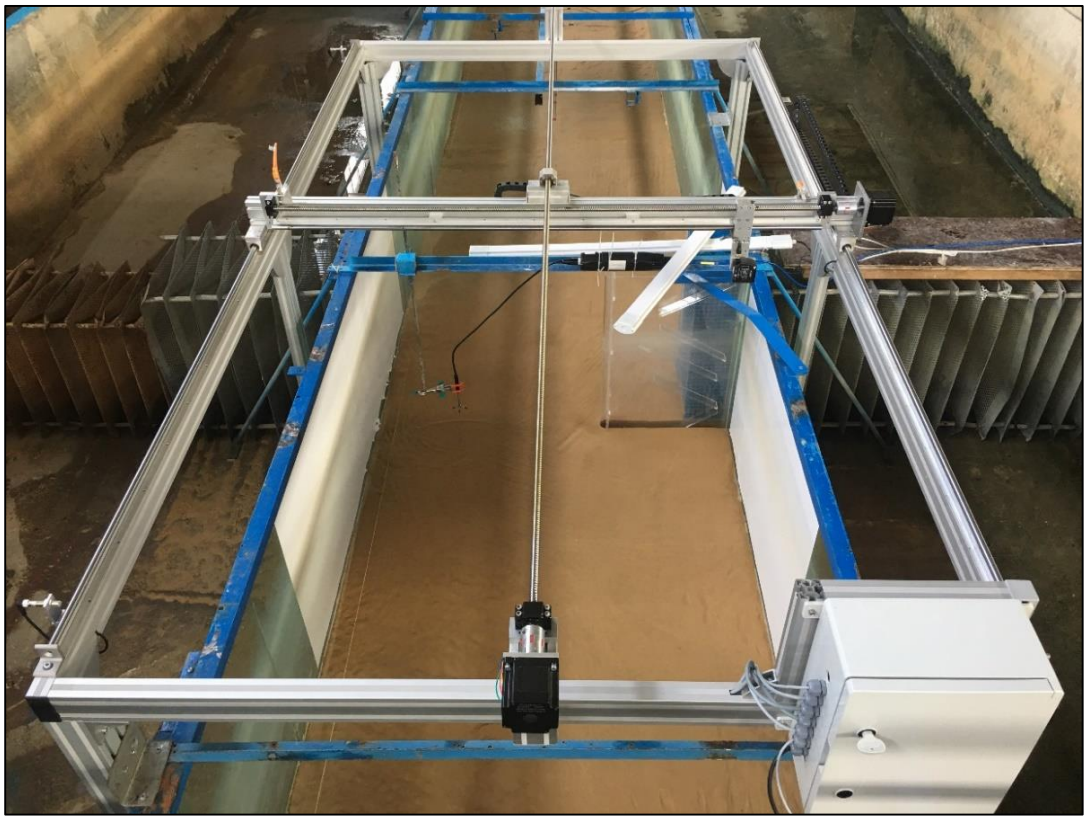

Figure 4.5. Experimental setup with semi-automatic laser bed scanner

4.2. Methodology

Surface tension forces and viscosity are not usually serious parameters in coastal engineering problems since the gravitational forces and inertia are the governing parameters. Therefore, Hughes (1993) indicates that Froude Law is often applied to physical models in coastal engineering. Froude number of the model (m) and the Froude number of the prototype (p) must be equal according to Froude Law. Froude number can be calculated with below given equation.

$$F_r = \sqrt{\frac{u^2}{gl}} \tag{4.1}$$

u represents the particle velocity of water, l is the characteristic length (diameter, depth, width, etc.) and g is the gravitational acceleration, in equation (4.1).

Froude similarity between prototype and model is given in equation (4.2).

$$(F_r)_p = (F_r)_m \tag{4.2}$$

The ratio between model and prototype in terms of length scale, and time scale are given in equation (4.3) and (4.4), respectively.

$$\lambda_L = \frac{L_m}{L_p} \tag{4.3}$$

$$\lambda_t = \sqrt{\lambda_L} \tag{4.4}$$

In the above given equations, λ_L is the length scale, λ_t is the time scale and L_m and L_p indicate the model length and prototype length, respectively.

The governing parameter of this study is the dimensionless KC number that may be described as a stroke to width ratio. It is easy to determine the KC number for the regular waves which have the same wavelength and wave height for each wave. However, when random waves are considered, wave analysis must be done carefully. KC number for random oscillatory flow can be calculated by below given equations (4.5) and (4.6).

$$KC_r = \frac{\left(\sqrt{2}\sigma_U\right)T_z}{B} = \frac{U_{m,r}.T_z}{B} \tag{4.5}$$

$$\sigma_U = U_{rms} = \sqrt{m_{0U}} \tag{4.6}$$

In above given equations, *Tz* represents mean value of zero-up crossing period of wave series, σ_U is the root mean square of the measured flow velocity. Finally, m_0 is the zeroth spectral moment of the measured flow velocity (Sumer and Fredsøe 2006).

The results of performed experiments are presented in non-dimensional scale. In order to do that, scour depth was non-dimensionalized with the structure width *B*. However, to present time dimensionless, equation (4.7) is used.

$$t^* = \frac{\sqrt{g(s-1){d_{50}}^3}}{B^2} t \tag{4.7}$$

In the above given equation; g is the gravitational acceleration which is g = 9.81 m/s^2 and s = 2.65, is the relative density of the sediment, d_{50} is the sediment diameter in meters, B is the width of the structure in meters, and finally, t is time in seconds (Fuhrman et al. 2014). By calculating the above equation, dimensionless time coefficient *t*/t=0.003401* can be found.

The time scale of scour processes is also an important parameter. Time scale represents the time that passes from starting of scour processes to the significant scour occurs.

$$T^* = \int_0^{t^*_{max}} \frac{S_{max} - S}{S_{max}} dt^* \tag{4.8}$$

In equation (4.8), T^* is time scale of scour process, S_{max} is the equilibrium scour, S is the scour that occurs in a certain time, t^* is dimensionless time and finally, t^*_{max} time that passes for the equilibrium scour occurs.

4.3. Wave Conditions

Three different types of waves are used in the scope of this study. Those waves are regular waves, random waves, and solitary waves. At the beginning of the experimental study, those waves need to be determined and generated their time series. In order to select appropriate wave, firstly, plain fixed bottom was constructed into the inner flume. At the beginning of the study, regular waves are used to make comparison with the study of Sumer and Fredsøe (1997) and properties of regular waves that are used in this part of the study are given below in Table 4.1.

Table 4.1. *Properties of the Regular Waves*

	H (m)	*T (s)*	*H/L*	U_m *(m/s)*	T_U *(s)*	*KC*
reg-1	0.063	1.047	0.040	0.076	1.059	1.333
reg-2	0.096	1.423	0.039	0.131	1.431	3.135
reg-3	0.128	1.796	0.039	0.178	1.798	5.337
reg-4	0.106	1.615	0.037	0.188	1.603	5.019

In order to make a reliable comparison between scour depths and wave characteristics, three different random waves are selected for corresponding KC numbers in the order of 1, 3, and 5. Those three waves have approximately the same wave steepness which is 0.04. However, steepness effect is also considered in this project. While KC is around 5.5, 3 different random waves determined with the steepness values of 0.03, 0.02 and 0.01, respectively. Random waves that are used in this study are listed in Table 4.2 below.

Table 4.2. *Properties of the Random Waves*

	H_m *(m)*	H_s *(m)*	T_p *(s)*	H_s/L_s	K_r	$U_{m,r}$	T_{mU} *(s)*	*KC*
rand-1	0.046	0.074	1.210	0.04	0.191	0.075	1.212	1.510
rand-2	0.066	0.106	1.661	0.04	0.202	0.139	1.553	3.608
rand-3	0.081	0.131	2.015	0.04	0.209	0.179	1.828	5.443
rand-4	0.064	0.107	2.478	0.03	0.271	0.164	2.047	5.610
rand-5	0.058	0.101	3.025	0.02	0.252	0.143	2.345	5.571
rand-6	0.038	0.068	2.388	0.01	0.419	0.113	2.929	5.500

In the above Table 4.2, H_m is mean wave height, H_s is the significant wave height, T_p is peak wave period, K_r is reflection coefficient of wave flume and corresponding KC numbers are calculated with the structure width B=0.06 m, and water depth is constant for all cases, h=0.4 m. This structure width and water depth are kept the same for both

random and regular waves. Reflection coefficient K_r values are calculated by using Goda and Suzuki (1976) approach.

When rand-4, rand-5, and rand-6 waves are considered, they have similar KC numbers. These waves are selected in order to compare their equilibrium scour depths since they have different steepness values. On the other hand, there are differences between wave periods and T_{mU} (mean period of oscillating flow), this gap caused because these waves are rather long and also consisting capillary waves. While recording these waves, wave gauges also recorded the capillary waves at water surface.

Besides random and regular waves, solitary waves were used as well in the physical model experiments. Solitary waves are generated in 3 different water depths which are 0.4 m, 0.3 m, and 0.2 m. There are also three different wave heights in each water depth which means nine individual solitary waves are used in this study. Furthermore, 3 of those waves have approximately the same wave height with different water depth. In this way, water depth effect can be examined for the same wave height. Unlike regular and random waves, period of a solitary wave converges to infinity. Hence, there is a necessity to define wave properties dimensionless because their KC number goes to infinity. Solitary wave properties are given below in Table 4.3.

Table 4.3. *Properties of the Solitary Waves*

	h (m)	*H (m)*	*h/B*	*H/B*	U_m *(m/s)*
sol-40-1	0.40	0.075	6.667	1.256	0.372
sol-40-2	0.40	0.054	6.667	0.892	0.270
sol-40-3	0.40	0.033	6.667	0.551	0.184
sol-30-1	0.30	0.093	5.000	1.544	0.434
sol-30-2	0.30	0.076	5.000	1.265	0.395
sol-30-3	0.30	0.056	5.000	0.928	0.288
sol-20-1	0.20	0.115	3.333	1.920	0.614
sol-20-2	0.20	0.096	3.333	1.602	0.540
sol-20-3	0.20	0.076	3.333	1.273	0.469

In Table 4.3, h is water depth, H is wave height, and U_m is the maximum horizontal velocity of the water particles. Above mentioned random, regular and solitary waves' properties are obtained in a state with plain fixed bottom and without structure in the flume. Random and regular waves' time series consists of 1000 individual waves.

4.4. Hydrodynamic Tests

In these tests, first, the blockage effect was investigated. It affects the flow regime at the head of structure. If there is a blockage effect, it means flume width is insufficient. Hence, distance between glass walls may have to be enlarged. In order to inspect whether blockage effect exists or not, transverse velocity distribution measurements have been done. Afterward, flow visualization experiments are performed in order to investigate the vortices occurring around the structure.

4.4.1. Transverse Velocity Distribution Measurements

To see if the flume width has adequate clearance, velocity measurements have been carried out in front of the breakwater head. Those measurements are performed with an ADV at certain distances from breakwater head to the glass wall in the transverse direction and are compared with undisturbed velocities of each wave conditions. ADV measurements are performed at a 5cm distance from the bottom for all cases. Velocity distribution between the head of the breakwater and glass wall is given in Figure 4.6 for regular, in Figure 4.7 for random waves and in Figure 4.8 for solitary waves.

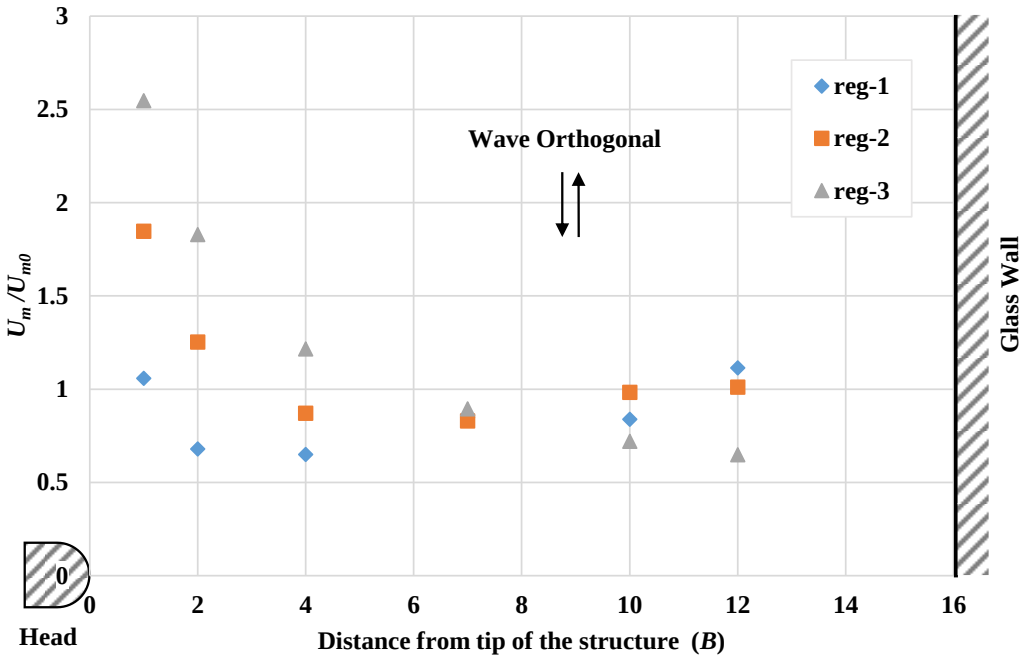

Figure 4.6. Velocity distribution for regular waves

Figure 4.6 indicates that for the reg-1 wave which has KC in the order of O(1), the blockage effect is almost not existed. However, for the reg-2 (KC=3.135) and reg-3 (KC=5.337), maximum horizontal velocities are 1.85 and 2.55 times higher at the 1B distance in front of the structure, respectively. In addition to that, when numerical and physical model results are compared with each other in terms of velocity distributions in transverse axis, horizontal velocities converge to undisturbed velocities on a shorter distance in physical model tests than numerical models. When Figure 3.7 and Figure 4.6 are compared with each other this difference is understood.

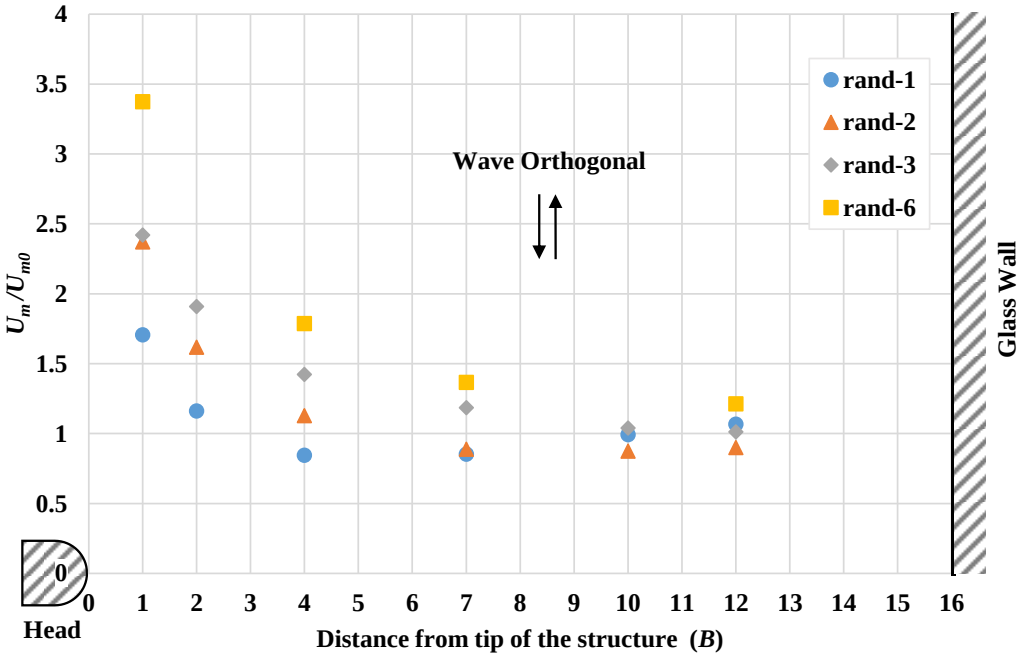

Figure 4.7. Velocity distribution for random waves

For the examined random waves, the ratio between maximum horizontal velocities and undisturbed velocities tend to approach to 1 at 10B distance from breakwater head.

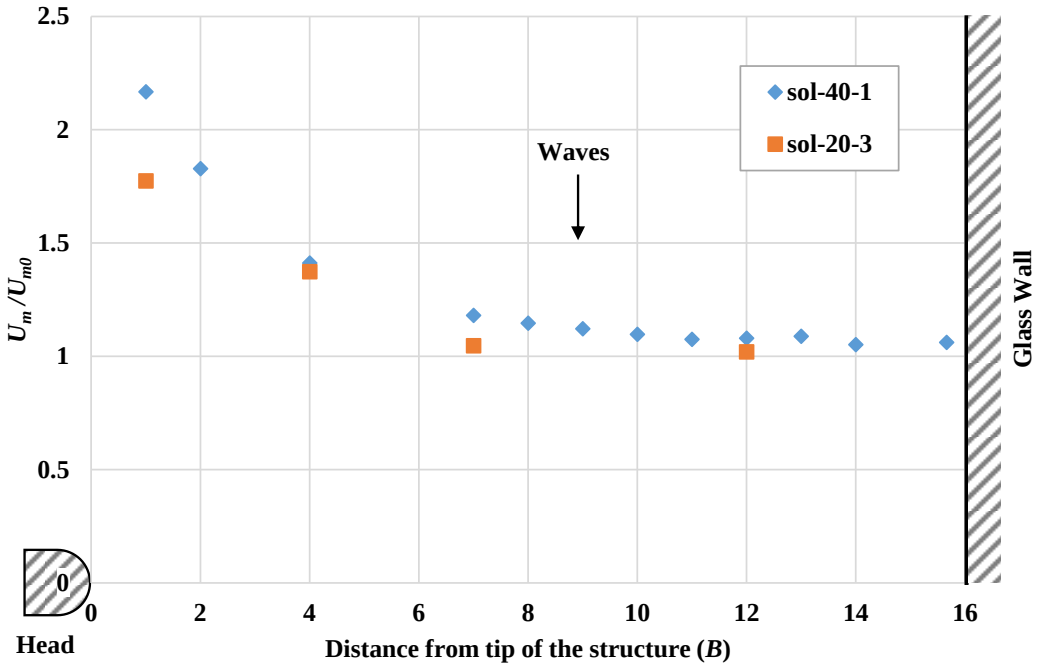

Figure 4.8. Velocity distribution for solitary waves

As seen from Figure 4.6, Figure 4.7, and Figure 4.8, the blockage effect does not exist after 10B distance from breakwater head. Hence, the flume width of 1.5 m was found to be adequate.

4.4.2. Flow Visualization Tests

In the scope of this study, flow visualization experiments are performed for two types of structures which are round head and sharp-edged head structures. Vortex formation is recorded via underwater cameras for three different regular waves and seven different solitary waves. Each experiment was performed at least three times to obtain consistent results. These experiments are performed with bright colored dye that solves in water. The dye injected with a silicon hose to the flow right before the passage of crest of a wave spreads around the structure, and the diffusion of dye is

recorded. To measure distance at the bottom of the flume, 2 cm x 2 cm grid is applied to the bottom (Figure 4.9).

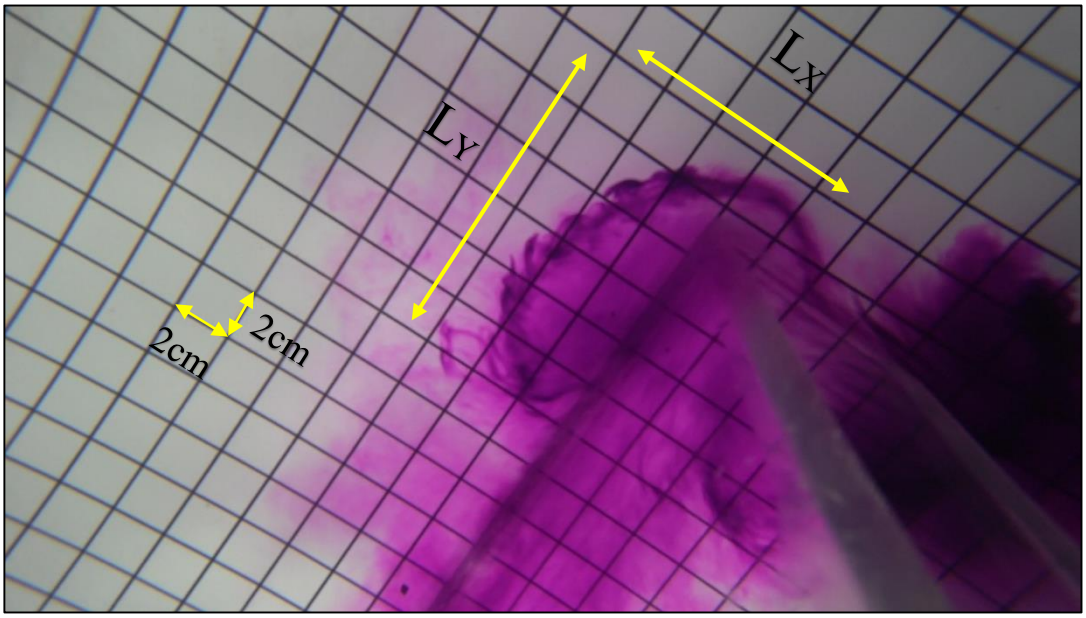

Figure 4.9. Flow visualization for sharp-edged structure

In Figure 4.9, vortex formation can be seen for the sharp-edged structure under regular waves that have a KC number of 3.135. The dimensions of the vortices are measured and listed below in Table 4.4, and Table 4.5 for regular and solitary waves, respectively.

Table 4.4. *Vortex dimensions under regular waves*

Structure Type	*KC*	L_X/B	L_Y/B
Sharp-edged head	1.333	-	-
Sharp-edged head	3.135	1.50	1.83
Sharp-edged head	5.337	2.61	2.94
Round head	1.333	-	-
Round head	3.135	1.33	1.67
Round head	5.337	2.78	3.56

When KC number is in the order of O(1), lee-wake vortices are not formed. In this point of view, it is said that physical and numerical model results are in agreement.

Table 4.5. *Vortex dimensions under solitary waves*

Structure Type	*Wave*	*h (m)*	U_m *(m/s)*	*H/B*	L_X/B	L_Y/B
Sharp-edged head	sol-40-1	0.4	0.372	1.256	1.54	2.38
Round head	sol-40-1	0.4	0.372	1.256	2.33	2.39
Round head	sol-40-2	0.4	0.270	0.892	1.83	1.83
Round head	sol-40-3	0.4	0.184	0.551	1.56	1.44
Round head	sol-30-2	0.3	0.395	1.265	1.69	1.67
Round head	sol-20-1	0.2	0.614	1.920	2.89	2.78
Round head	sol-20-2	0.2	0.540	1.602	2.22	2.39
Round head	sol-20-3	0.2	0.469	1.273	1.79	1.75

In Table 4.5, lee-wake vortex dimensions are presented in dimensionless forms with the maximum horizontal velocities. The biggest vortex occurs in the case sol-20-1, which has the maximum horizontal velocity of all. In this case vortex dimensions reach up to almost three times the structure width in both axes.

Vortex dimensions obtained for regular waves from 2D and 3D numerical simulations, as well as physical model tests, are presented in Figure 4.10. To make integrant comparison between vortex dimensions under solitary wave action, results are presented in Table 4.5 and Figure 4.11.

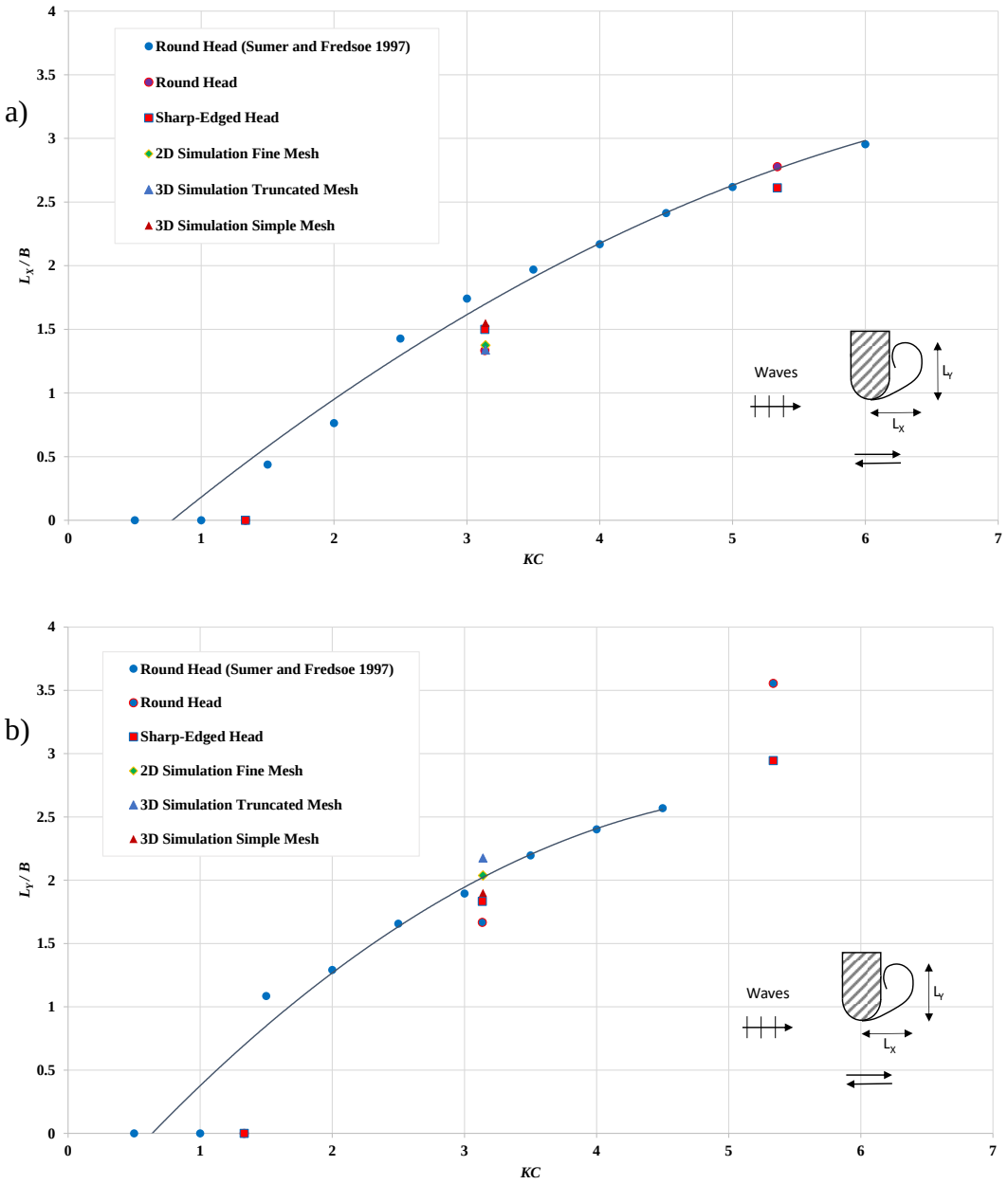

Figure 4.10. Dimensions of Lee-Wake vortices under regular waves a) X direction b) Y direction

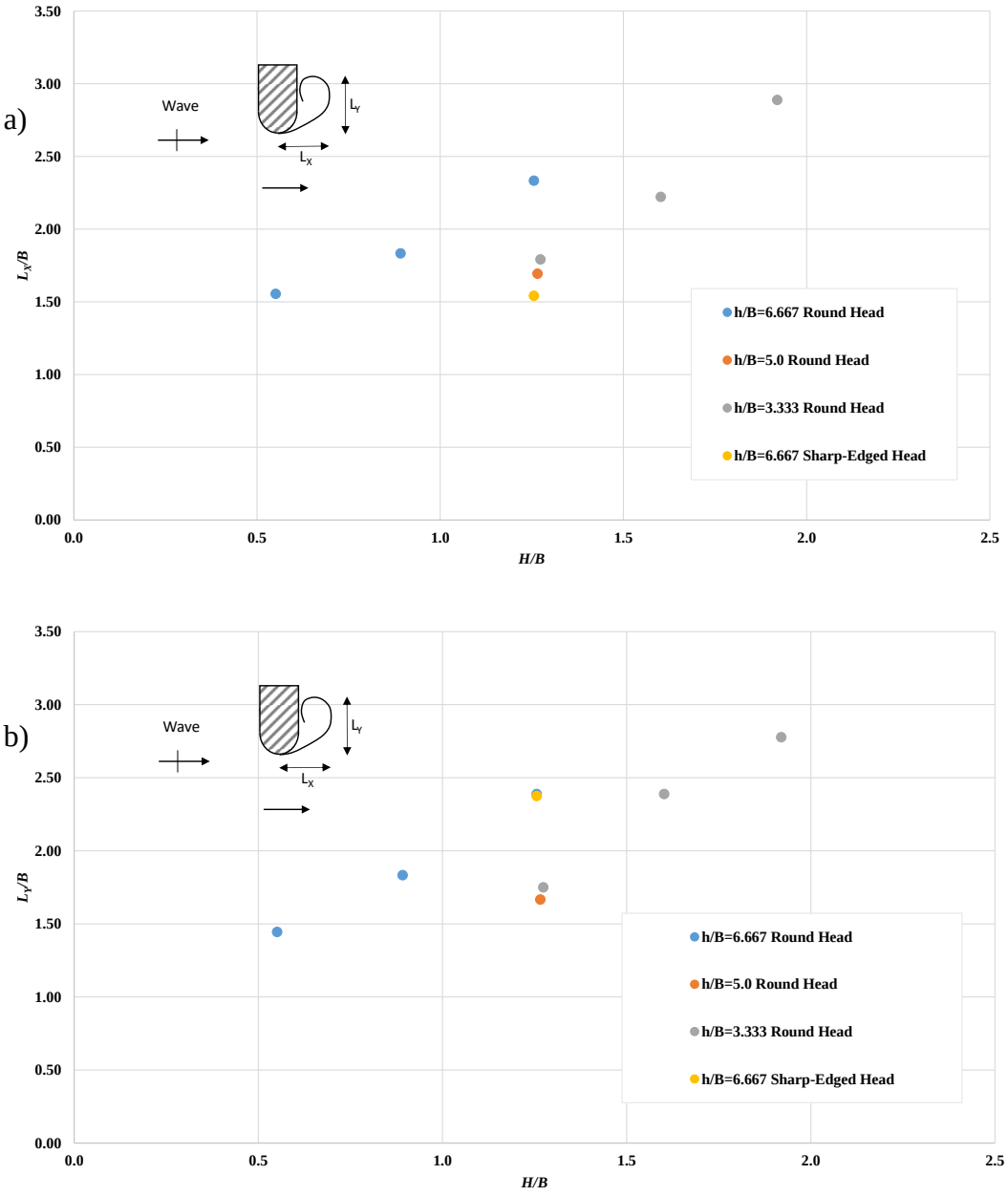

Figure 4.11. Dimensions of Lee-Wake vortices under solitary waves a) X direction b) Y direction

As seen from Figure 4.10, vortex dimensions are consistent for both physical and numerical models with the results of Sumer and Fredsøe (1997). On the other hand, Figure 4.11 indicates that when h/B is constant, vortex dimensions increase in both directions while H/B increases. Additionally, for the constant H/B ratio, vortex dimensions are higher in h/B=6.667 case than the h/B=5.0 case. However, there is no significant difference between h/B=5.0 and h/B=3.333 cases under the same H/B ratio. Finally, there is a significant decreasing in vortex dimension on X direction between round head and sharp-edged structures under same wave, although L_Y/B is unchanged for sharp-edged structure.

4.5. Scour Tests

Scour experiments constitute a large part of this study. In order to investigate the effect of structure shape, two different types of breakwater model are used. Additionally, not only random and regular waves were used in this part, but also scouring processes are examined under solitary waves. After completion of hydrodynamic tests and flow visualization experiments, the false bottom is removed, and sediment is filled in between inlet and outlet slopes. The sediment used in this study has a median diameter d_{50}=0.21mm. Grain size distribution curve of the sediment is given in Figure 4.12.

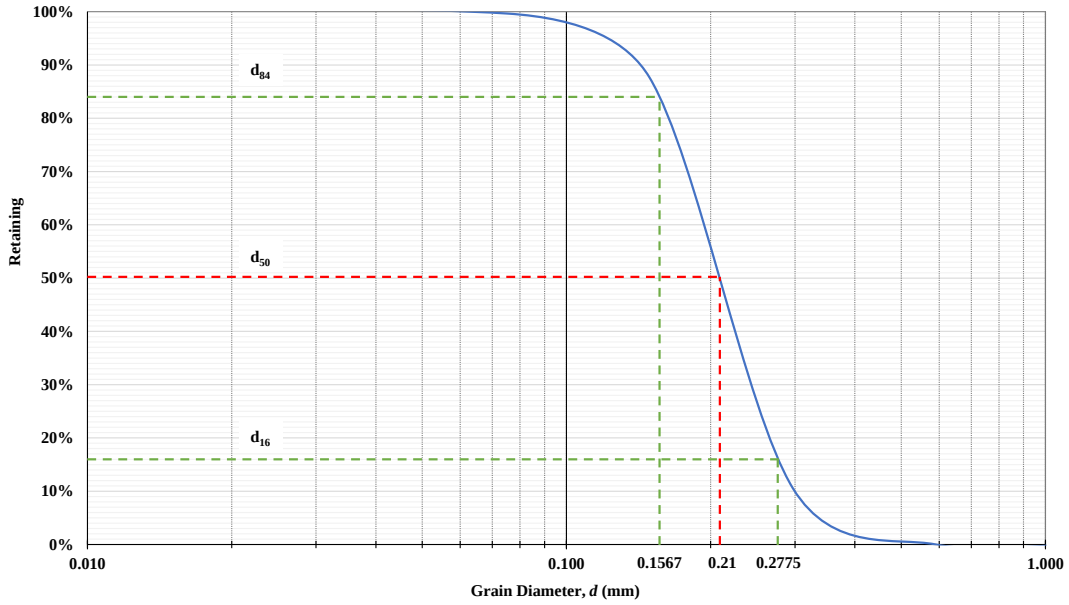

Figure 4.12. Grain size distribution curve

As seen from Figure 4.12, d_{16} indicates that 16% of the grains are bigger than 0.2775 mm diameter, and d_{84} indicates that 16% of the grains are smaller than 0.1567 mm diameter. Gradation coefficient of the sediment is calculated as 1.3308 with the equation below. As the gradation coefficient approaches to 1.0, the sediment becomes uniformly distributed. In this study sediment is defined as narrow graded since gradation coefficient is lower than 1.5.

$$S_g = \frac{\left({}^{d_{84}}/_{d_{50}} + {}^{d_{50}}/_{d_{16}}\right)}{2} \tag{4.9}$$

This part of the study divides into two main sections in the point of structure shape. Firstly, sharp-edged head breakwater model is used. Secondly, the round head structure placed into the flume and proceeded with it. Thereupon, it becomes possible to make comparison between scour depths under the same waves for different types of structures.

To perform a scour experiment, firstly, sediment bottom must be flattened, and the initial bottom state should be scanned. After completion of scanning, wave flume should be filled up very slowly to prevent undesired sediment movement. When the setup is ready, the experiment is carried out. To preserve the scour profile, wave flume must be drained very slowly. Finally, bottom state will be scanned. Filling up and draining the wave flume take approximately 12 hours for each process. Thus, one set of experiment takes two days.

In scour experiment, ADV measurements are performed at a distance of 10B perpendicular from head of the structure. 10B distance was picked out from velocity distribution experiments and is the distance that the blockage effect becomes insignificant.

Scour tests performed until the scour depth reaches the equilibrium state which means scouring process stops and no more scouring occurs. For the regular waves, scouring processes reaches the equilibrium state in 20-30 minutes depending on KC number. However, in random waves this process takes approximately 2-3 hours that consists of at least 6 - 7 time-series which has 1000 waves individually. Unlike regular and random waves, determining the equilibrium scour depth on solitary waves is different. In this study, it is said that if the scour depth doesn't change for the last 5 individual waves, the bottom evolution is completed. The measured dimensionless scour depths and scour depths given by Sumer and Fredsøe (1997) study for corresponding KC numbers are given in Table 4.6 for sharp-edged structure and in Table 4.7 for round read structure.

Table 4.6. *Scour Experiments for Sharp-Edged Head Structure*

Wave	T (s)	U_m (m/s)	$U_{m,r}$ (m/s)	KC	S (mm)	S/B_{meas}	$S/B_{(SF97)}$	T^*
rand-1	1.208	-	0.070	1.403	48	0.800	-	10.499
rand-2	1.607	-	0.119	3.182	98	1.625	-	2.123
rand-3	1.891	-	0.170	5.347	174	2.892	-	3.021
rand-4	1.973	-	0.165	5.417	192	3.200	-	3.679
reg-2	1.437	0.133	-	3.184	54	0.900	0.278	0.226

Table 4.7. *Scour Experiments for Round Head Structure*

Wave	*T (s)*	U_m *(m/s)*	$U_{m,r}$ *(m/s)*	*KC*	*S (mm)*	S/B_{meas}	$S/B_{(SF97)}$	T^*	*Number of Waves*
rand-1	1.208	-	0.070	1.403	16	0.267	-	4.023	-
rand-2	1.607	-	0.119	3.182	76	1.267	-	3.175	-
rand-3	1.891	-	0.170	5.347	142	2.367	-	3.010	-
rand-4	1.973	-	0.165	5.417	166	2.767	-	4.871	-
rand-5	2.161	-	0.154	5.528	149	2.483	-	4.436	-
rand-6	2.481	-	0.132	5.445	162	2.700	-	5.434	-
reg-1	1.058	0.079	-	1.390	0	0.000	0.035	-	-
reg-2	1.437	0.133	-	3.184	11	0.183	0.150	0.022	-
reg-2	1.437	0.133	-	3.184	10	0.167	0.150	0.027	-
reg-3	1.776	0.150	-	4.432	48	0.792	0.210	0.026	-
reg-3	1.776	0.150	-	4.432	49	0.817	0.210	0.035	-
reg-4	1.603	0.188	-	5.019	39	0.650	0.235	0.031	-
sol-40-1	-	0.396	-	-	176	2.933	-	-	46
sol-40-2	-	0.306	-	-	138	2.300	-	-	48
sol-40-3	-	0.205	-	-	92	1.533	-	-	50
sol-30-1	-	0.473	-	-	187	3.117	-	-	50
sol-30-2	-	0.407	-	-	138	2.300	-	-	35
sol-30-3	-	0.314	-	-	123	2.042	-	-	40
sol-20-1	-	0.591	-	-	125	2.083	-	-	35
sol-20-2	-	0.534	-	-	125	2.083	-	-	45
sol-20-3	-	0.435	-	-	113	1.883	-	-	45

In the above given Table 4.6 and Table 4.7, S indicates the equilibrium scour depth in mm and S/B indicates it in dimensionless form. In Figure 4.13, the scoured sediment bottom around the transparent acrylic breakwater model with a round head is given.

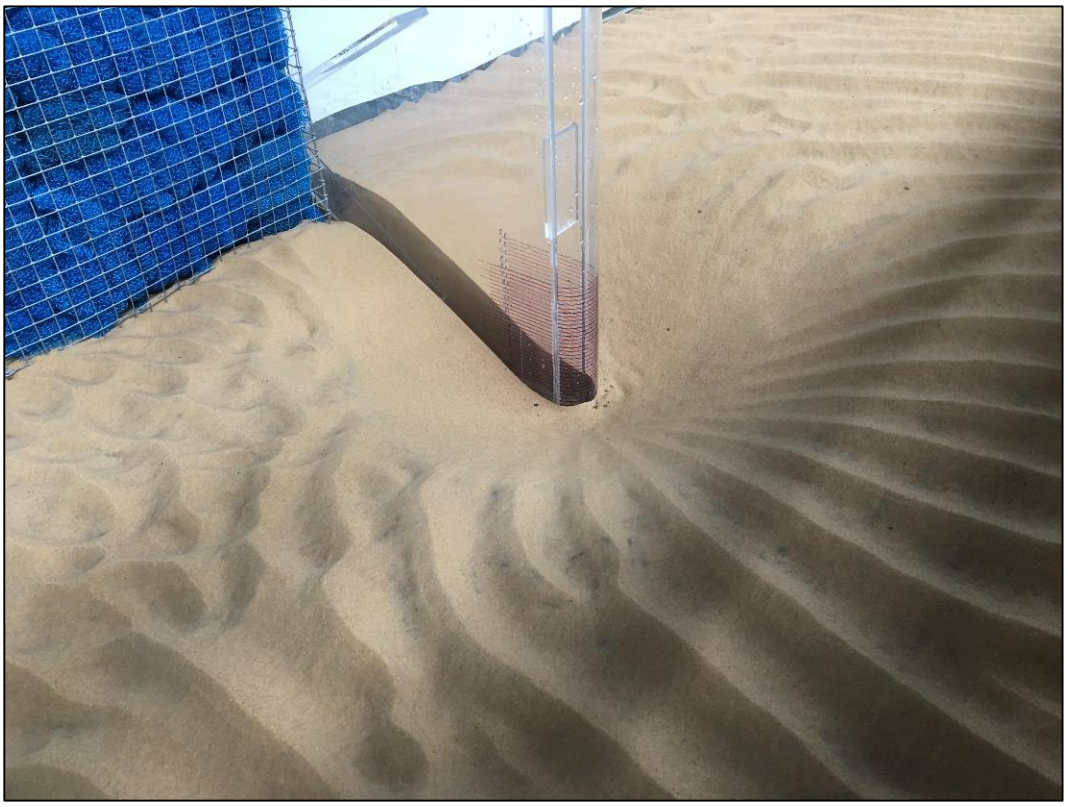

Figure 4.13. Round head structure model with scour hole (after KC=5.347, ir-3)

In order to present the results of scour experiments under regular and random waves in a more illustrative way, results that given in Table 4.6, and Table 4.7 are also given as figures in Figure 4.14.

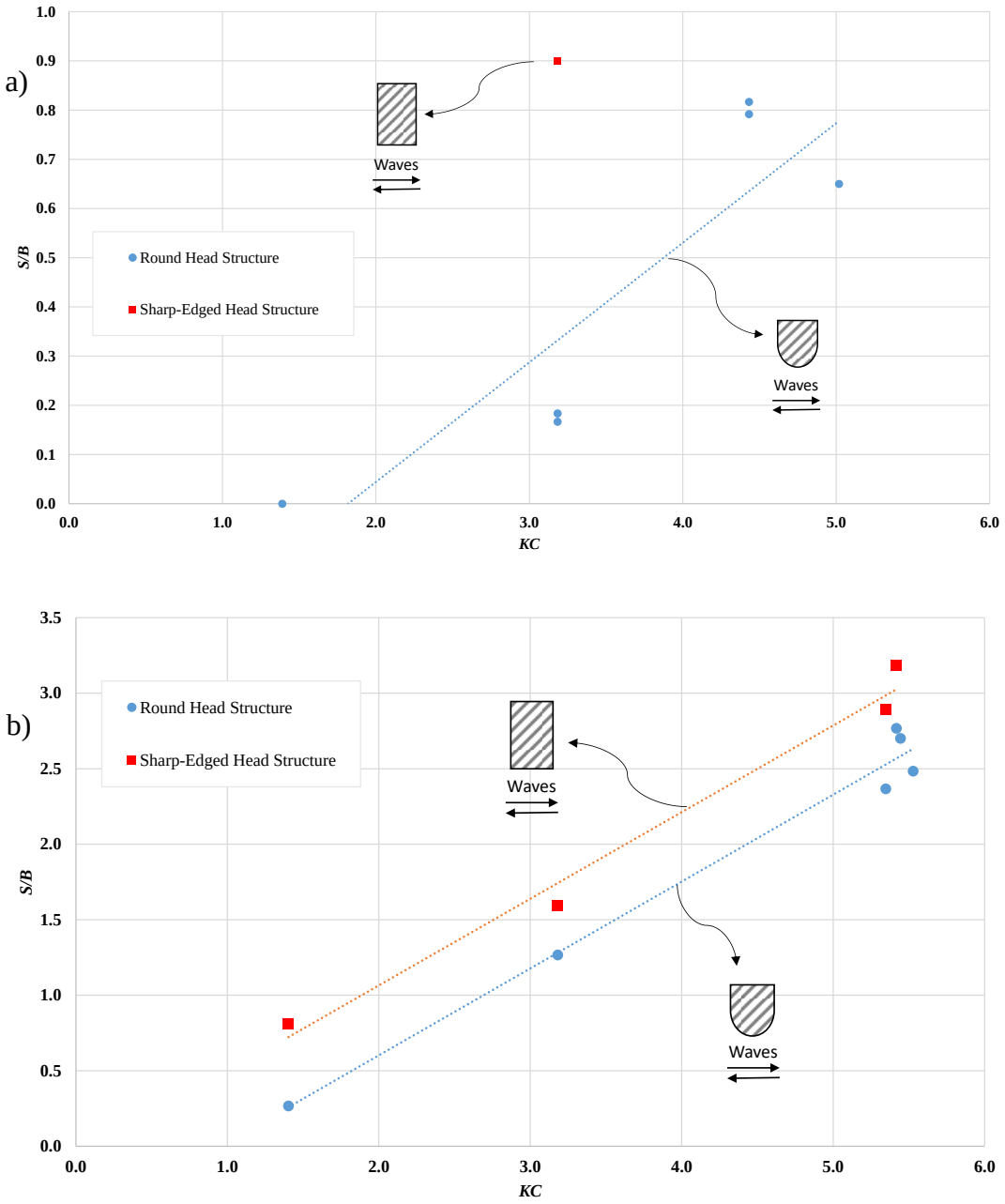

Figure 4.14. Equilibrium scour depths for a) regular waves, b) random waves

Figure 4.14 indicates that scour depth increases with the increasing KC number for both regular and random waves. When KC numbers are around 5.5, four different wave series with different steepness values are investigated. Regardless of the steepness of the wave, there is no significant difference in equilibrium scour depth for the same breakwater model. On the other hand, scour depths under random waves are from 20% to 25% higher for the sharp-edged head structure than the round head structure.

While KC numbers are around 5.5, four random waves are tested for round head structures. Although their KC numbers are close to each other, steepness values of these waves vary between 0.008 and 0.04. Equilibrium scour depths of mentioned waves are presented in Figure 4.15.

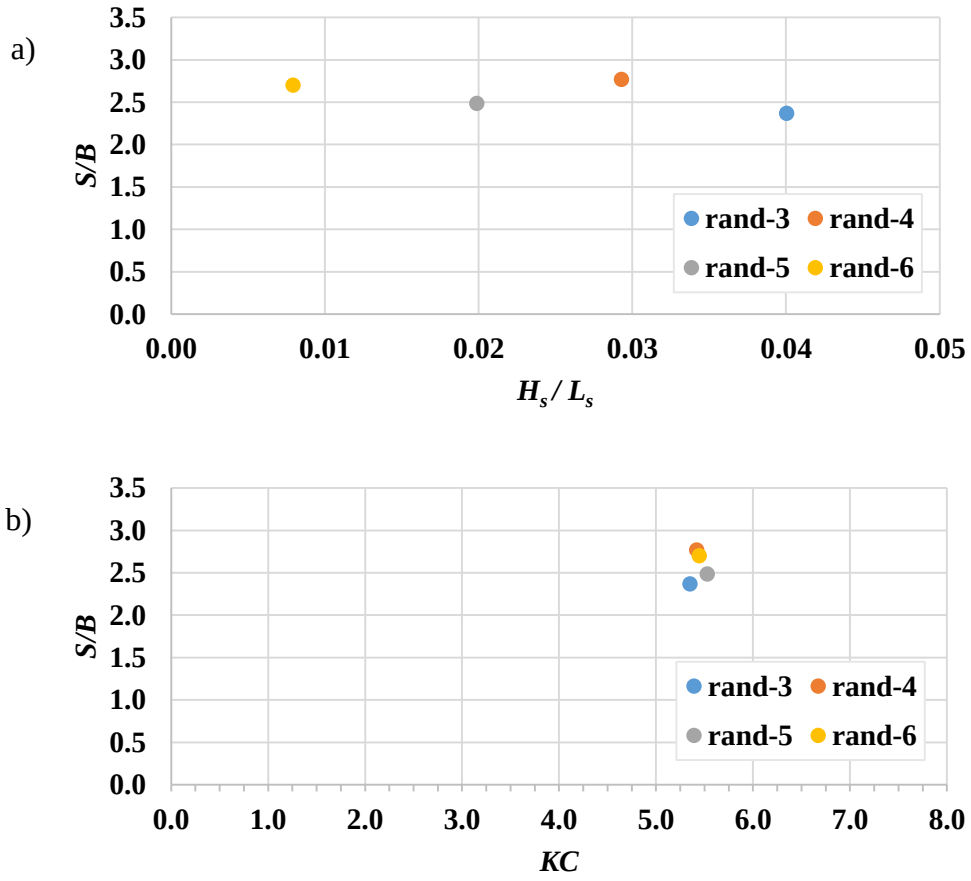

Figure 4.15. Equilibrium scour depths corresponding to a) Steepness values b) KC numbers

Figure 4.15 indicates that while KC number is approximately 5.5, equilibrium scour depths are around 2.5. However, when these waves are compared with each other in terms of wave steepness, they have different values. Hence, there is no significant relation between wave steepness and equilibrium scour depth, and KC number is the main governing parameter.

Results of scour tests that performed in the scope of this study for both regular and random waves, and results from Sumer and Fredsøe (1997) are presented in Figure 4.16 to make a comparison in between.

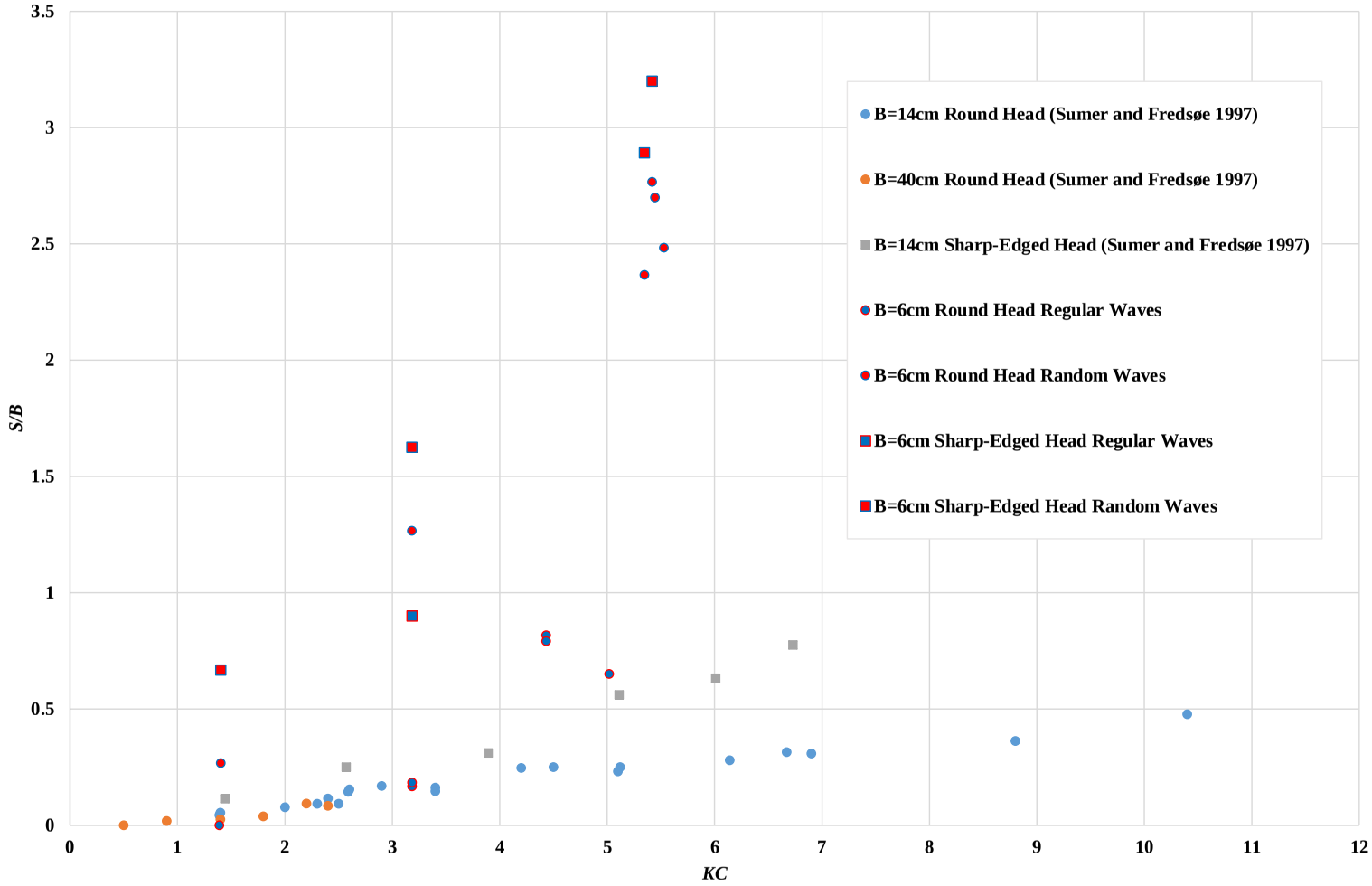

Figure 4.16. Comparison of equilibrium scour depths for regular and random waves

For the breakwater model, which has round head, equilibrium scour depths corresponding to wave heights for solitary waves are given in Figure 4.17.

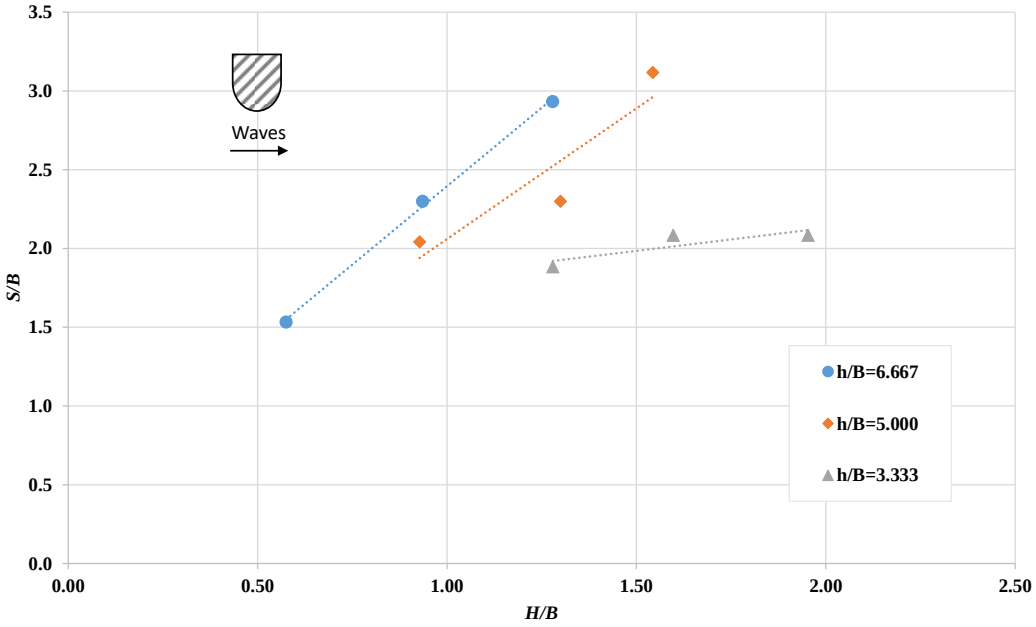

Figure 4.17. Equilibrium scour depths for round head structure under solitary waves

In Figure 4.17, for the constant h/B ratio, equilibrium scour depth usually tends to increase with the increasing H/B. When H/B is constant, but h/B varies, which means the same wave height with different water depth, equilibrium scour depth increases while water depth increases.

Rather than scour depths, dimensions of scour holes are also measured. These dimensions are compered each other with corresponding KC numbers. For the regular and solitary waves, vortex dimensions and scour hole dimensions are compared as well. Figure 4.18 shows the scour hole dimensions for regular and random waves with corresponding KC numbers.

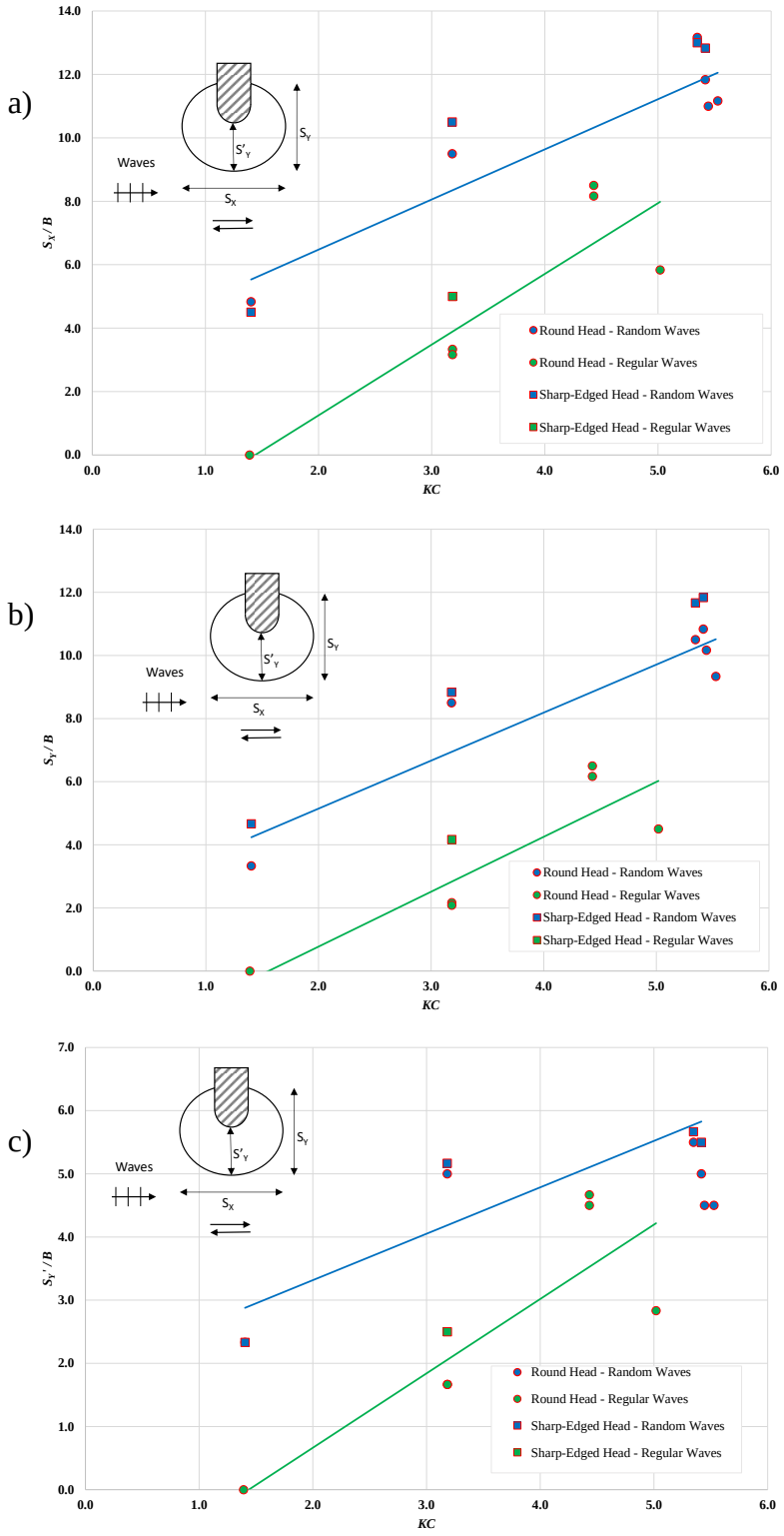

Figure 4.18. Scour hole dimensions for regular and random waves a) S_X length, b) S_Y length, c) S'_Y length

In Figure 4.18, S_X is the length of the scour hole in flow direction and S_Y is the length of the scour hole in transverse direction. As seen from Figure 4.18, like scour depths, dimensions of the scour hole are increasing with increasing KC number. For the same KC number but different structure shapes, scour hole dimensions are slightly higher for the sharp-edged structures. This situation caused due to the fact that the equilibrium scour depths are higher for the sharp-edged head structures than the round head structures under same wave condition. In Figure 4.19, scour hole dimensions under solitary waves are given.

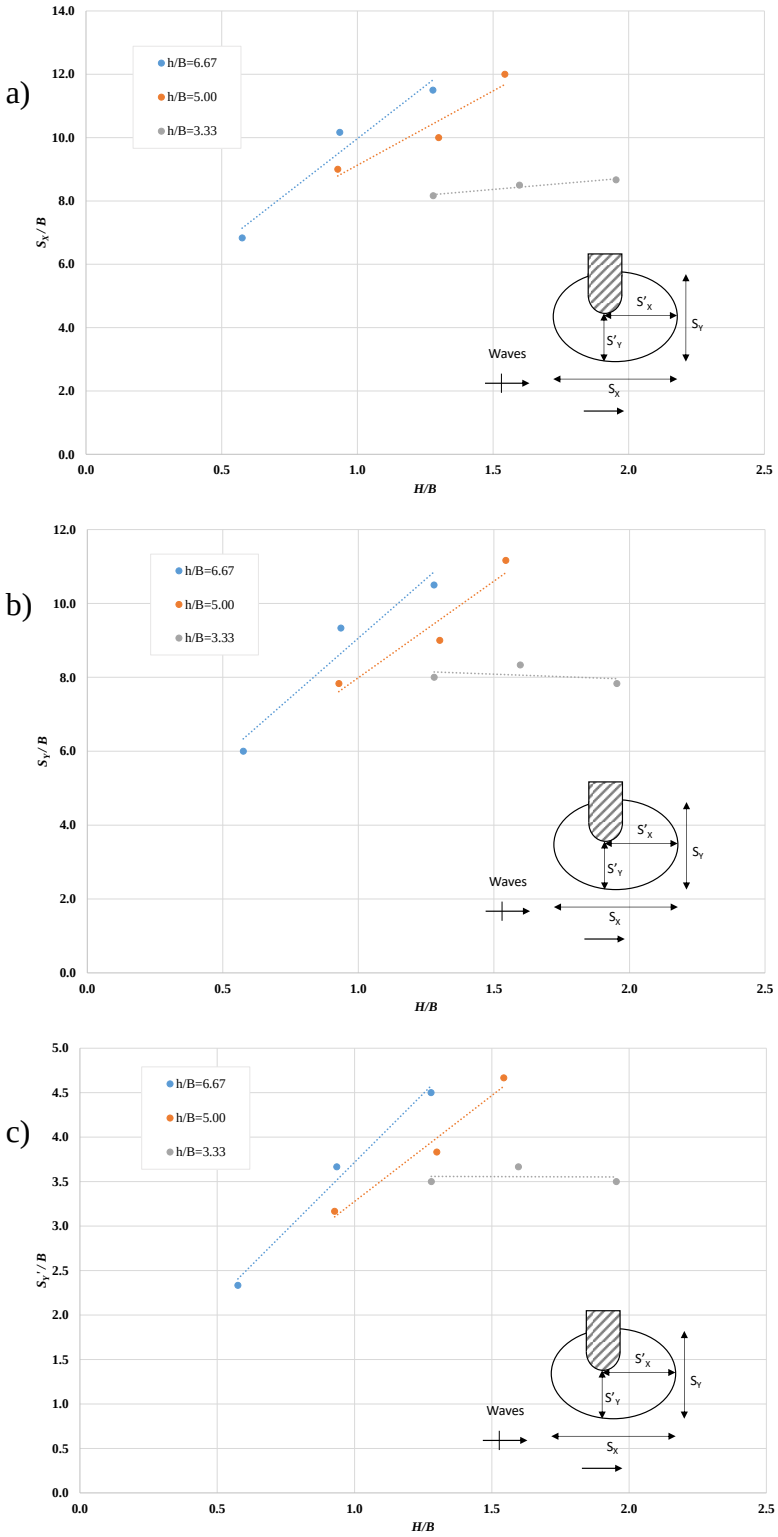

Figure 4.19. Scour hole dimensions for solitary waves a) S_X length, b) S_Y length, c) S'_Y length

As given in Figure 4.19, scour hole dimensions are usually increasing with increasing wave height to structure width ratio (H/B) for solitary waves which have the same water depths. Except for the h/B=3.333 cases, scour hole dimensions are not significantly different from each other. Scour hole dimensions are found directly related to the scour depths.

Vortex dimensions and scour hole dimensions are also compared in between for solitary waves. S'_X and S_Y values are used in order to compare them properly, due to the fact that solitary waves do not have symmetrical scour holes like regular waves. In Figure 4.20, comparison between vortex dimensions and scour hole dimensions are presented for solitary waves.

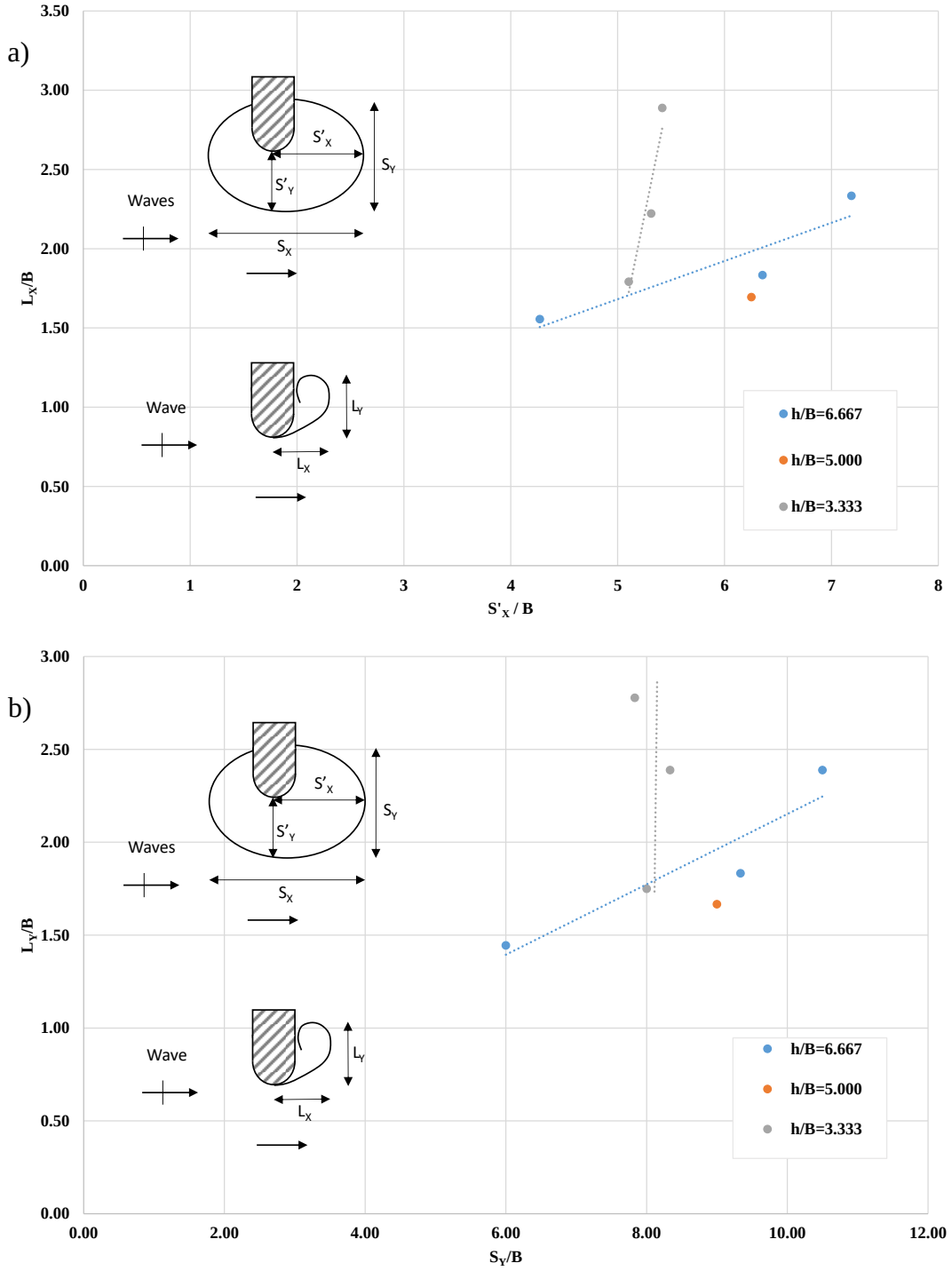

Figure 4.20. Comparison between scour hole dimensions and vortex dimensions for solitary waves a) X direction, b) Y direction

Figure 4.20 shows that with the increasing vortex dimensions, scour hole dimensions are also increasing for h/B=6.667 cases. For h/B=3.333 cases, although vortex dimensions are different from each other, scour hole dimensions are not significantly different due to the fact that they have similar scour depths.

CHAPTER 5

CONCLUSIONS

Wave induced scouring processes under different types of waves are investigated for both round head and sharp-edged head structures in this study. It is understood that the scour depth is mostly governed by KC number, although structure shape affects it as well. In order to understand hydrodynamic processes, flow visualization experiments and velocity distributions in front of the structure head are also examined.

Besides physical model experiments, hydrodynamic processes studied numerically as well by using an open-source CFD environment OpenFOAM®. Both 2D and 3D simulations are run, and the results of these simulations are compared with each other. In order to obtain optimum computational mesh for numerical model studies, different types and sizes of models are created. Those models also divided into four different sizes of cells to obtain an adequate model.

Conclusions obtained from this study are presented below.

- It is understood that the dimensions of a numerical model have serious effects on the results, and determining the optimum model with adequate cell size is vital.
- Vortex dimensions measured from physical model experiments increase with the increasing KC numbers for regular waves. On the other hand, when the vortex dimensions compared for different types of structures, although there are minor differences, no significant changes were observed.
- Vortex dimensions obtained for regular waves from physical model tests and numerical simulations are found to be in good agreement with Sumer and Fredsøe (1997).

- When the transverse velocity distributions on a straight line from the tip of the breakwater head to the flume wall are examined, it is observed that the velocity values converge to the undisturbed velocities beyond 10B distance which means blockage effect due to converging flow becomes insignificant beyond this distance. Therefore, ADV measurements are performed at 10B distance in scour experiments.
- It is observed that scour depths are from 20% to 25% higher for the sharp-edged structures than the round head structures under random waves.
- While KC number is in the order of 1.4 for regular waves, no scour is observed for the round head structure.
- For two different structure types, scour depths increases with the increasing KC number under both regular and random waves.
- In order to compare scour depths for different wave series, four different wave series used that have KC numbers in the order of 5.5 and different wave steepness values. It is observed that the wave steepness does not affect scour depth for different wave series which have the same KC number.
- When scour depths for regular and random waves were compared for the same KC numbers, scour depth is greater for random waves. For instance, when KC number is around 3, scour depth is seven times higher for random waves than the regular waves. On the other hand, when KC number is around 5.0 equilibrium scour depth is 3.3 times higher for random waves. The nature of random waves might cause this phenomenon. Random waves are composed of individual waves which has different individual KC numbers. A random wave series have many large waves as well as many small waves. Since the volume of sediment transported for a given time is correlated to the water particle velocities of 3^{rd} power, larger amounts of sediments are carried away for the same KC numbers of regular waves.
- Besides, scour depth differences between regular and random waves, there is also difference for time scale of scour processes. Regular waves reach

equilibrium state at least 25 times faster than random waves under same KC numbers when they are compared in dimensionless time scale.

- For solitary waves, as a general trend, scour depth increases with the increasing wave height for round head structures. However, the largest wave which has H/B=1.95 (H=11.7 cm) wave height to breakwater width ratio in h/B=3.333 (h=20 cm) cases does not have the largest scour depth. The largest scour depth is observed in h/B=5.0 and H/B=1.54 (h=30 cm water depth for 9.3 cm wave height) case.
- When wave heights are around H/B=1.3 (H=7.6 cm), largest scour is observed in h/B=6.667 (h=40 cm) case, and smallest is observed in h/B=3.333 (h=20 cm) case. In other words, scour depth increases with the increasing water depth.
- Maximum scour depth under solitary waves occur at the leeward of the structure rather than the tip of the breakwater head as in regular and random waves.

Finally, future recommendations for this study can be listed as follows.

- Different size of sediment might be used rather than d_{50}=0.21 mm, and this way sediment size comparison would be done.
- Breakwater model orientation in this study was kept constant. However, waves can approach from different angles to the breakwater. By changing the model placement with various angles, the effect of the angle of approach would be observed.
- Although it is understood that the dimensionless KC number mainly governs the scour process, various KC numbers different than the tested range in this study (1.5 - 5.5) could also be studied, varying the structure width and the wave conditions.
- The backfilling process is another serious case, and it should be considered as well on future studies.

- Scour experiments performed without any rubble base or protective layer in this study. Future studies may be performed with toe protection to investigate its effect.

REFERENCES

Baranya, S., Olsen, N. R. B., Stoesser, T., and Sturm, T. (2012). "Three-Dimensional Rans Modeling of Flow Around Circular Piers using Nested Grids." *Engineering Applications of Computational Fluid Mechanics*, Taylor & Francis, 6(4), 648–662.

Baykal, C., Sumer, B. M., Fuhrman, D. R., Jacobsen, N. G., and Fredsoe, J. (2015). "Numerical investigation of flow and scour around a vertical circular cylinder." *Philosophical Transactions of the Royal Society A: Mathematical, Physical and Engineering Sciences*, 373(2033).

Baykal, C., Sumer, B. M., Fuhrman, D. R., Jacobsen, N. G., and Fredsøe, J. (2017). "Numerical simulation of scour and backfilling processes around a circular pile in waves." *Coastal Engineering*, Elsevier, 122(January), 87–107.

Carreiras, J., Larroudé, P., Seabra-santos, F., and Mory, M. (2000). *Wave Scour Around Piles*. 27th International Conference on Coastal Engineering (ICCE), Sydney, Australia.

Dalrymple, R. A. (1989). "Physical Modelling of Littoral Processes." *Recent Advances in Hydraulic Physical Modelling*, R. Martins, ed., Springer Netherlands, Dordrecht, 567–588.

Dey, S., Sumer, M. B., and Fredsøe, J. (2006). "Control of Scour at Vertical Circular Piles under Waves and Current." *Journal of Hydraulic Engineering*, American Society of Civil Engineers, 132(3), 270–279.

Eroğlu, N., Özbek, T., and Demiröz, E. (2001). "Dikdörtgen Kesitli Doğrusal Yatak Üzerinde Yerleştirilmiş Düşey Plak Şeklindeki Mahmuzun Oyulma Sınırlarının Belirlenmesi." *İMO Teknik Dergi*, 57(12), 2331–2353.

Escauriaza, C., and Sotiropoulos, F. (2011a). “Lagrangian model of bed-load transport in turbulent junction flows.” *Journal of Fluid Mechanics*, Cambridge University Press, 666, 36–76.

Escauriaza, C., and Sotiropoulos, F. (2011b). “Initial stages of erosion and bed form development in a turbulent flow around a cylindrical pier.” *Journal of Geophysical Research: Earth Surface*, John Wiley & Sons, Ltd, 116(F3).

Ettema, R., Melville, B., and Barkdoll, B. (1998). “Scale Effect in Pier-Scour Experiments.” *Journal of Hydraulic Engineering*, American Society of Civil Engineers, 124(6), 639–642.

Franco, L. (1994). “Vertical breakwaters: the Italian experience.” *Coastal Engineering*, 22(1), 31–55.

Fuhrman, D. R., Baykal, C., Mutlu Sumer, B., Jacobsen, N. G., and Fredsøe, J. (2014). “Numerical simulation of wave-induced scour and backfilling processes beneath submarine pipelines.” *Coastal Engineering*, Elsevier B.V., 94, 10–22.

Goda, Y., and Suzuki, Y. (1976). “Estimation of incident and reflected waves in random wave experiments.” *in: Proc. Fifteenth Coastal Engng. Conf. (Hawaii Univ. U.S.a., Jul.11-17,1976)*, 1, New Yo, 828–845.

Göthel, O., and Zielke, W. (2007). “Numerical Modeling of Scour at Offshore Wind Turbines.” *Coastal Engineering 2006*, World Scientific Publishing Company, 2343–2353.

Güney, M. Ş., Özgenç Aksoy, A., and Bombar, G. (2011). *Kare Kesitli Köprü Orta Ayağı Etrafında Zamanla Değişen Akım Nedeniyle Oluşan Yerel Oyulmalar*. V. Ulusal Su Mühendisliği Sempozyumu, İstanbul, Turkey.

Hughes, S. A. (1993). *Physical Models and Laboratory Techniques in Coastal Engineering*. *Advanced Series on Ocean Engineering*, World Scientific.

Jacobsen, N. G., Fredsoe, J., and Jensen, J. H. (2014). "Formation and development of a breaker bar under regular waves. Part 1: Model description and hydrodynamics." *Coastal Engineering*, Elsevier B.V., 88, 182–193.

Kamphuis, J. W. (1991). "Physical Modeling." *Handbook of Coastal and Ocean Engineering*, J. B. Herbich, ed., Gulf Publishing, Houston, Texas, USA, 1049–1066.

Kim, Y. C. (2009). "Handbook of Coastal and Ocean Engineering." World Scientific.

Larsen, B. E., Fuhrman, D. R., Baykal, C., and Sumer, B. M. (2017). "Tsunami-induced scour around monopile foundations." *Coastal Engineering*, Elsevier Ltd, 129(August), 36–49.

Le Mehaute, B. (1990) "Similitude", *Ocean Engineering Science*, B. Le Mehaute, Ed., Vol 9, Part B in the series The Sea, John Wiley and Sons, New York, pp 955-980.

Lim, S. (1997). "Equilibrium Clear-Water Scour around an Abutment." *Journal of Hydraulic Engineering*, American Society of Civil Engineers, 123(3), 237–243.

Liu, X., and García, M. H. (2008). "Three-Dimensional Numerical Model with Free Water Surface and Mesh Deformation for Local Sediment Scour." *Journal of Waterway, Port, Coastal, and Ocean Engineering*, American Society of Civil Engineers, 134(4), 203–217.

Melville, B. W., and Raudkivi, A. J. (1977). "Flow Characteristics in Local Scour At Bridge Piers." *Journal of Hydraulic Research*, Taylor & Francis, 15(4), 373–380.

Melville, B. W., and Raudkivi, A. J. (1996). "Effects of Foundation Geometry on Bridge Pier Scour." *Journal of Hydraulic Engineering*, American Society of Civil Engineers, 122(4), 203–209.

Melville, B. W., and Sutherland, A. J. (1988). “Design Method for Local Scour at Bridge Piers.” *Journal of Hydraulic Engineering*, American Society of Civil Engineers, 114(10), 1210–1226.

Nielsen, A. W., Sumer, B. M., Fredsøe, J., and Christensen, E. D. (2010). *Scour Protection around Offshore Wind Turbines. Monopiles*. 5th International Conference on Scour and Erosion (ICSE-5), San Francisco, California, USA.

Olsen, N. R. B., and Kjellesvig, H. M. (1998). “Three-dimensional numerical flow modeling for estimation of maximum local scour depth.” *Journal of Hydraulic Research*, Taylor & Francis, 36(4), 579–590.

Olsen, N. R. B., and Melaaen, M. C. (1993). “Three-Dimensional Calculation of Scour Around Cylinders.” *Journal of Hydraulic Engineering*, American Society of Civil Engineers, 119(9), 1048–1054.

Oumeraci, H. (1994). “Review and analysis of vertical breakwater failures — lessons learned.” *Coastal Engineering*, Elsevier, 22(1–2), 3–29.

Raudkivi, A. J. (1986). “Functional Trends of Scour at Bridge Piers.” *Journal of Hydraulic Engineering*, American Society of Civil Engineers, 112(1), 1–13.

Raudkivi, A. J. (1998). *Loose Boundary Hydraulics*. CRC Press.

Raudkivi, A. J., and Ettema, R. (1977). “Effect of Sediment Gradation on Clear Water Scour.” *Journal of the Hydraulics Division*, 103(10), 1209–1213.

Raudkivi, A. J., and Ettema, R. (1983). “Clear-Water Scour at Cylindrical Piers.” *Journal of Hydraulic Engineering*, American Society of Civil Engineers, 109(3), 338–350.

Roulund, A., Sumer, B. M., Fredsøe, J., and Michelsen, J. (2005). “Numerical and experimental investigation of flow and scour around a circular pile.” *Journal of Fluid Mechanics*, Cambridge University Press, 534, 351–401.

Stahlmann, A. (2014). “Numerical and Experimental Modeling of Scour at Foundation Structures for Offshore Wind Turbines.” *Journal of Ocean and Wind Energy*, 1(2), 82–89.

Stahlmann, A., and Schlurmann, T. (2012). “Investigations on scour development at tripod foundations for offshore wind turbines: Modeling and application.” *Proceedings of the Coastal Engineering Conference*, 1–11.

Sumer, B. M., Christiansen, N., and Fredsoe, J. (1992a). “Time Scale Of Scour Around A Vertical Pile.” *The Second International Offshore and Polar Engineering Conference*, International Society of Offshore and Polar Engineers, San Francisco, California, USA.

Sumer, B. M., Christiansen, N., and Fredsøe, J. (1993). “Influence of Cross Section on Wave Scour around Piles.” *Journal of Waterway, Port, Coastal, and Ocean Engineering*, American Society of Civil Engineers, 119(5), 477–495.

Sumer, B. M., and Fredsøe, J. (1997). “Scour at the head of a vertical-wall breakwater.” *Coastal Engineering*, 29(3–4), 201–230.

Sumer, B. M., and Fredsøe, J. (2001). “Scour around Pile in Combined Waves and Current.” *Journal of Hydraulic Engineering*, American Society of Civil Engineers, 127(5), 403–411.

Sumer, B. M., and Fredsøe, J. (2006). *Hydrodynamics Around Cylindrical Structures*. *Advanced Series on Ocean Engineering*, World Scientific.

Sumer, B. M., Fredsøe, J., and Christiansen, N. (1992b). “Scour Around Vertical Pile in Waves.” *Journal of Waterway, Port, Coastal, and Ocean Engineering*, American Society of Civil Engineers, 118(1), 15–31.

Takahashi, S. (1996). *Design of Vertical Breakwaters*. Port and Airport Reseach Institute, Japan.

Yanmaz, M. A., and Altınbilek, D. H. (1991). “Study of Time-Dependent Local Scour around Bridge Piers.” *Journal of Hydraulic Engineering*, American Society of Civil Engineers, 117(10), 1247–1268.

Zhao, M., and Cheng, L. (2008). “Numerical Modeling of Local Scour below a Piggyback Pipeline in Currents.” *Journal of Hydraulic Engineering*, American Society of Civil Engineers, 134(10), 1452–1463.

Zhao, M., Cheng, L., and Zang, Z. (2010). “Experimental and numerical investigation of local scour around a submerged vertical circular cylinder in steady currents.” *Coastal Engineering*, Elsevier B.V., 57(8), 709–721.

Zhao, M., Zhu, X., Cheng, L., and Teng, B. (2012). “Experimental study of local scour around subsea caissons in steady currents.” *Coastal Engineering*, Elsevier B.V., 60(1), 30–40.

APPENDICES

A. Scour Patterns and Development Curves for Sharp-Edged Head Structures

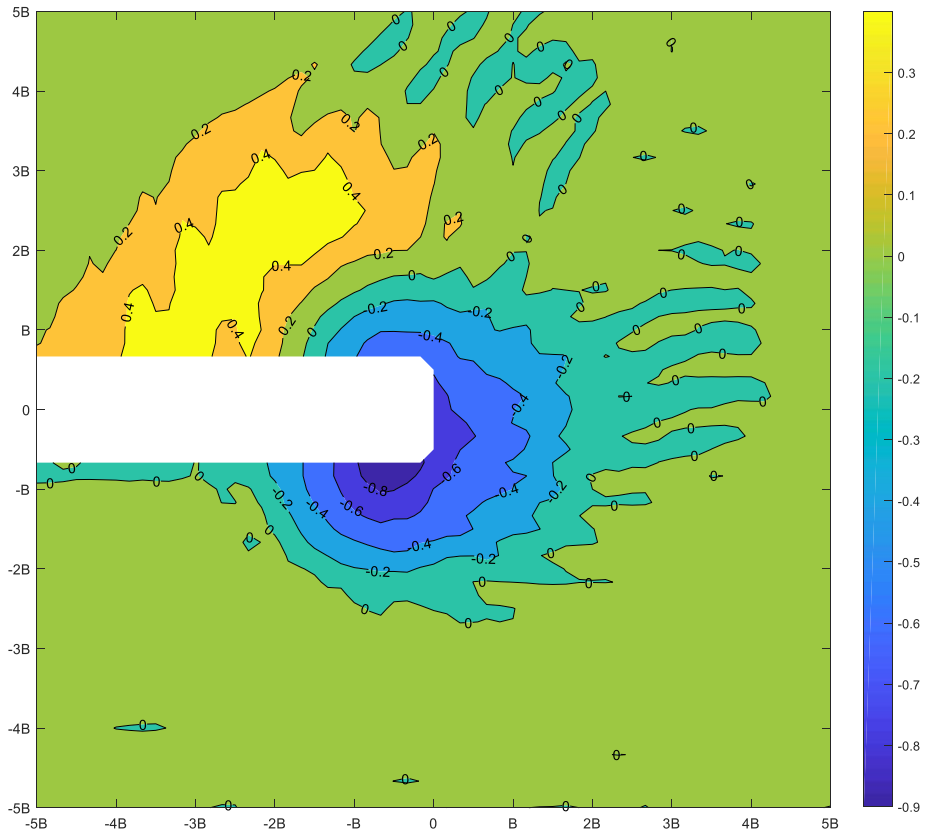

Figure 0.1. Sharp-edged head structure scour pattern (S/B) under ir-1 wave (KC=1.403)

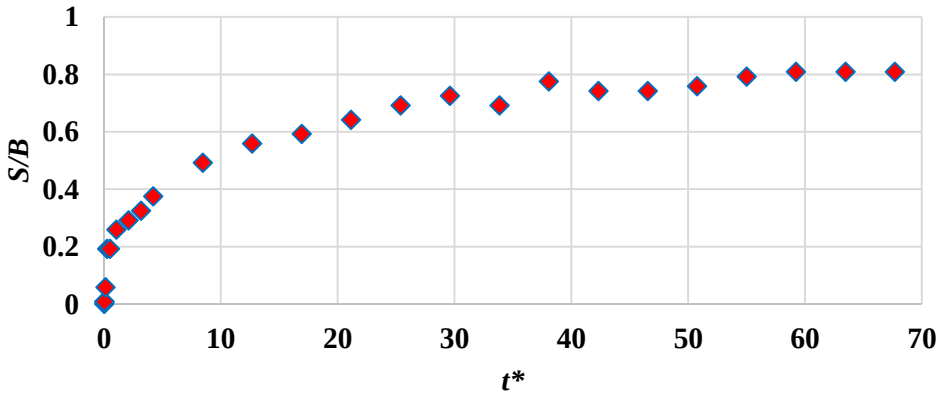

Figure 0.2. Sharp-edged head structure scour development (S/B) under ir-1 wave (KC=1.403)

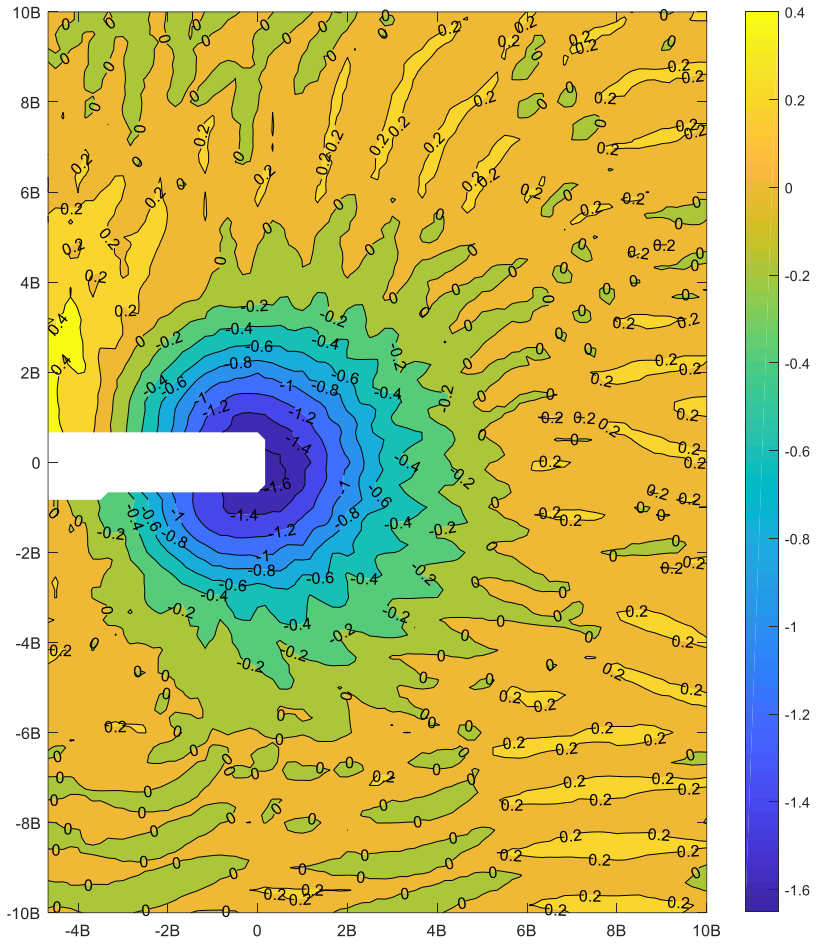

Figure 0.3. Sharp-edged head structure scour pattern (S/B) under ir-2 wave (KC=3.182)

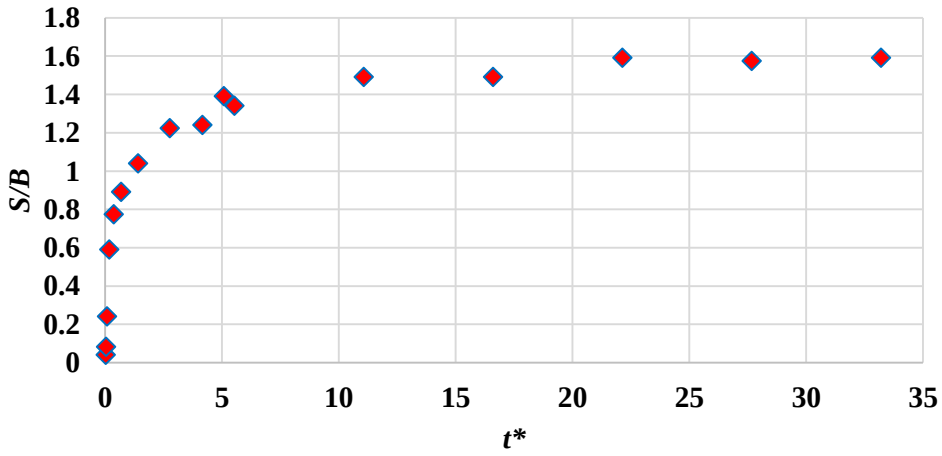

Figure 0.4. Sharp-edged head structure scour development (S/B) under ir-2 wave (KC=3.182)

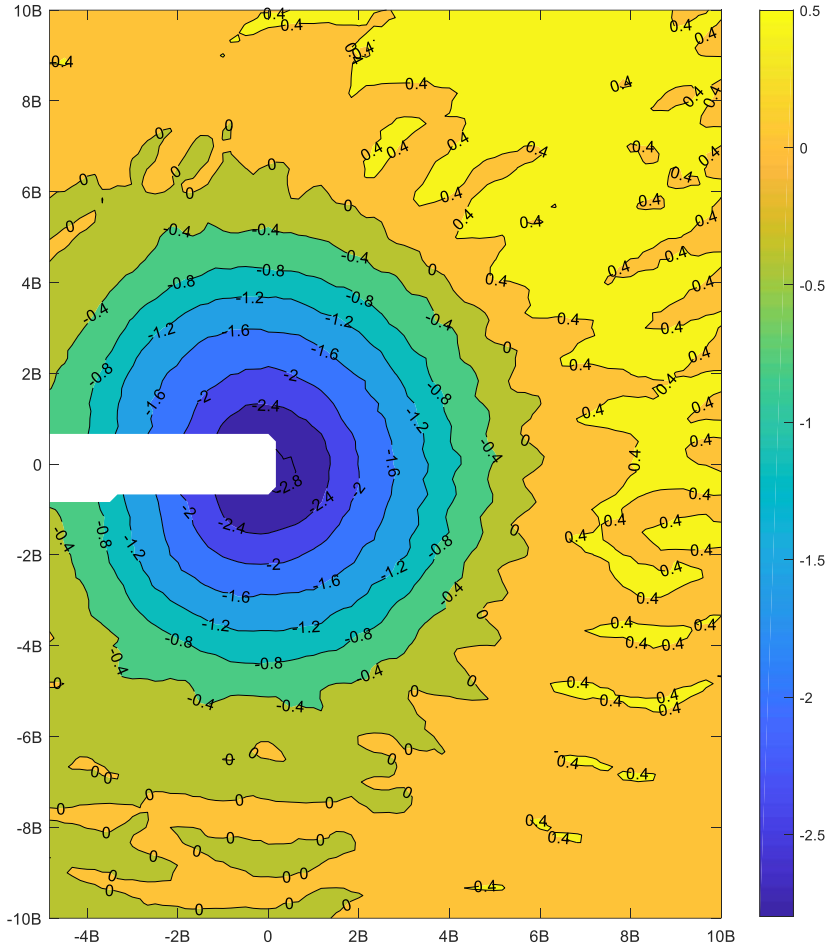

Figure 0.5. Sharp-edged head structure scour pattern (S/B) under ir-3 wave (KC=5.347)

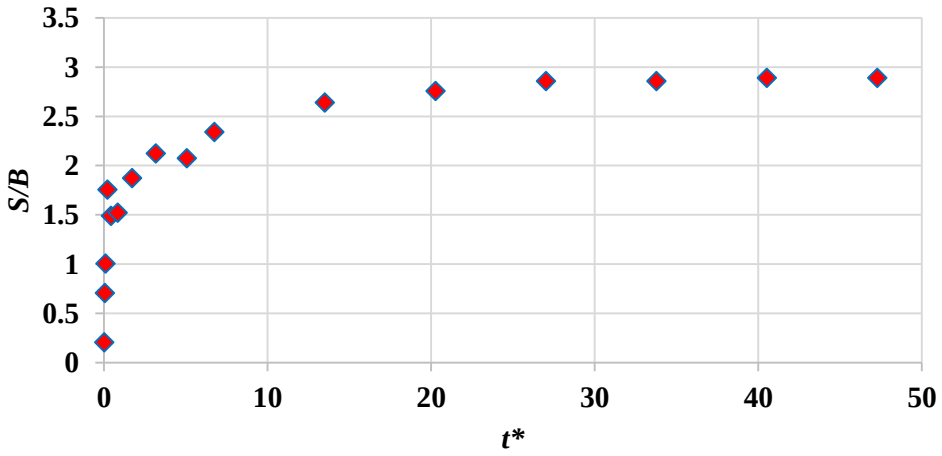

Figure 0.6. Sharp-edged head structure scour development (S/B) under ir-3 wave (KC=5.347)

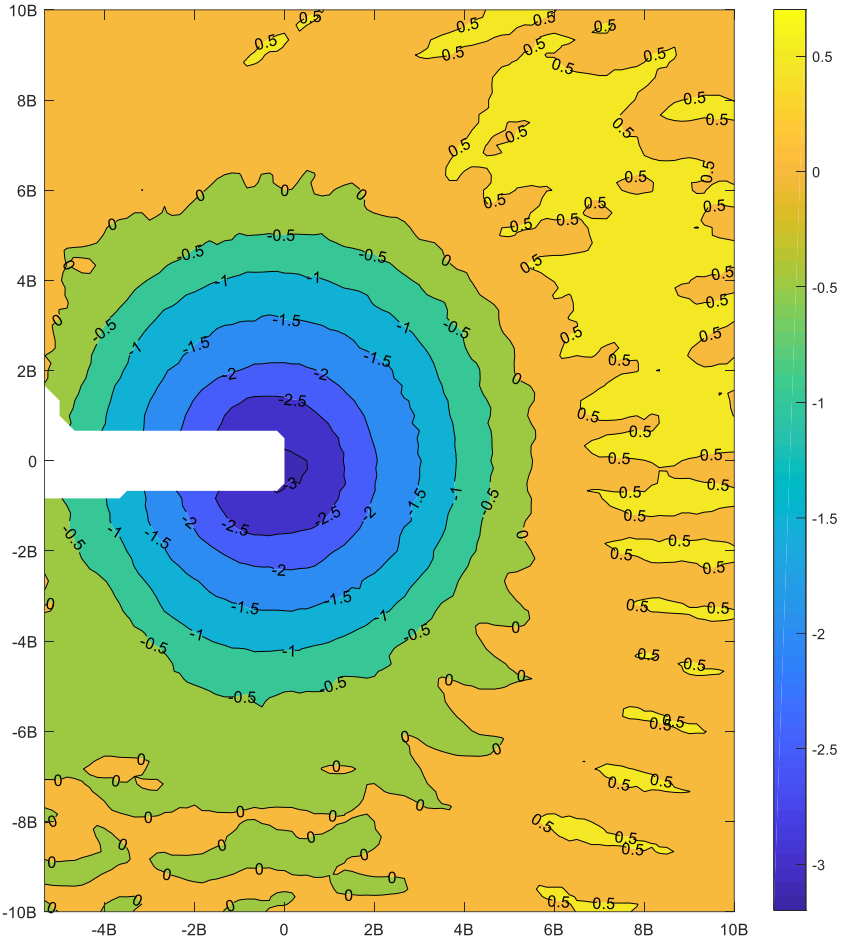

Figure 0.7. Sharp-edged head structure scour pattern (S/B) under ir-4 wave (KC=5.417)

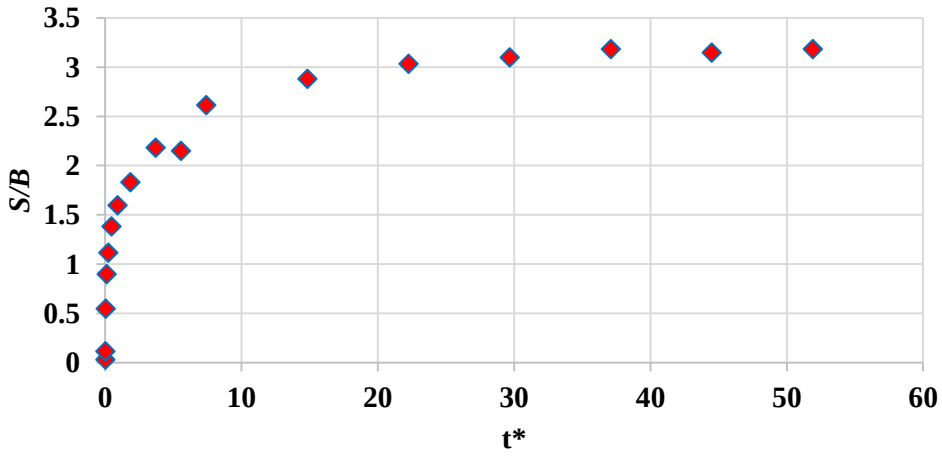

Figure 0.8. Sharp-edged head structure scour development (S/B) under ir-4 wave (KC=5.417)

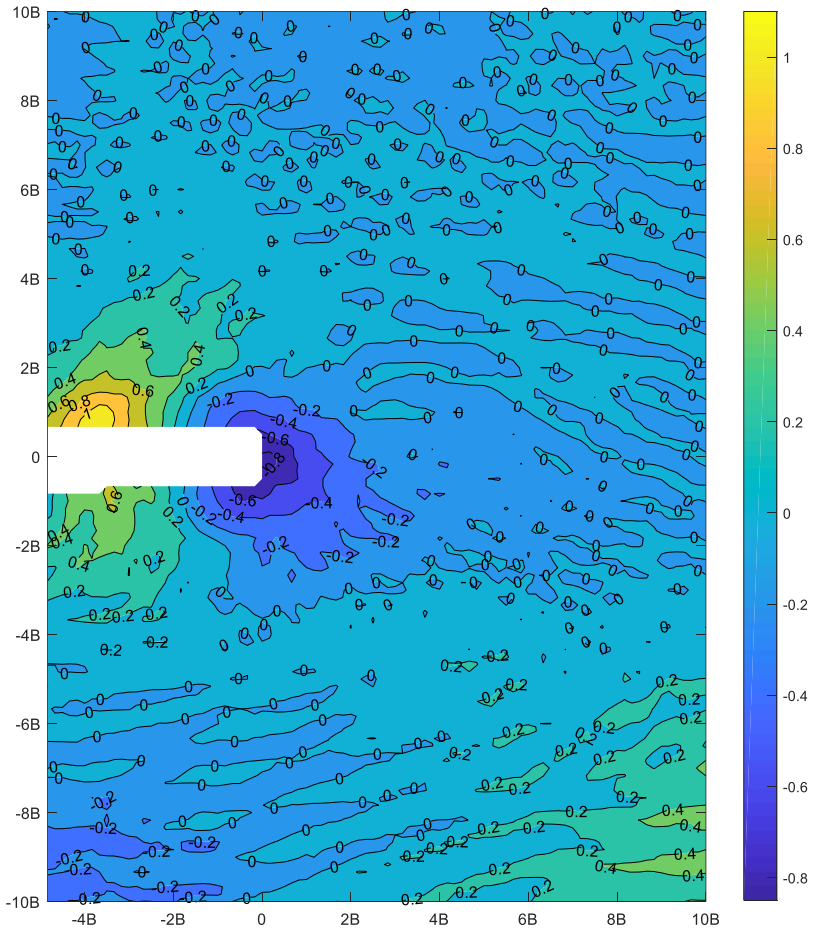

Figure 0.9. Sharp-edged head structure scour pattern (S/B) under reg-2 wave (KC=3.184)

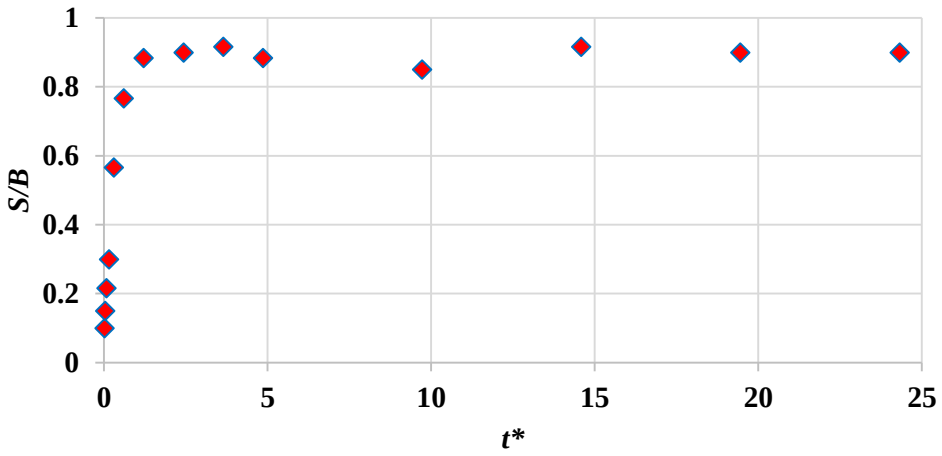

Figure 0.10. Sharp-edged head structure scour development (S/B) under reg-2 wave (KC=3.184)

B. Scour Patterns and Development Curves for Round Head Structures

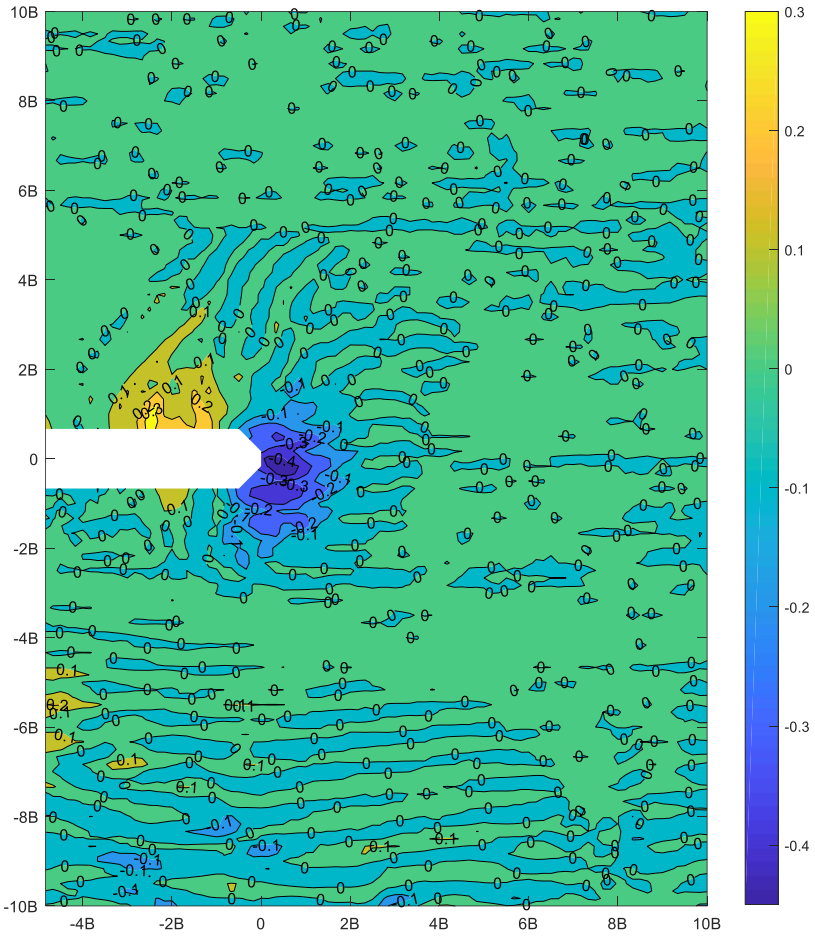

Figure 0.11. Round head structure scour pattern (S/B) under ir-1 wave (KC=1.403)

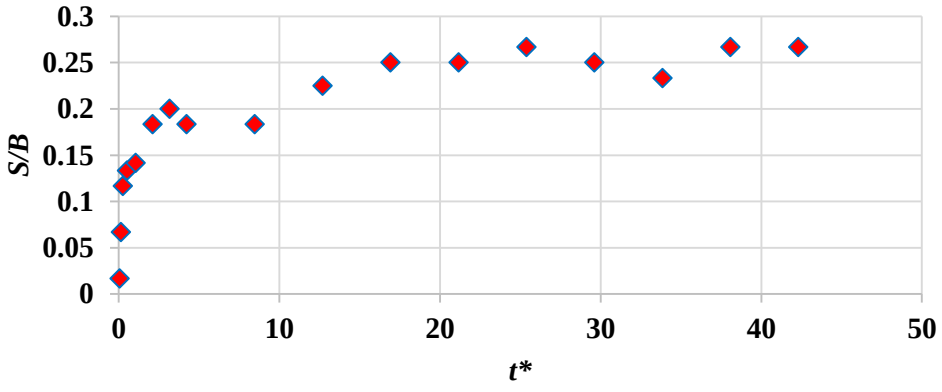

Figure 0.12. Round head structure scour development (S/B) under ir-1 wave (KC=1.403)

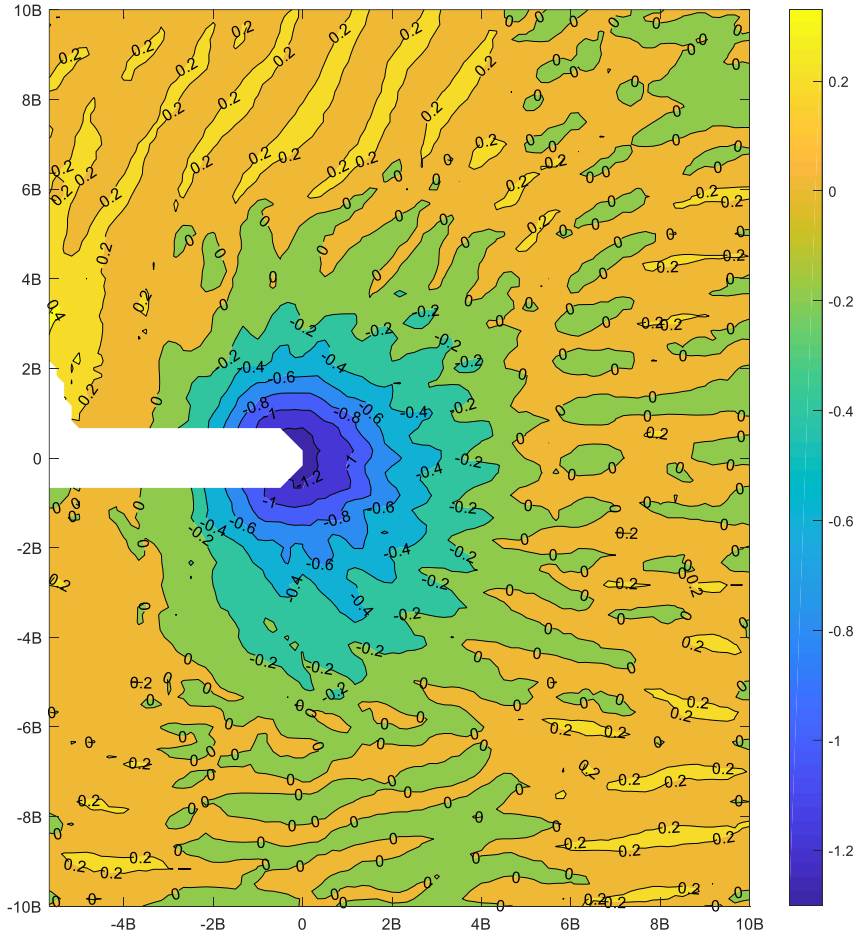

Figure 0.13. Round head structure scour pattern (S/B) under ir-2 wave (KC=3.182)

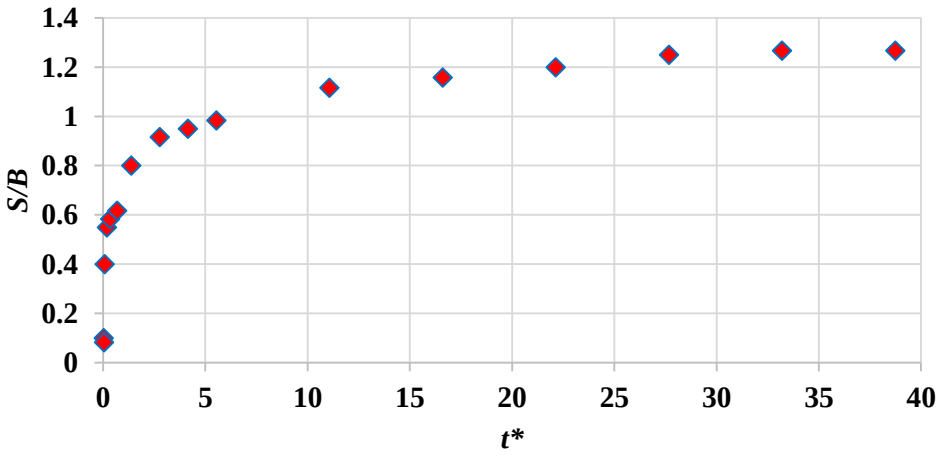

Figure 0.14. Round head structure scour development (S/B) under ir-2 wave (KC=3.182)

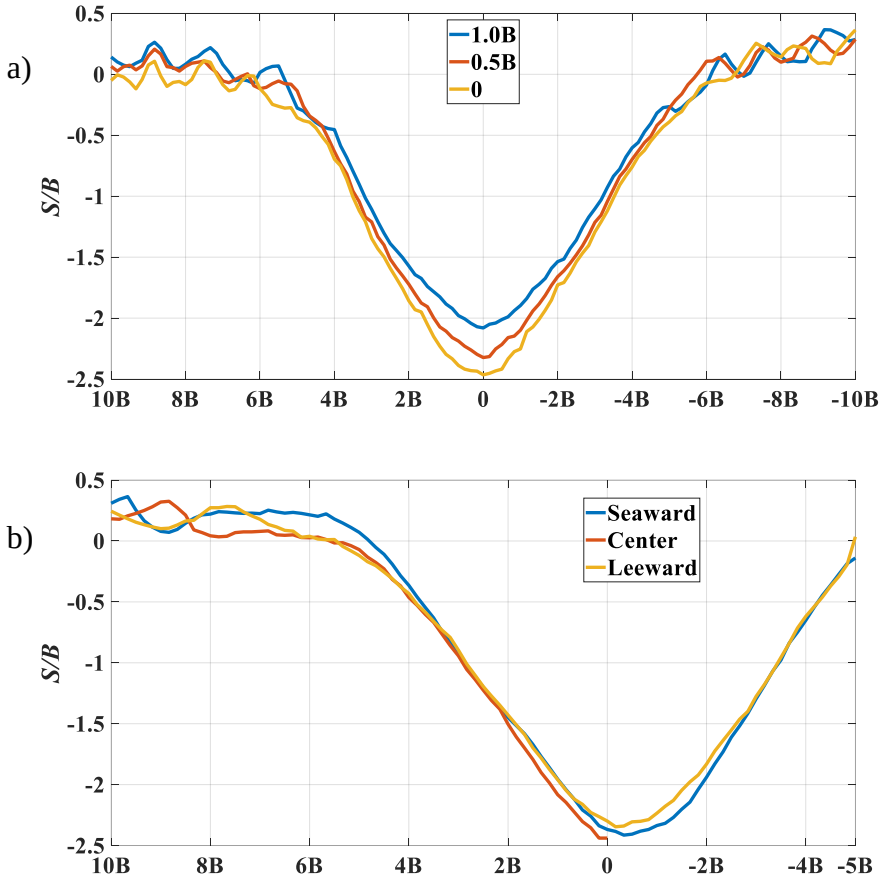

Figure 0.15. Round head structure scour profiles under ir-3 wave (KC=5.347) a) X direction b) Y direction

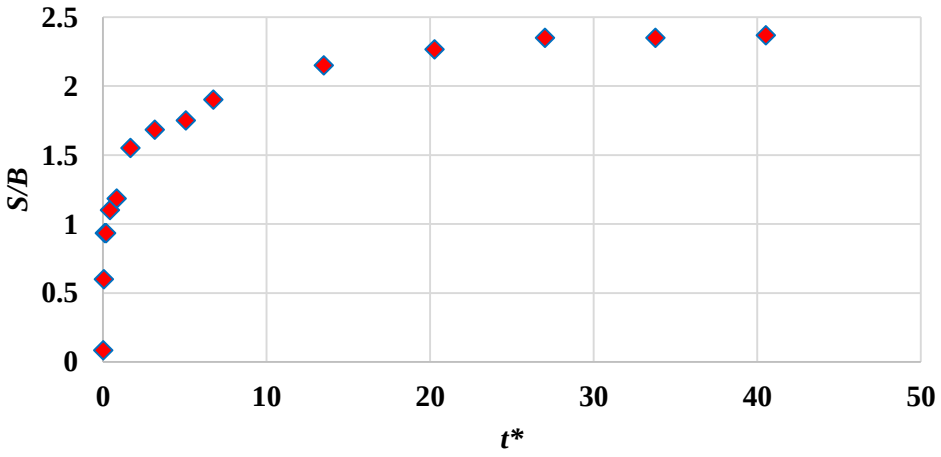

Figure 0.16. Round head structure scour development (S/B) under ir-3 wave (KC=5.347)

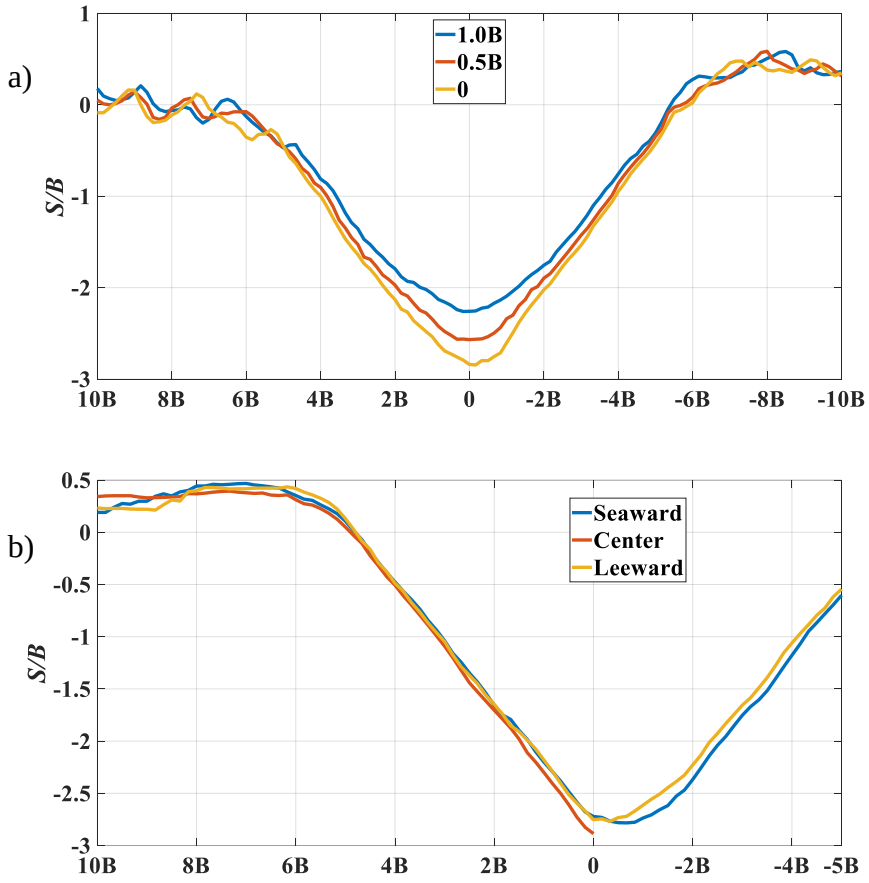

Figure 0.17. Round head structure scour profiles under ir-4 wave (KC=5.417) a) X direction b) Y direction

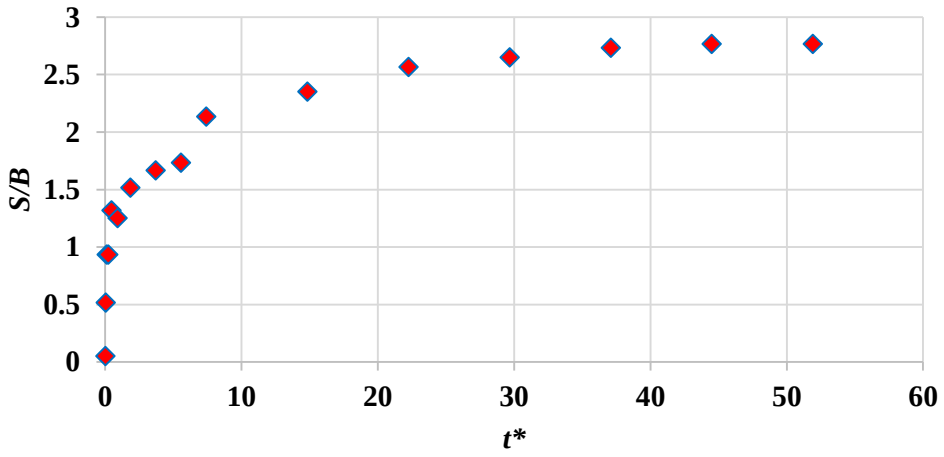

Figure 0.18. Round head structure scour development (S/B) under ir-4 wave (KC=5.417)

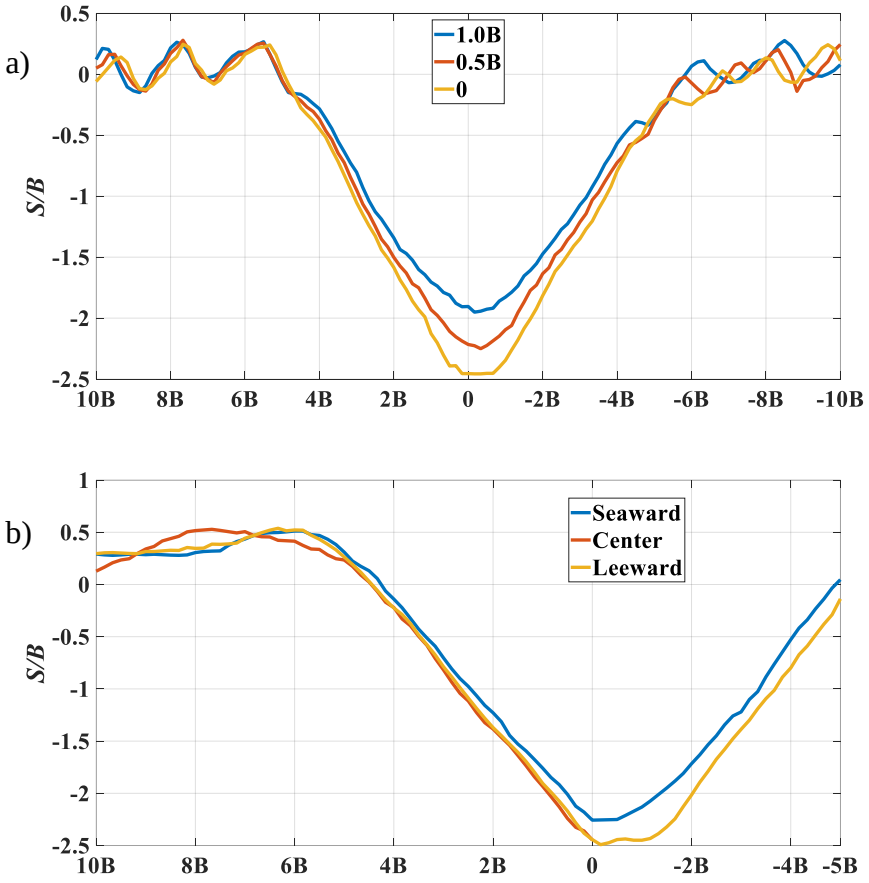

Figure 0.19. Round head structure scour profiles under ir-5 wave (KC=5.528) a) X direction b) Y direction

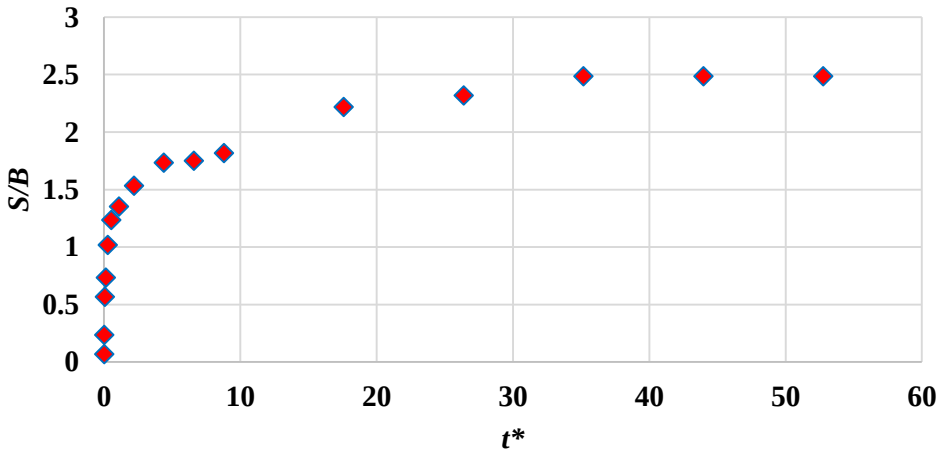

Figure 0.20. Round head structure scour development (S/B) under ir-5 wave (KC=5.528)

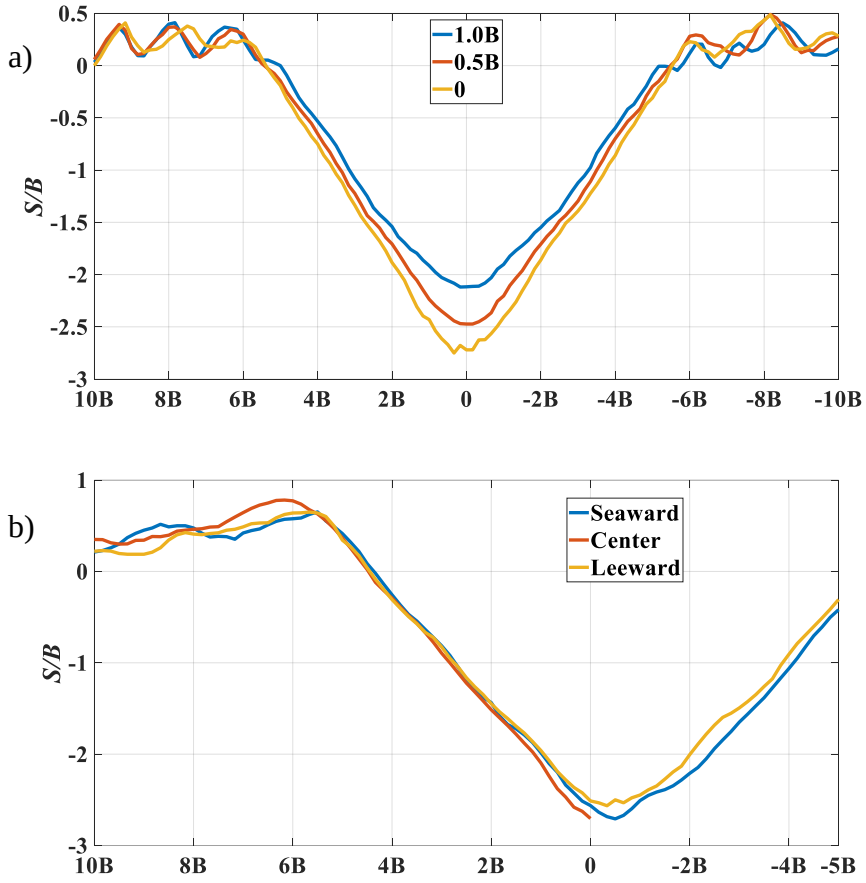

Figure 0.21. Round head structure scour profiles under ir-6 wave (KC=5.445) a) X direction b) Y direction

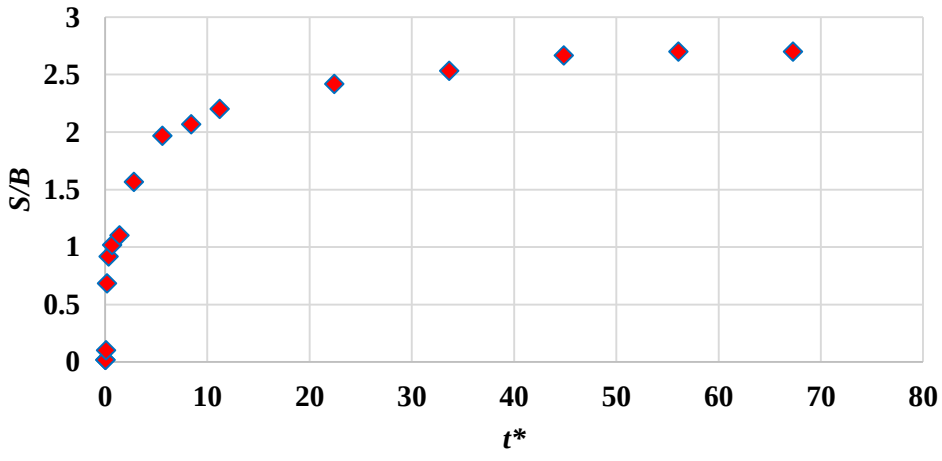

Figure 0.22. Round head structure scour development (S/B) under ir-6 wave (KC=5.445)

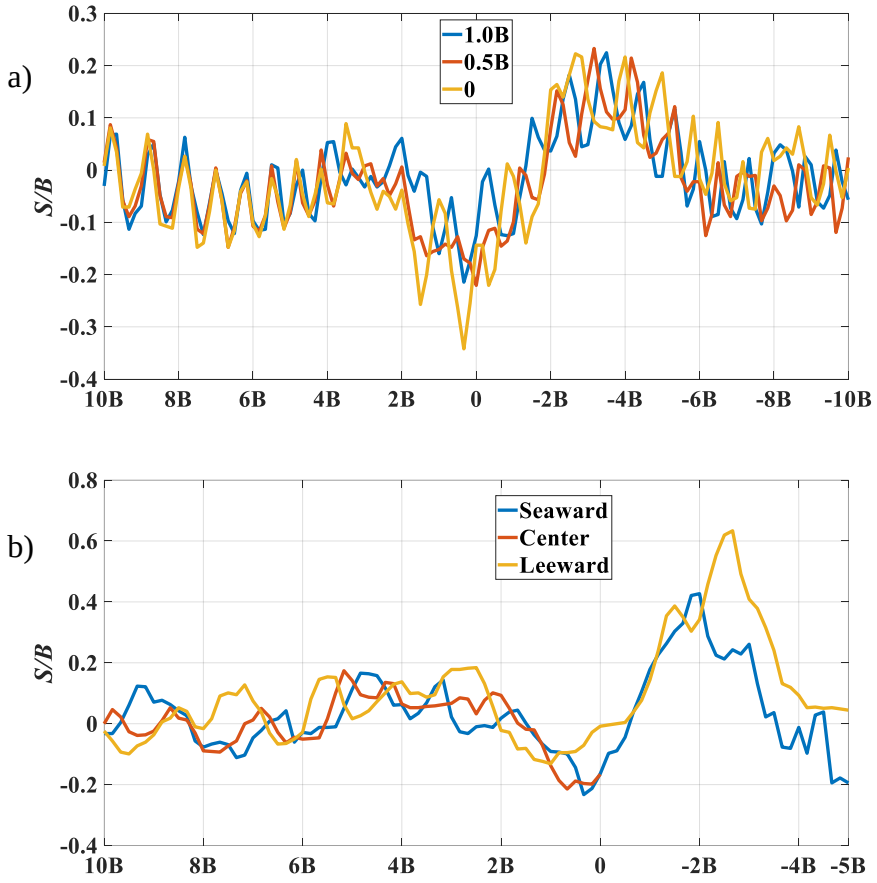

Figure 0.23. Round head structure scour profiles under first test of reg-2 wave (KC=3.184) a) X direction b) Y direction

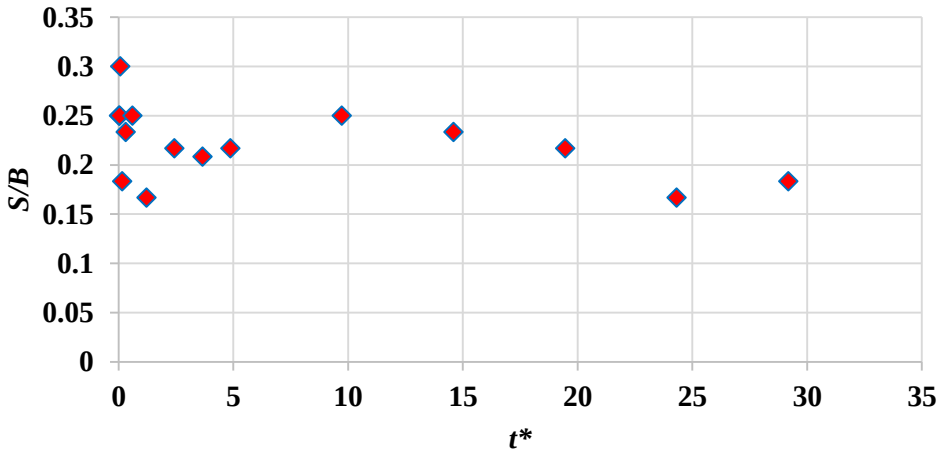

Figure 0.24. Round head structure scour development (S/B) under first test of reg-2 wave (KC=3.184)

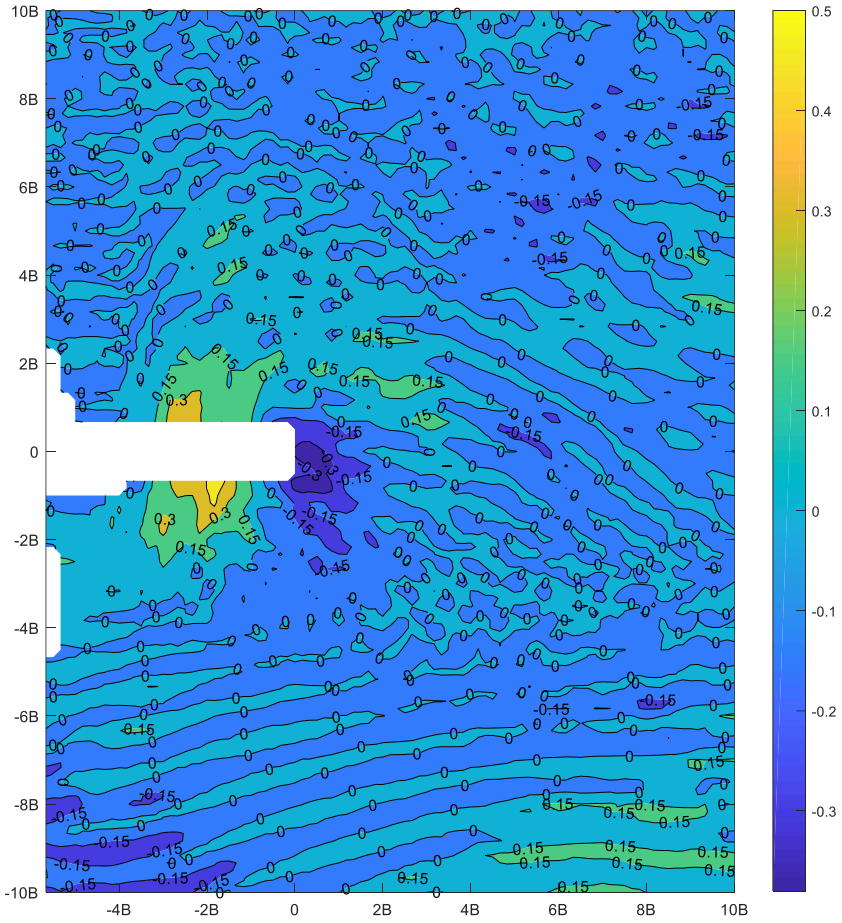

Figure 0.25. Round head structure scour pattern (S/B) under second test of reg-2 wave (KC=3.184)

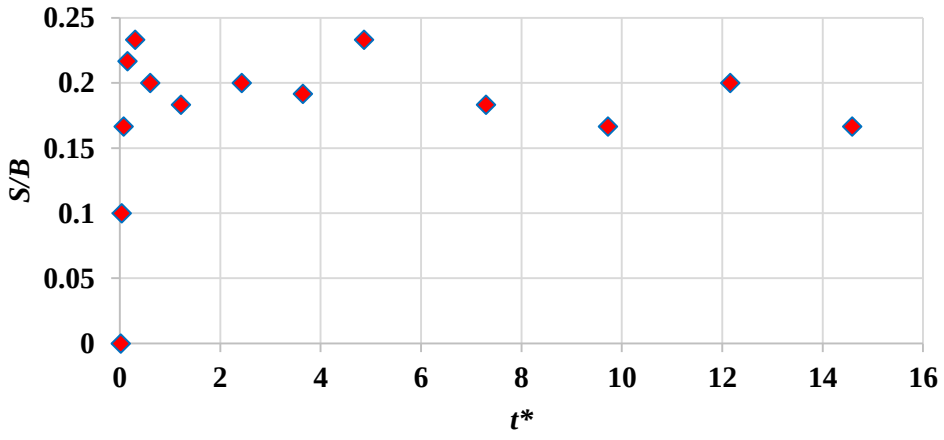

Figure 0.26. Round head structure scour development (S/B) under second test of reg-2 wave (KC=3.184)

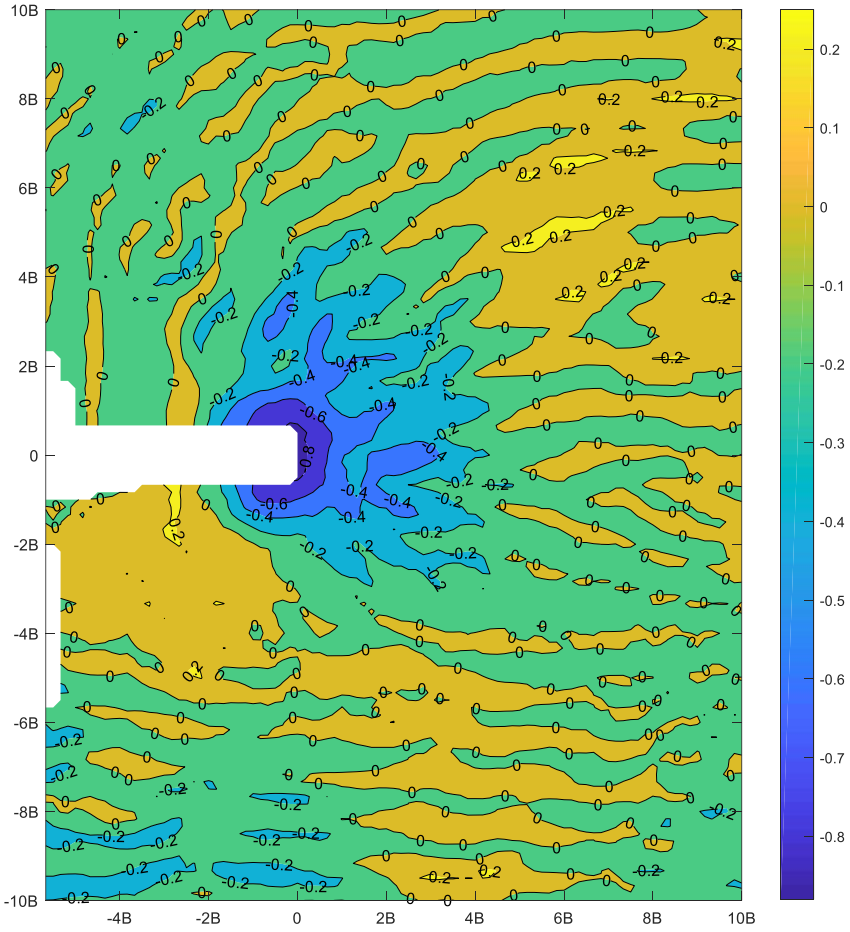

Figure 0.27. Round head structure scour pattern (S/B) under first test of reg-3 wave (KC=4.432)

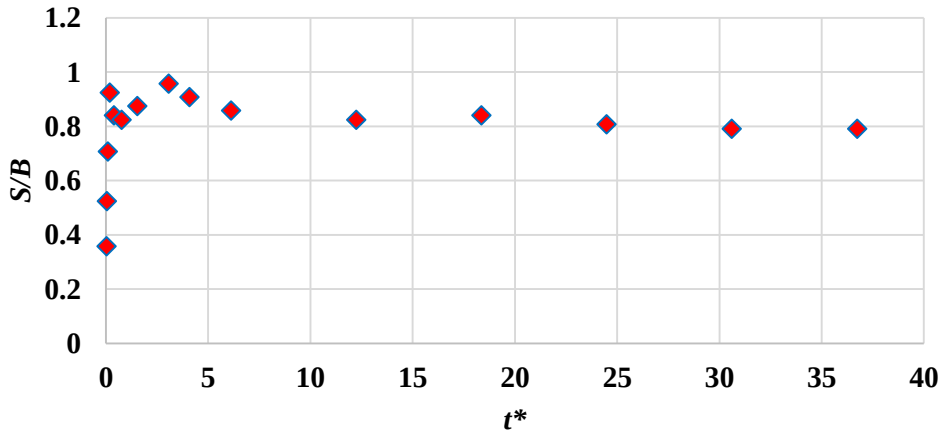

Figure 0.28. Round head structure scour development (S/B) under first test of reg-3 wave (KC=4.432)

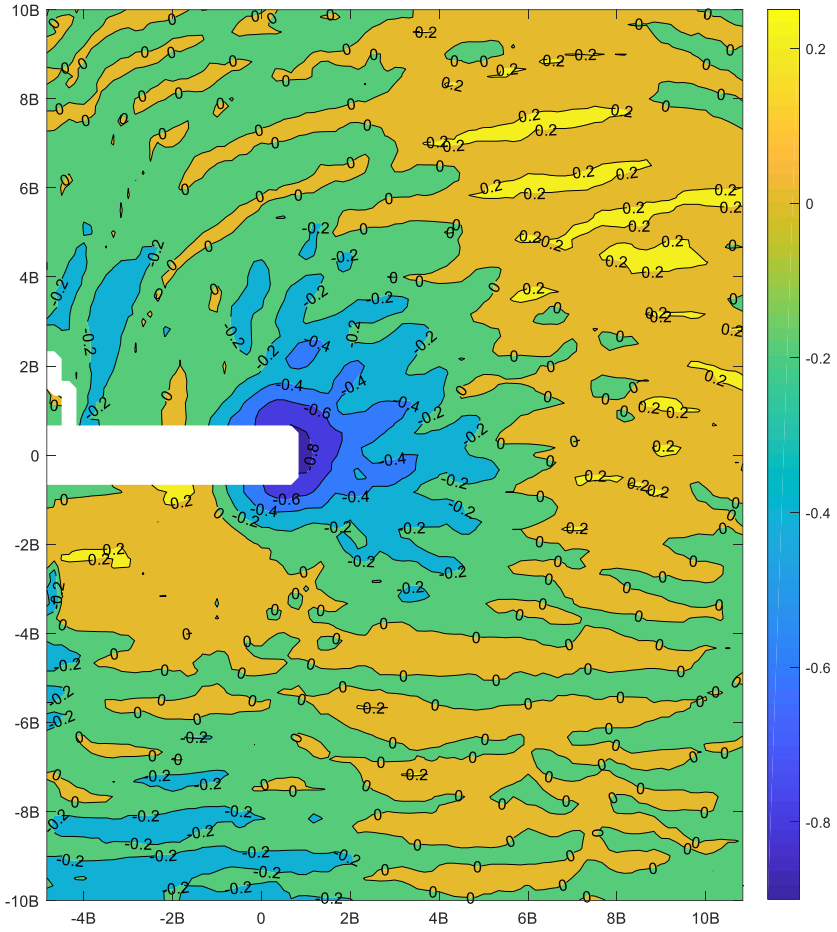

Figure 0.29. Round head structure scour pattern (S/B) under second test of reg-3 wave (KC=4.432)

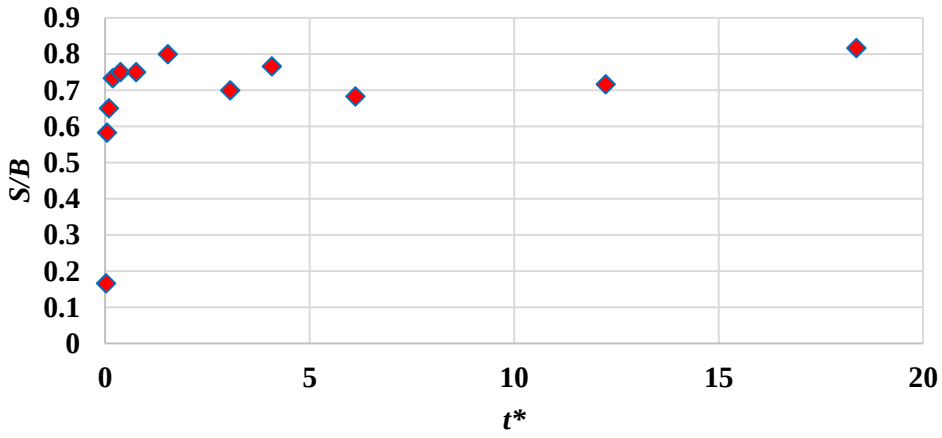

Figure 0.30. Round head structure scour development (S/B) under second test of reg-3 wave (KC=4.432)

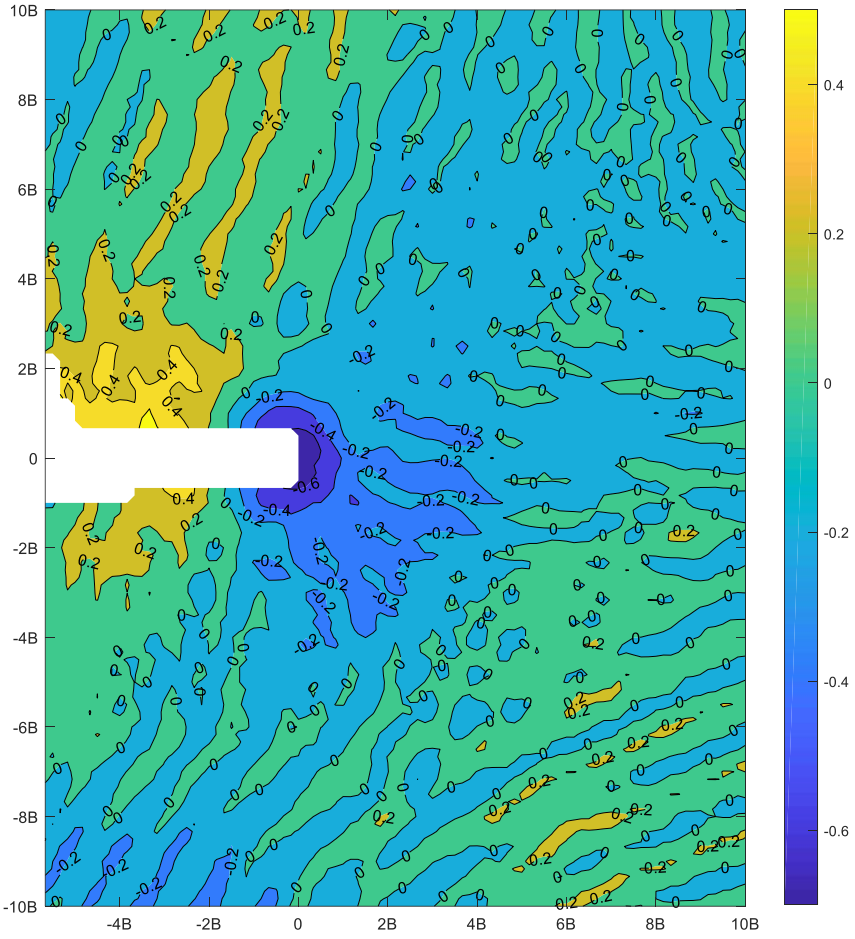

Figure 0.31. Round head structure scour pattern (S/B) under reg-4 wave (KC=5.019)

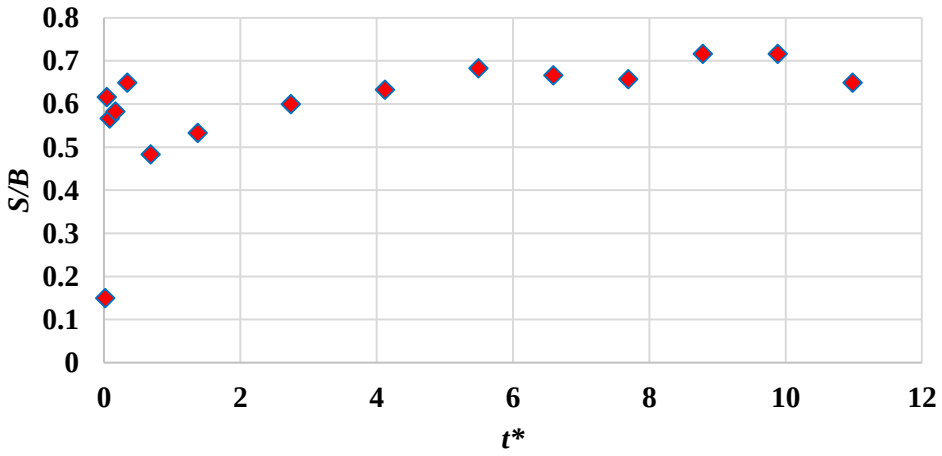

Figure 0.32. Round head structure scour development (S/B) under reg-4 wave (KC=5.019)

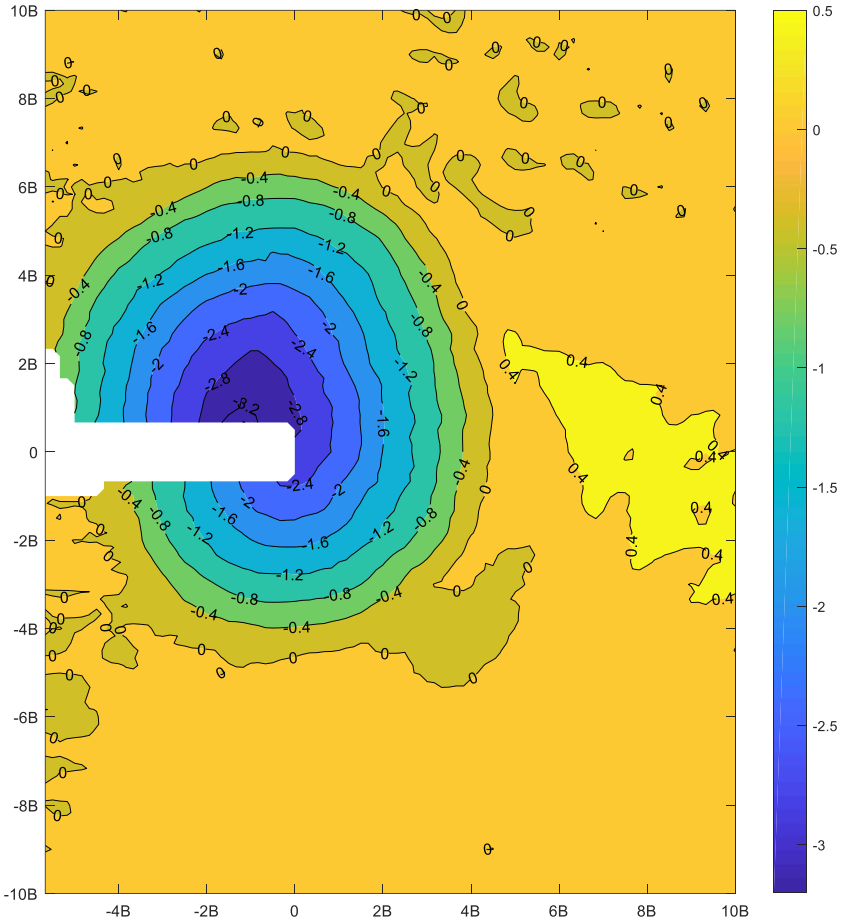

Figure 0.33. Round head structure scour pattern (S/B) under sol-40-1 wave (h=40cm, H=7.7cm)

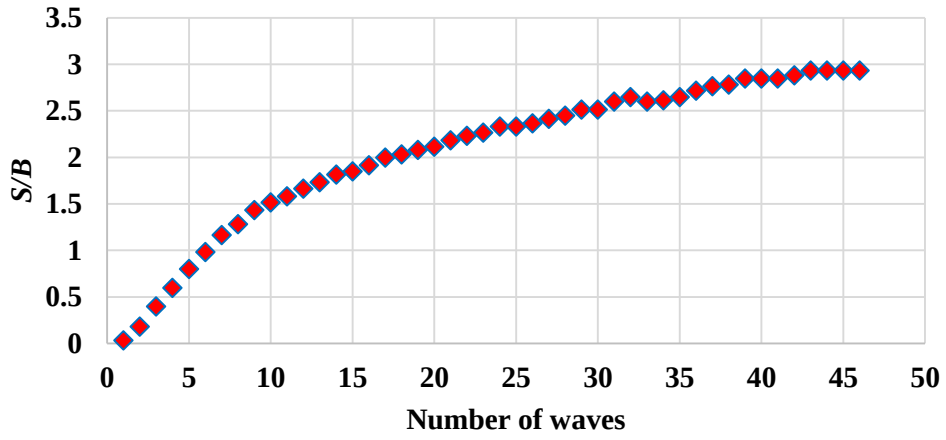

Figure 0.34. Round head structure scour development (S/B) under sol-40-1 wave (h=40cm, H=7.7cm)

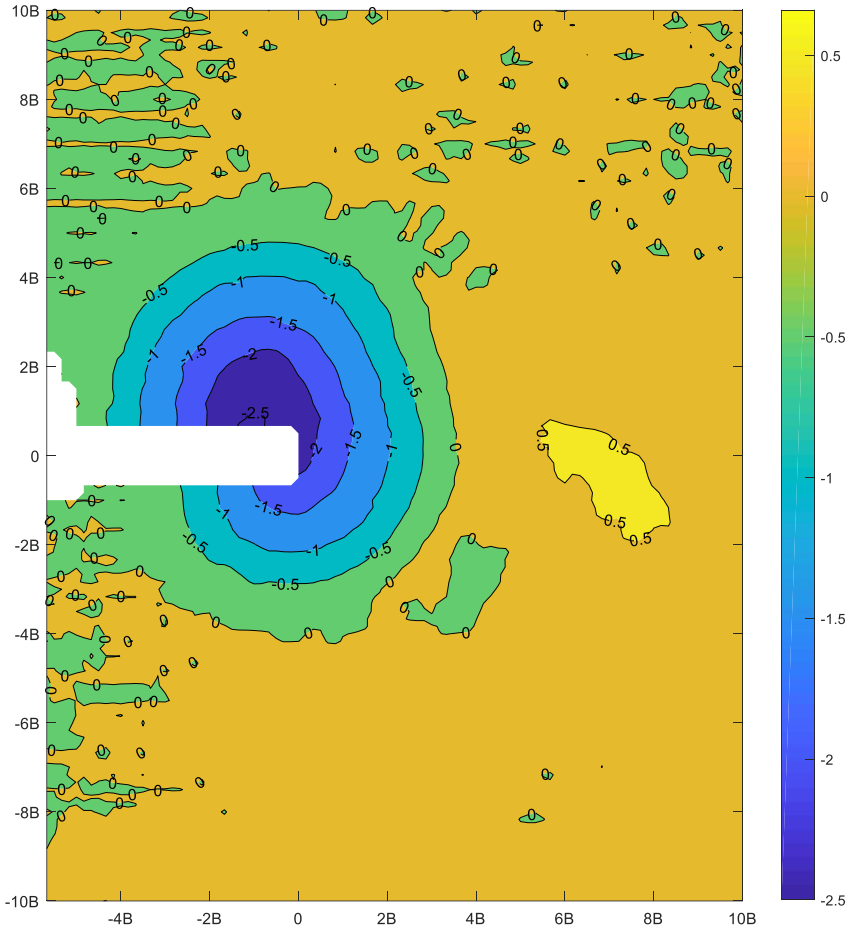

Figure 0.35. Round head structure scour pattern (S/B) under sol-40-2 wave (h=40cm, H=5.6cm)

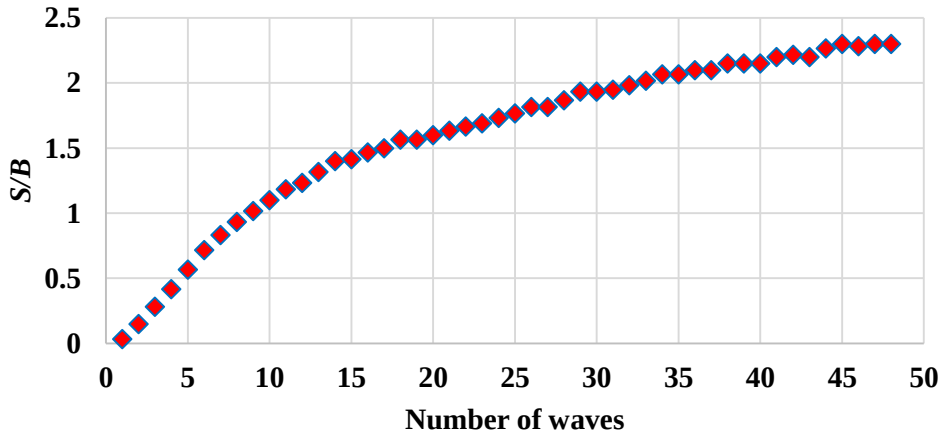

Figure 0.36. Round head structure scour development (S/B) under sol-40-2 wave (h=40cm, H=5.6cm)

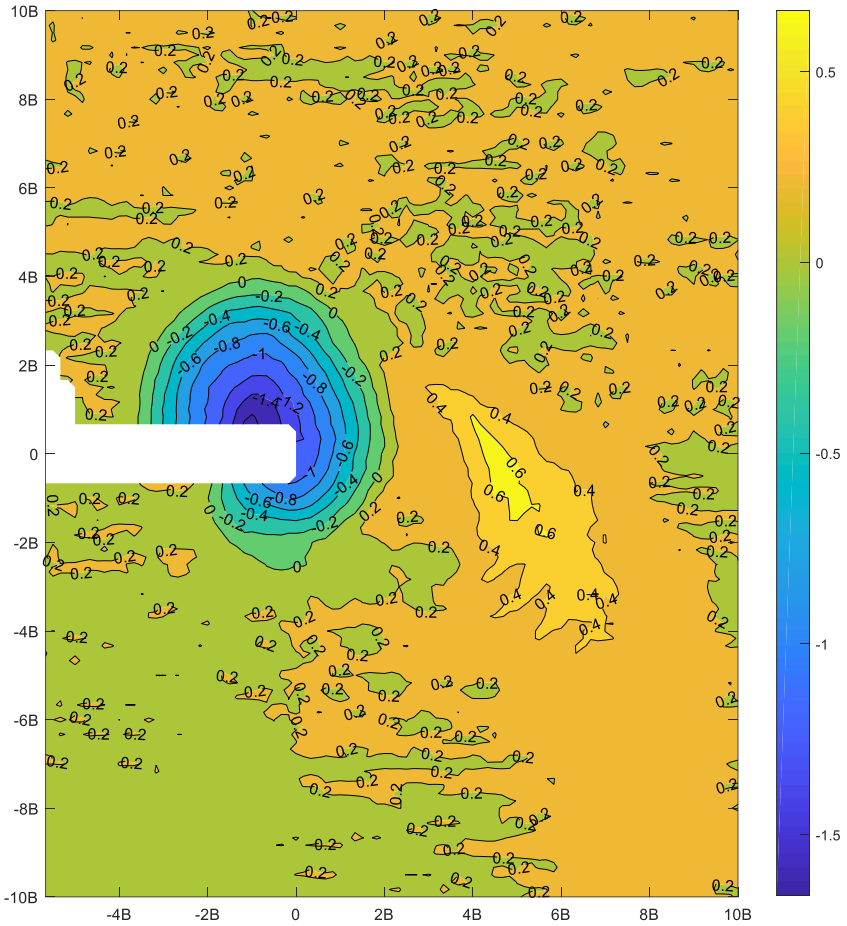

Figure 0.37. Round head structure scour pattern (S/B) under sol-40-3 wave (h=40cm, H=3.5cm)

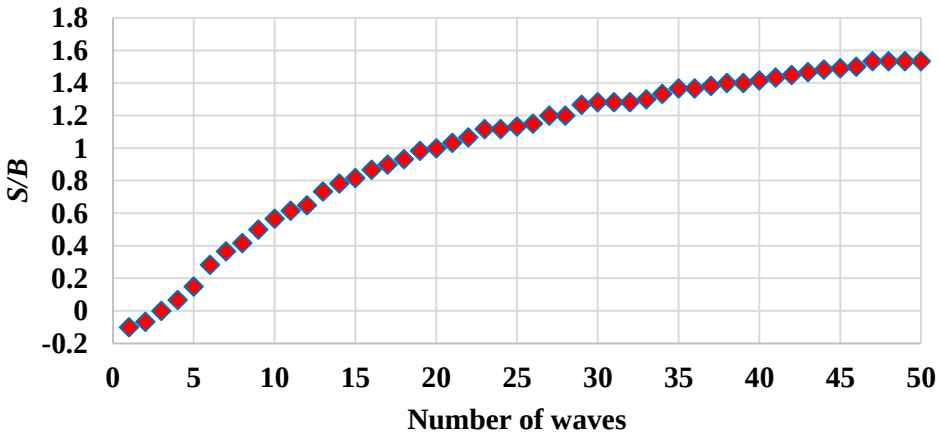

Figure 0.38. Round head structure scour development (S/B) under sol-40-3 wave (h=40cm, H=3.5cm)

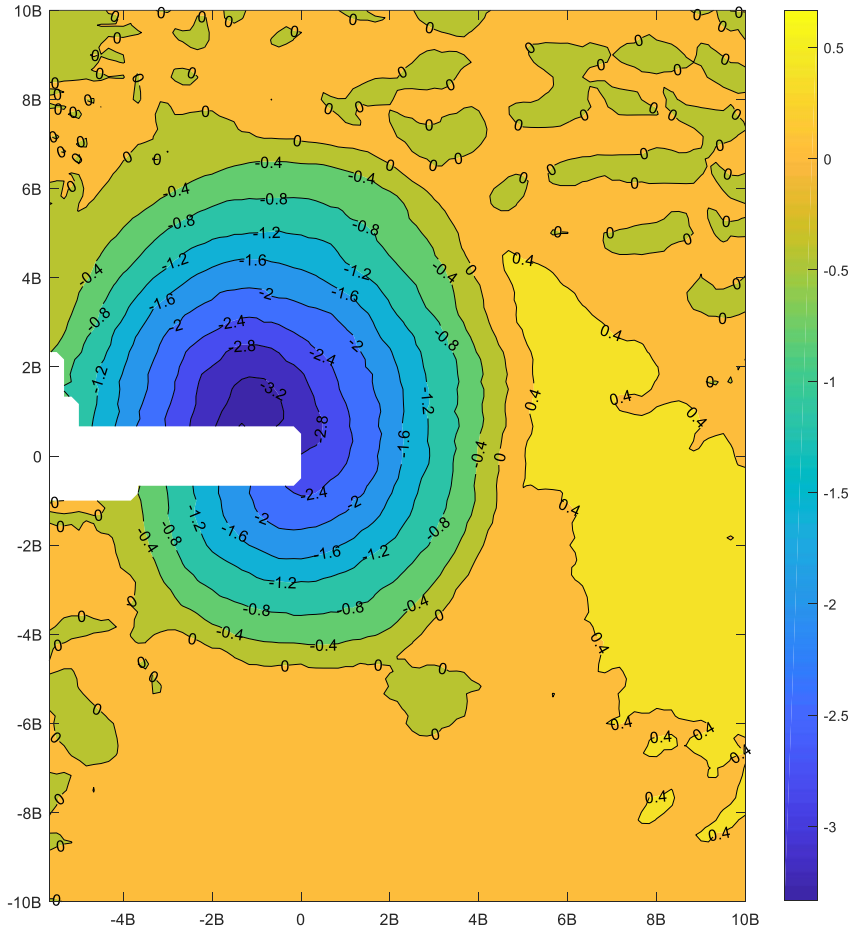

Figure 0.39. Round head structure scour pattern (S/B) under sol-30-1 wave (h=30cm, H=9.3cm)

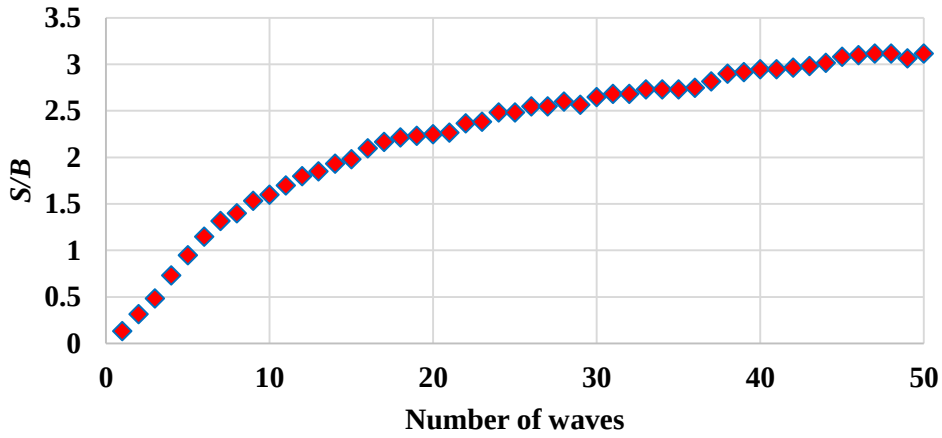

Figure 0.40. Round head structure scour development (S/B) under sol-30-1 wave (h=30cm, H=9.3cm)

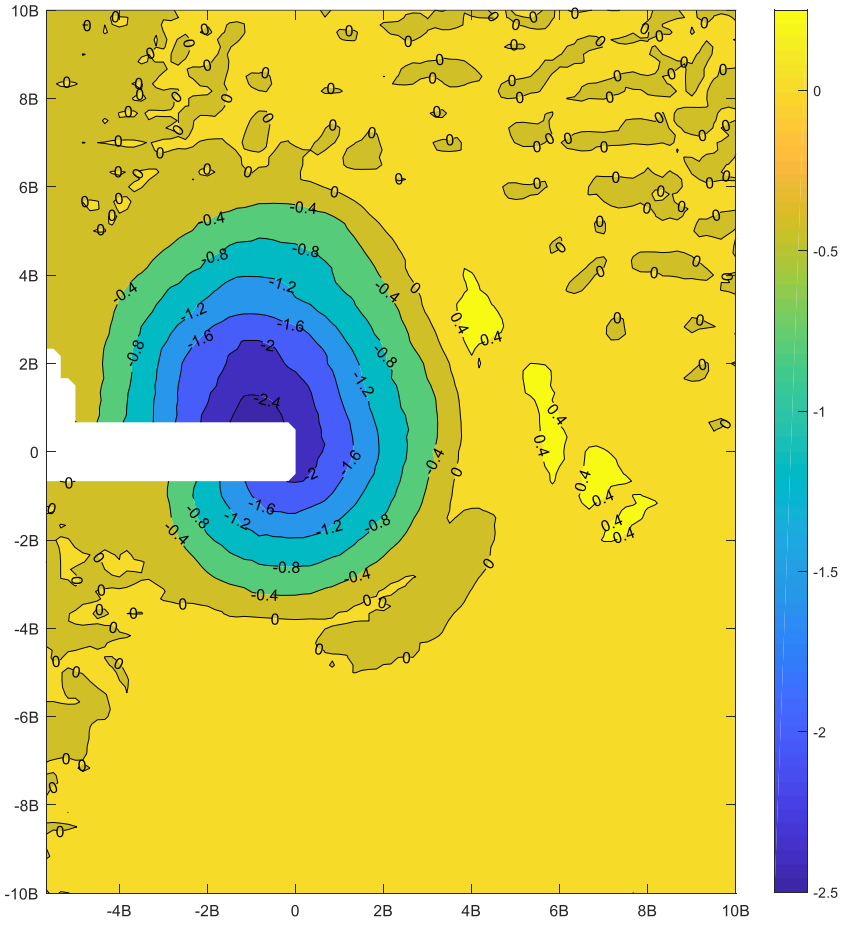

Figure 0.41. Round head structure scour pattern (S/B) under sol-30-2 wave (h=30cm, H=7.8cm)

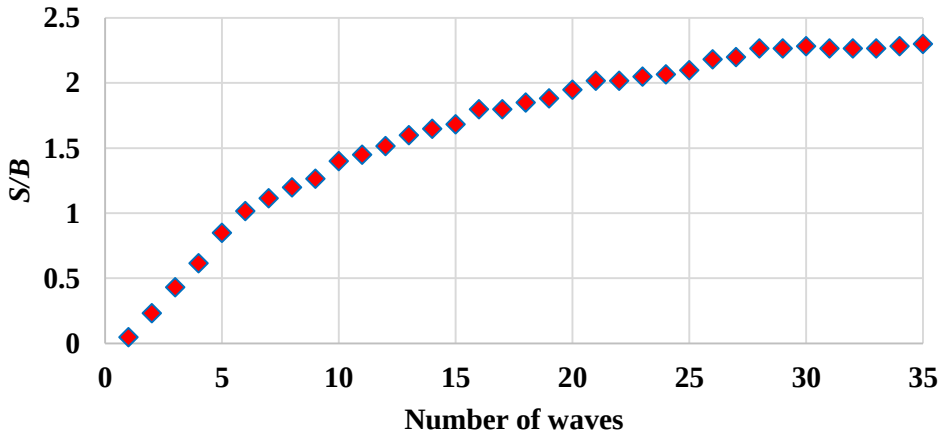

Figure 0.42. Round head structure scour development (S/B) under sol-30-2 wave (h=30cm, H=7.8cm)

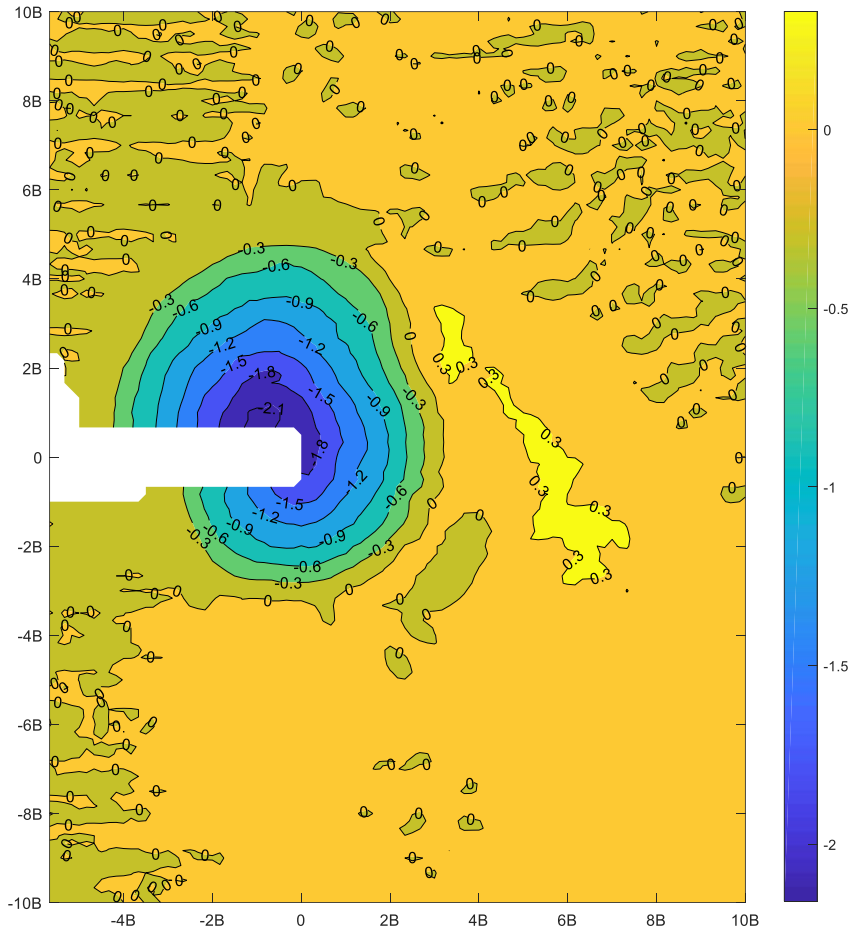

Figure 0.43. Round head structure scour pattern (S/B) under sol-30-3 wave (h=30cm, H=5.6cm)

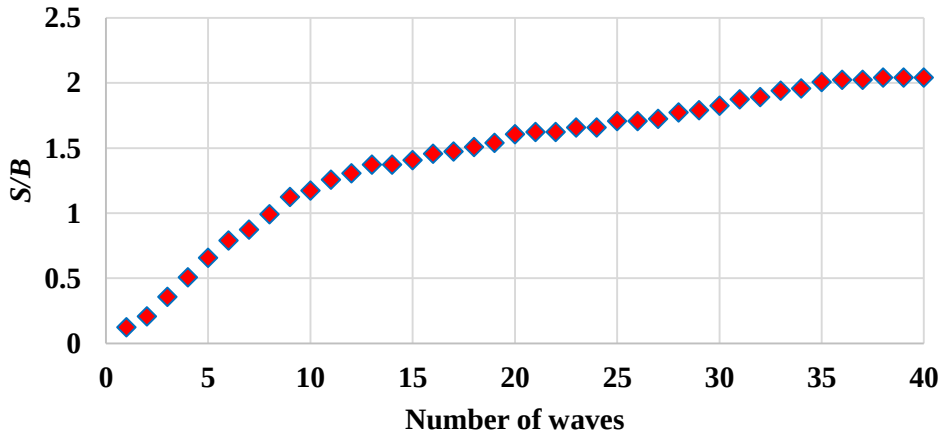

Figure 0.44. Round head structure scour development (S/B) under sol-30-3 wave (h=30cm, H=5.6cm)

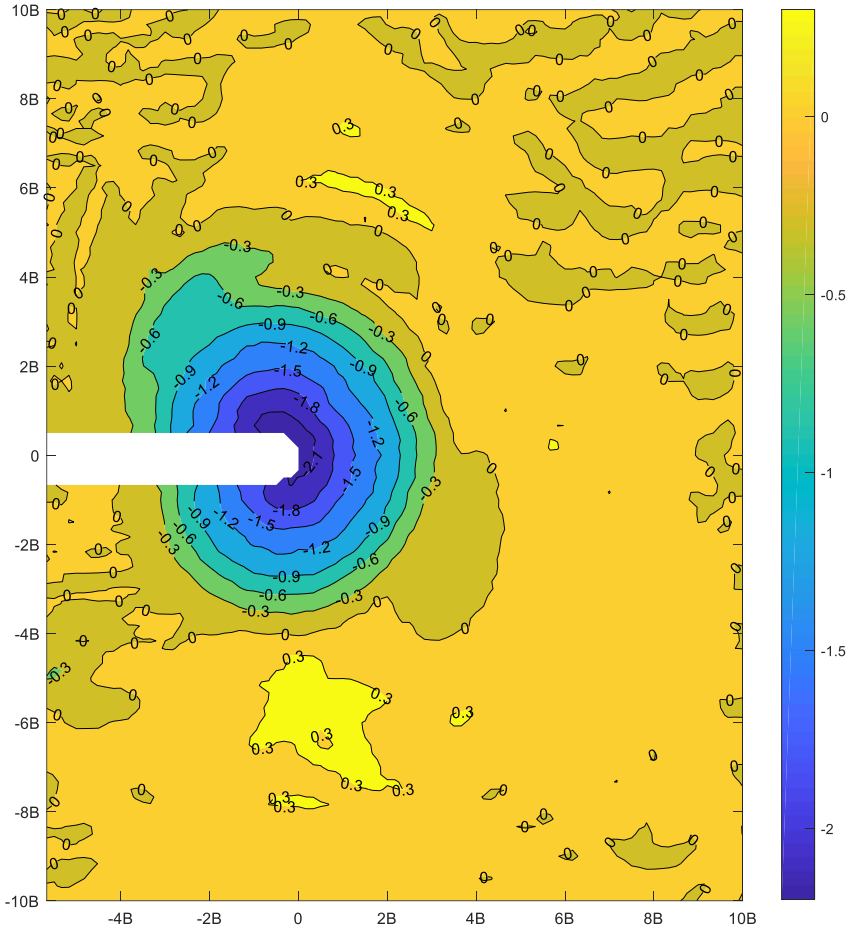

Figure 0.45. Round head structure scour pattern (S/B) under sol-20-1 wave (h=20cm, H=11.7cm)

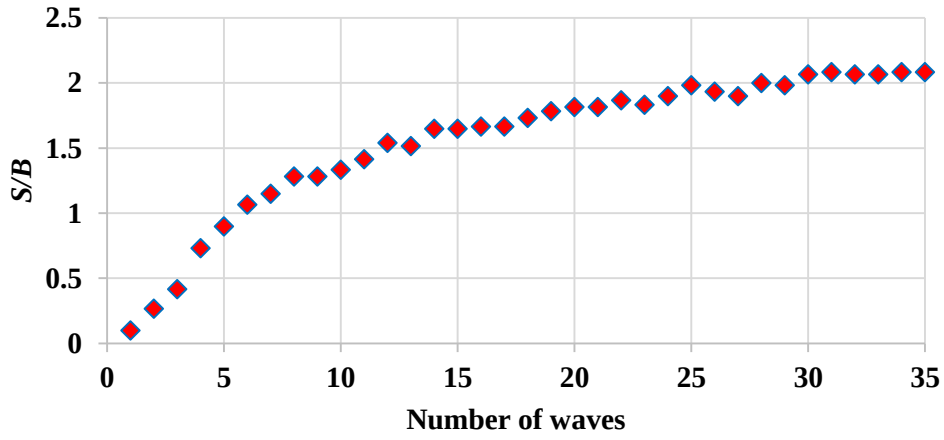

Figure 0.46. Round head structure scour development (S/B) under sol-20-1 wave (h=20cm, H=11.7cm)

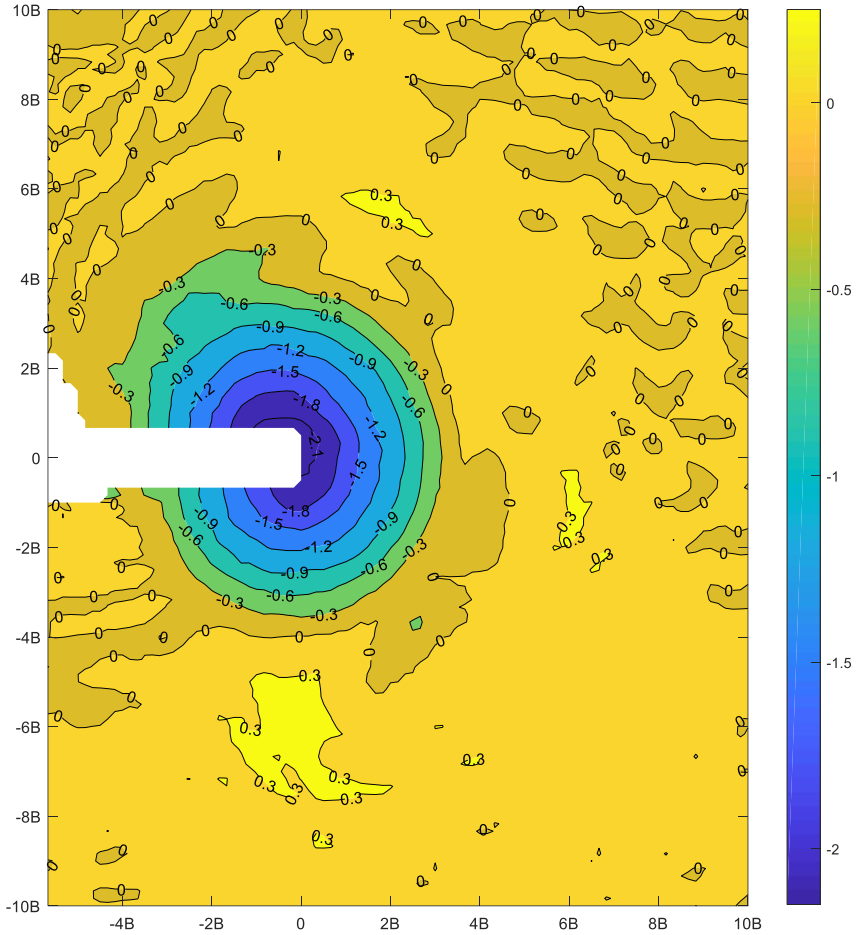

Figure 0.47. Round head structure scour pattern (S/B) under sol-20-2 wave (h=20cm, H=9.6cm)

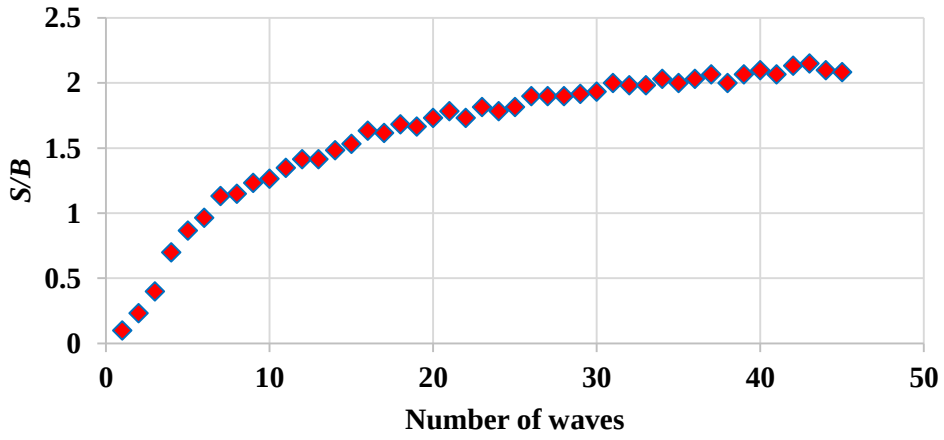

Figure 0.48. Round head structure scour development (S/B) under sol-20-2 wave (h=20cm, H=9.6cm)

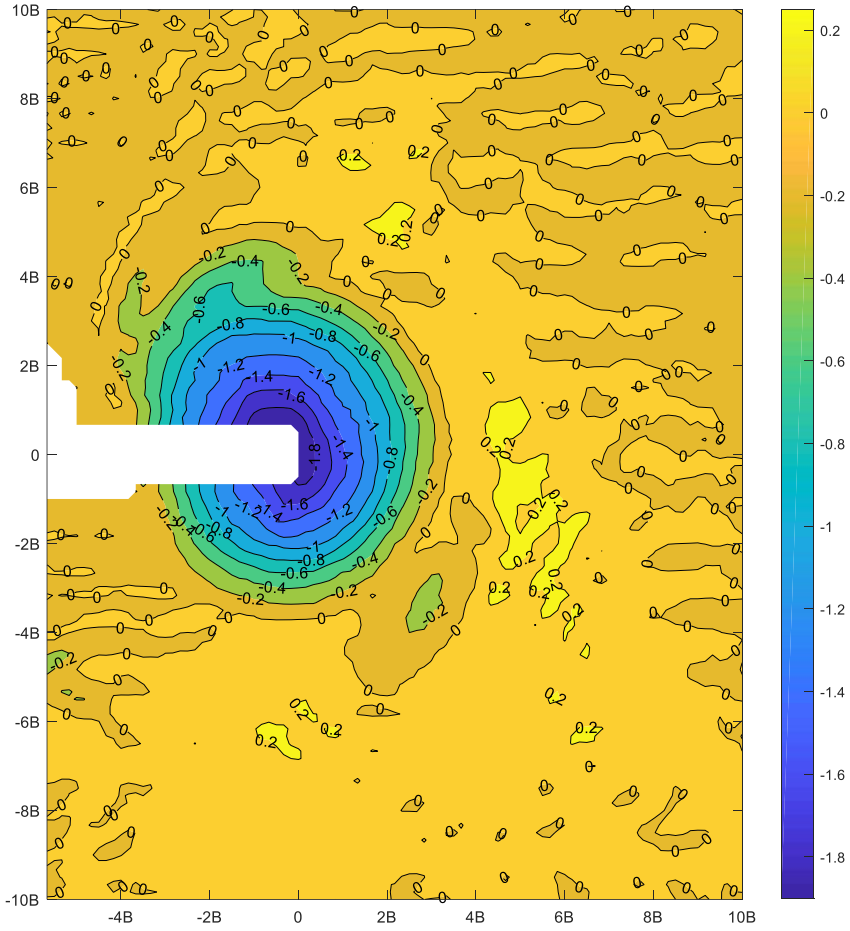

Figure 0.49. Round head structure scour pattern (S/B) under sol-20-3 wave (h=20cm, H=7.7cm)

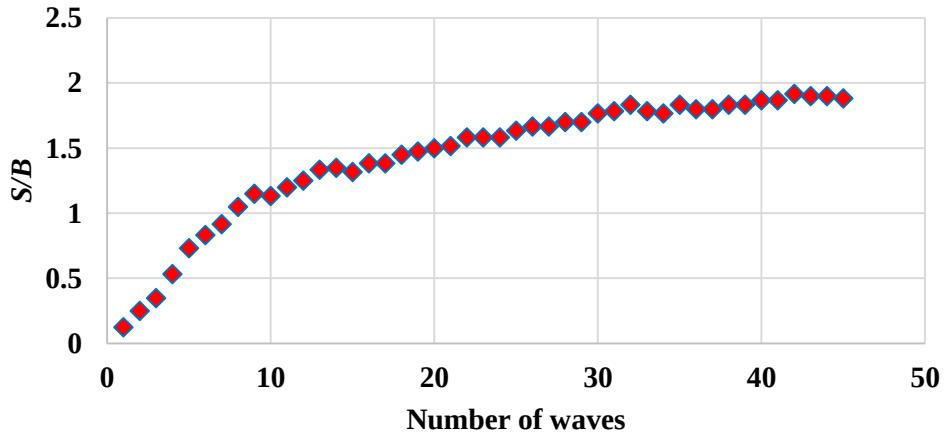

Figure 0.50. Round head structure scour development (S/B) under sol-20-3 wave (h=20cm, H=7.7cm)